Disentangling the Role of CHOP in Mitochondrial Dysfunction

Inaugural-Dissertation

zur

Erlangung des Doktorgrades

der Mathematisch-Naturwissenschaftlichen Fakultät

der Universität zu Köln

vorgelegt von

Sophie Melissa Kaspar

aus München

Köln, 2019

Berichterstatter: Prof. Dr. Aleksandra Trifunovic
Prof. Dr. Rudolf Wiesner

Tag der mündlichen Prüfung: 13. Februar 2020

Table of Contents

List of Figures

List of Tables

Abbreviations

°C	Degree Celcius
^{35}S-met	Radioactive methionine isotope
A	Adenosine
ADP	Adenosine diphosphate
AFG3L2	AFG3-like protein 2
AKT	RAC-alpha serine/threonine-protein kinase
AMP	Adenosine monophosphate
AMPK	5'-AMP-activated protein kinase
APS	Ammonium persulfate
ASNS	Asparagine synthetase
ATF	Activating transcription factor
ATFS-1	Stress activated transcription factor 1 (C.elegans)
ATP	Adenosine triphosphate
BiP	Binding-immunoglobulin protein
BN	Blue native
bp	Base pairs
BSA	Bovine serum albumin
C	Cytosine
CI	Complex I
CII	Complex II
CIII	Complex III
CIV	Complex IV
CV	Complex V
C/EBP	CCAAT-enhancer-binding protein
CAA	Chloroacetamide
cAMP	Cyclic AMP
cDNA	Complementary DNA
CHOP	C/EBP-homologous protein
Ci	Curie
Ckmm	Muscle creatine kinase
CLPP	Caseinolytic mitochondrial matrix peptidase proteolytic subunit
clpp-1	Caseinolytic mitochondrial matrix peptidase proteolytic subunit (C.elegans)
COX	Cytochrome c oxidase
Cre	Bacteriophage P1 derived site-specific recombinase
Cyt	Cytochrome
DARS2	Mitochondrial aspartyl-tRNA synthetase
DBD	DNA binding domain
(d)dH_2O	(Double) distilled Water
DKO	Double knock-out

DMSO	Dimethyl sulfoxide
DNA	Deoxyribonucleic acid
DNase	Deoxyribonuclease
dNTP	Desoxy-ribonucleoside triphosphate
dsRNA	Double-stranded ribonucleic acid
DTT	Dithiothreitol
e.g.	*Exempli gratia*
ECL	Enhanced chemiluminescence
EDTA	Ethylenediaminetetraacetic acid
EGTA	Ethylene glycol tetraacetic acid
eIF2α	α subunit of the eukaryotic initiation factor 2
ER	Endoplasmatic reticulum
EtBr	Ethidiumbromide
ETC	Electron transport chain
EtOH	Ethanol
ETS	Electron transfer system
FAO	Fatty acid oxidation
FC	Fold change
FCCP	Carbonylcyanide p-(trifluoromethoxy)phenylhydrazone
Fe-S	Iron-sulfur
fl	Floxed, loxP flanked
FMN	Flavin mononucleotide
G	Gunanine
g	Gravitational acceleration ($9.81 m/s^2$)
GBP5	Guanylate-binding protein 5
GCN2	general control non-derepressible protein 2
h	Hour
H&E	Hematoxylin and eosin
H_2O_2	Hydrogen peroxide
HCl	Hydrogen chloride
HEPES	4-(2-hydroxyethyl)-1-piperazineethanesulfonic acid
HRI	Heme-regulated inhibitor
HRP	Horseradish peroxidase
HSP	Heavy strand promoter
IAA	Iodoacetamide
IMM	Inner mitochondrial membrane
IMS	Intermembrane space
IRE1a	Inositol-requiring protein 1
ISR	Integrated stress response
KCl	Potassium chloride
KCN	Potassium cyanide

kDa	Kilo Dalton
KO	Knock-out
LONP-1	Lon protease homolog, mitochondrial (C.elegans)
LONP1	Lon protease homolog, mitochondrial
LSP	Light strand promoter
M	Molar (g/mol)
MEFs	Mouse embryonic fibroblasts
MeOH	Methanol
mA	Milli-Ampere
mg	Milli-gram
$MgCl_2$	Magnesium chloride
min	Minute
ml	Milli-litre
mM	Milli-molar
mRNA	(Messenger) ribonucleic acid
mt	Mitochondrial
mtARS	Mitochondrial aminoacyl-tRNA synthetase
mtDNA	Mitochondrial DNA
mtEF	Mitochondrial elongation factor
MTHFD2	Mitochondrial methylenetetrahydofolate dehydrogenase
mtIF	Mitochondrial initiation factor
mtLSU	Mitochondrial large ribosomal subunit
mTOR	Mammalian target of rapamycin
mtRF	Mitochondrial release factor
mtRRF1	Mitochondrial ribosomal release factor 1
MTS	Mitochondrial targeting sequence
mtSSB	Mitochondrial single strand binding protein
mtSSU	Mitochondrial small ribosomal subunit
NaCl	Sodium chloride
NAD^+	Nicotinamide adenine dinucleotide (oxidised)
NADH	Nicotinamide adenine dinucleotide (reduced)
NADP+	Nicotinamide adenine dinucleotide phosphate (oxidised)
NADPH	Nicotinamide adenine dinucleotide phosphate (reduced)
NaF	Sodium fluoride
NaH_2PO_4	Monosodium phosphate
NaN_3	Sodium azide
NaOH	Sodium hydroxide
nDNA	Nuclear DNA
NES	Nuclear export sequence
ng	Nano-gram
NLRP3	NACHT, LRR and PYD domains-containing protein 3

NLS	Nuclear localisation signal
O_2	Molecular oxygen
OMM	Outer mitochondrial membrane
ORF	Open reading frame
OXPHOS	Oxidative phosphorylation
p	Postnatal day
PAGE	Polyacrylamide gel electrophoresis
PARP	protein poly-ADP-ribosyltransferase
PBS(T)	Phosphate buffered saline (with Tween)
PCR	Polymerase chain reaction
PERK	PKR-like ER kinase
PKR	Double-stranded RNA-dependent protein kinase
POLG	DNA polymerase gamma
POLRMT	DNA-directed RNA polymerase, mitochondrial
PYCR1	Pyrroline-5-carboxylate reductase
qPCR	Quantitative polymerase chain reaction
RC	Respiratory chain
RNase	Ribonuclease
ROS	Reactive oxygen species
rpm	Revolutions per minute
rRNA	Ribosomal ribonucleic acid
RT	Room temperature
RT-PCR	Reverse transcription polymerase chain reaction
SD	Standard deviation
SDH	Succinate dehydrogenase
SDS	Sodium dodecyl sulfate
sec	Second
SHMT2	Mitochondrial serine hydroxymethyltransferase
SU	Subunit
TAD	Transactivation domain
TBE	Tris borate EDTA
TBS(T)	Tris buffered saline (with Tween)
TCA	Tircarboxylic acid cycle, citrate cycle, Krebs cycle
TE	Tri-EDTA buffer
TEAB	Triethylammonium bicarbonate
TEFM	Transcription elongation factor of mitochondria
TEFM	Transcription elongation factor, mitochondrial
TEM	Transmission electron microscopy
TEMED	Tetramethylethylenediamine
TES	[Tris(hydroxymethyl)methyl]-2-aminoethanesulfonic acid
TF	Transcription factor

TFAM	transcription factor A, mitochondrial
TFB2M	Mitochondrial transcription factor B2
tg	Transgene
Tris	Trisaminomethane
tRNA	Transfer ribonucleic acid
Tween	Polyethylene glycol sorbitan monolaurate
U	Units
uORF	Upstream open reading frame
UPR	Unfolded protein response
V	Volt
v/v	Volume per volume
w/v	Weight per volume
WT	Wild type
ΔOTC	Truncated ornithine transcarbamylase
µg	Micro-gram
µL	Micro-litre
µM	Micro-molar

Abstract

Maintenance of mitochondrial homeostasis is essential for a broad spectrum of signalling, metabolic and energetic processes. Consequently, mitochondrial dysfunction is linked to the development of a wide range of myopathies and many common diseases, including type 2 diabetes, Parkinson's and Alzheimer's diseases.

In response to disturbed mitochondrial proteostasis, an organelle-specific stress response is initiated, which results in an adaptive transcriptional response partially sharing the signature of the integrated stress response (ISR).

However, the exact sequence of events of the signalling cascade resulting in the activation of a nuclear response remains elusive. CHOP was one of the first transcription factors (TFs) proposed to play a role in response to impaired mitochondrial proteostasis. Although - due to the lack of a functional DNA-binding domain - CHOP needs to form heterodimers with other TFs in order to activate or suppresses respective target genes.

The present study aims to investigate the molecular aspects and *in vivo* functions of CHOP in a murine model of mitochondrial dysfunction. Therefore, DARS2/CHOP double-deficient mice, from now referred to as double knock-out (DKO) mice, were generated. Disruption of mitochondrial translation by heart and skeletal muscle-specific knock-out of the mitochondrial aspartyl-tRNA synthetase *Dars2* (DARS2 KO) results in severe mitochondrial dysfunction and causes the death of the animals with approximately seven weeks of age. Additional deletion of *Chop* even further reduces the lifespan to less than three weeks, suggesting an existential role of the TF within the initiated stress-signalling pathway. Our data indicate that CHOP's impact arises from the regulation of another TF: ATF4. The analysis of transcriptomic data uncovered excessive transcriptional activation of ATF4 targets in DKO mice. Those massive changes were further confirmed on the protein level and coincide with the rapid deterioration of the animal's health status.

Co-immunoprecipitation experiments revealed the TF C/EBPβ as the most abundant CHOP interactor in hearts of DARS2 KO mice. Further experiments in cell culture showed that under normal conditions, mitochondrial dysfunction triggers CHOP and C/EBPβ protein expression. C/EBPβ has three isoforms: LAP*, LAP and LIP. In comparison to the isoforms LAP* and LAP, LIP exhibited a disproportionate increase under conditions of mitochondrial dysfunction. Our experiments confirmed opposite effects of LAP and LIP on *Atf4* transcription. Whereas LAP promoted *Atf4* transcription, LIP acted as a transcriptional repressor of *Atf4*. Notably, CHOP deficiency in the context of mitochondrial dysfunction resulted in an impaired response of LIP in particular, which failed to increase on the protein level as observed under wild type-like conditions. Hence

we propose, that the impairment of LIP accumulation upon mitochondrial dysfunction in a CHOP-deficient background results in loss of negative regulation of *Atf4* transcription in DKO animals. As a result, ATF4 is exceedingly active and causes an anabolic overstress of the mice. We propose to complement the current ISR model by a supplementary CHOP and LIP-driven regulatory layer, contributing to the transcriptional control of *Atf4* in the context of mitochondrial dysfunction.

Zusammenfassung

Zahlreiche zelluläre Kommunikations-, Stoffwechsel- und Energiebereitstellungs-Prozesse sind stark von der Aufrechterhaltung der mitochondriellen Homöostase abhängig. Folglich sind mitochondrielle Dysfunktionen eng mit einem weiten Spektrum an Erkrankungen, unter anderem vielen Myopathien aber auch allgemeineren Krankheiten (z.B. Typ 2 Diabetes, Parkinson und Alzheimer), verknüpft.

Die Störung der mitochondriellen Proteostase induziert eine Organellen-spezifische Stressantwort. Es folgt die Aktivierung einer adaptiven, transkriptionellen Antwort, welche über eine große Schnittmenge mit der sogenannten *Integrierten Stressantwort* (ISA) verfügt.

Allerdings ist der genaue Ablauf der Signalkaskade, die in die Aktivierung der nuklearen Antwort mündet, nur ansatzweise bekannt. Einer der ersten Transkriptionsfaktoren (TF), welcher mit der nuklearen Antwort infolge von einer gestörten mitochondriellen Proteostase in Verbindung gebracht wurde, ist CHOP. Aufgrund einer defizitären DNA-Bindungsdomäne von CHOP ist zu beachten, dass dieser TF für die Repression bzw. Aktivierung von Ziel-Genen auf die Bildung von Heterodimeren angewiesen ist.

Ziel der vorliegenden Studie ist die Untersuchung der molekularen Aspekte sowie *in vivo* Funktionen von CHOP in einem Mausmodell mit bestehender mitochondrieller Dysfunktion. Für diesen Zweck wurde eine DARS2/CHOP doppel-defizitäre Mauslinie generiert, welche nachfolgend als Doppel-Knockout (DKO)-Mauslinie bezeichnet wird. Die Herz- und Skelettmuskel-spezifische Deletion der mitochondriellen aspartyl-tRNA-Synthetase *Dars2* (DARS2 KO) resultiert in einer schweren mitochondriellen Dysfunktion und führt im Alter von etwa sieben Wochen zum Tod der Mäuse. Eine zusätzliche Deletion von *Chop* führt zu einer weiteren Verkürzung der Lebenserwartung auf weniger als drei Wochen, was auf eine essenzielle Funktion von CHOP im Rahmen der induzierten Stressantwort hindeutet. Unseren Daten zufolge hat die Wirkung von CHOP ihren Ursprung in der Regulation eines weiteren TFs: ATF4. Die Auswertung der Transkriptom-Daten offenbarte eine exzessive, transkriptionelle Aktivierung von ATF4 Ziel-Genen in DKO-Mäusen. Diese massiven Veränderungen wurden ebenfalls auf Proteinebene bestätigt und gingen einher mit einer rapiden Verschlechterung des Allgemeinzustands der Tiere.

Der TF C/EBPβ wurde mittels Co-Immunpräzipitation als der am häufigsten auftretende Interaktionspartner von CHOP in Herzen von DARS2 KO-Mäusen identifiziert. Weiterführende Versuche auf Zellkulturebene zeigten, dass unter normalen Umständen

mitochondrielle Dysfunktion die Expression der Proteine CHOP und C/EBPβ induziert. C/EBPβ tritt in drei Isoformen auf: LAP*, LAP und LIP. Bei vorliegender mitochondrieller Dysfunktion wies LIP, im Gegensatz zu den beiden anderen Isoformen LAP* und LAP, einen überproportional starken Anstieg auf Proteinebene auf. Unsere Versuche bestätigten gegensätzliche Effekte von LAP und LIP auf die *Atf4*-Transkription. Während LAP sich positiv auf die *Atf4*-Transkription auswirkte, agierte LIP als trankriptioneller *Atf4*-Repressor. Bemerkenswerterweise resultierte die CHOP-Defizienz im Kontext mitochondrieller Dysfunktion in einer beeinträchtigten Antwort von LIP. Der auf Proteinebene beobachteter Anstieg des TFs LIP im Wildtyp versagte bei CHOP-Defizienz. Daraus leiten wir den Verlust der negativen Regulation der *Atf4*-Transkription aufgrund eines fehlenden Anstiegs von LIP auf Proteinebene bei Abwesenheit von CHOP als Ursache für den beobachteten Phänotyp in DKO-Tieren ab. Die resultierende übermäßige Aktivierung von ATF4 führt zu einer anabolischen Überlastung der Mäuse. Aufbauend darauf schlagen wir eine Erweiterung des gegenwärtigen Modells der ISA um eine zusätzliche CHOP- und LIP-gesteuerte regulatorische Ebene vor, welche zur transkriptionellen Kontrolle von *Atf*4 im Kontext mitochondrieller Dysfunktion beiträgt.

1 Introduction

The major difference between eukaryotic and prokaryotic cells is a distinct nuclear compartment separated by a double membrane from the cytoplasm. The high degree of compartmentalisation provided by the endomembrane system in eukaryotic cells eases a spatial separation and thereby allows the simultaneous operation of cellular processes requiring different micro-environments. Mitochondria represent one of the oldest endomembrane systems in eukaryotes. They are the product of a long chain of evolutionary steps that started approximately 1.5 billion years ago when the atmosphere's oxygen levels dramatically increased. The seminal event of this evolutionary process was the engulfment of an aerobic α-proteobacterium by an ancestral eukaryotic cell, followed by a plethora of incidents comprising major events such as endosymbiotic gene transfer and the acquisition of additional metabolic functions beyond aerobic synthesis of ATP by mitochondria (Friedman and Nunnari, 2014; John and Whatley, 1975; Kurland and Andersson, 2000; Margulis, 1970; Timmis et al., 2004). According to the hypothesis proposed by Nick Lane and William Martin the complexity of eukaryotic life has its origin in the acquisition of mitochondria, enabling organisms to overcome the bioenergetic limitation of the prokaryotic genome size (Lane and Martin, 2010).

1.1 Mitochondrial structure and function

The outer appearance of mitochondria is subject to a certain variability reaching from a tubular network to spherical bodies, as reflected by the greek words for thread (“mitos”) and granule (“chondros”) from which the organelle’s name was derived. Whether the complex mitochondrial reticulum tends towards the one or the other is determined by the dynamic balance of fusion and fission events (Ernster and Schatz, 1981; Friedman and Nunnari, 2014; Westermann, 2010). Two membranes, the outer and inner mitochondrial membrane (OMM and IMM, respectively), separate the mitochondrial compartments, the intermembrane space (IMS) and the matrix, from the cytoplasm. Both membranes clearly distinguish from each other regarding features such as surface area/topology, lipid composition, membrane-embedded protein complexes or ion permeability. Whereas the OMM surrounds the organelle, the IMM is structured into the inner boundary and the cristae membrane. Cristae are infoldings of the IMM that are stabilized by the MICOS complex at cristae junctions, the interface of cristae and inner boundary membrane as well as a contact site between IMM and OMM (Ernster and Schatz, 1981; Rampelt et al., 2017).

The mitochondrial matrix harbours multiple copies of the circular, polycistronic mitochondrial genome (mtDNA) as well as the whole mitochondrial genetic system ensuring maintenance, replication and transcription of mtDNA as well as the subsequent translation of mtDNA-encoded proteins (Jacobs and Holt, 1998). The outreach of the endosymbiotic gene transfer mentioned earlier becomes apparent from the ratio of nuclear DNA (nDNA) to mtDNA-encoded proteins: In mammalian cells, only 13 out of approximately 1500 mitochondrial proteins are encoded by the mtDNA, along with 22 tRNAs and two rRNAs. MtDNA-encoded proteins are unanimously part of the IMM-embedded oxidative phosphorylation system (OXPHOS), converting NADH and $FADH_2$ generated in the matrix to a proton gradient across the IMM and subsequently to ATP (Anderson et al., 1981; Lodish et al., 2008; Lopez et al., 2000).

Mitochondria house many metabolic pathways. Most central for energy metabolism is the TCA cycle, oxidising acetyl-CoA moieties to CO_2, thereby feeding NADH and $FADH_2$ to complex (C) I and CII, respectively. Acetyl-CoA is provided either by (i) carbohydrate breakdown through cytoplasmic glycolysis, (ii) β-oxidation of fatty acids in the matrix or (iii) mitochondrial ketone body oxidation and branched-chain amino acid (BCAA) catabolism (Akram, 2014; Spinelli and Haigis, 2018). Apart from its catabolic role, the TCA cycle fulfils also many anabolic functions as it provides numerous precursors for e.g. fatty acid, amino acid or heme synthesis (Owen et al., 2002). Consequently, mitochondria are biosynthetic hubs and, in addition to the before-mentioned synthetic

pathways, are also involved in essential processes such as iron-sulphur cluster and nucleotide synthesis. Aside from bioenergetics and biosynthesis, mitochondria make an important contribution to detoxification, as they ensure the conversion of toxic ammonia generated by amino acid catabolism into urea for excretion by means of the urea cycle (Spinelli and Haigis, 2018). Furthermore, mitochondria are known as signalling organelles, communicating for instance via reactive oxygen species (ROS), Ca^{2+} or acetyl-CoA, and are involved in cell fate-determining processes such as apoptosis (Chandel, 2015; Wang and Youle, 2009).

1.1.1 Replication, transcription and translation of the mammalian mitochondrial genome

MtDNA is a polycistronic organised, circular genome of 16.6 kb in mammals, present in 100 to 10.000 copies per cell (Figure 1.1). It consists of a guanine-rich heavy (H) strand, encoding the vast majority of transcripts, and a complement cytosine-rich light (L) strand. With 93% of coding sequences in total and entirely devoid of introns, mtDNA exhibit an extremely high gene density in comparison to nDNA. However, there is also a large non-coding region (NCR) with an approximate length of 1kb. The NCR contains several regulatory elements, such as the L-strand promoter (LSP), H-strand promoter (HSP) or the origin of replication of the H-strand (O_H) as well as the displacement loop (D-loop) region. The origin of replication of the L-strand (O_L) is located approximately 11 kb downstream of the O_H (Anderson et al., 1981; Andrews et al., 1999).

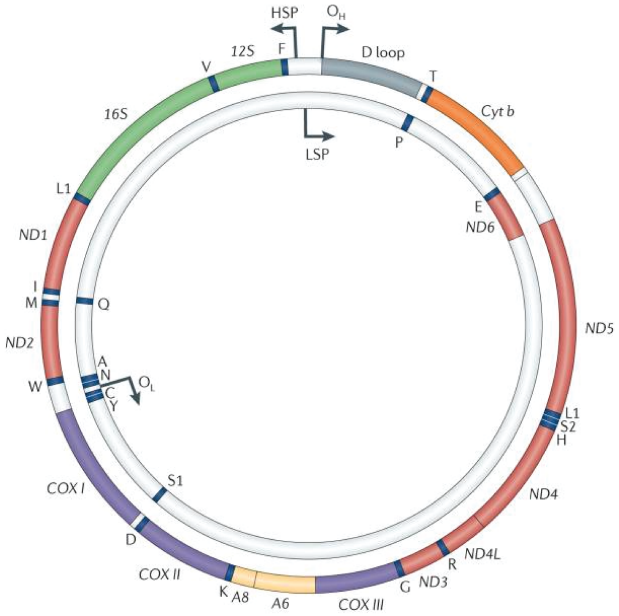

Figure 1.1: Organisation of the human mtDNA.

The vast majority of transcripts (twelve mRNAs, two rRNAs [marked in green] and 14 tRNAs [marked in blue]) is encoded on the H-strand of mtDNA. Consequently, the L-strand encodes one mRNA and eight tRNAs. Among the 13 proteins of the respiratory chain (RC) encoded by the mitochondrial genome are seven subunits (SUs) of CI [marked in red], one SU of CIII [marked in orange], three SUs of CIV [marked in violet] and two SUs of CV [marked in yellow]. CII is the only complex of the RC fully encoded by the nuclear genome. Non-coding regions are shown in white. The large NCR of about 1 kb comprises the HSP, LSP, O_H and the D loop. Reprinted from (Schon et al., 2012).

1.1.1.1 Replication

The mitochondrial genome is organised in nucleoids of ~100nm in diameter, with mtDNA and TFAM (transcription factor A, mitochondrial) as major components of these nucleoprotein complexes (Bogenhagen, 2012; Kukat et al., 2011). MtDNA in nucleoids can be stored, but also actively replicated. It has been shown, that mitochondrial division occurs at ER-mito contact points and that actively replicating nucleoids localize to those regions of future division, allowing coordination of mtDNA synthesis and mitochondrial division (Lewis et al., 2016).

Although other models were suggested in-between, the currently most widely accepted model of mtDNA replication is the strand displacement model (SDM) already proposed in the early 1970ies. The SDM is characterized by continuous synthesis of both, O_H and O_L (Robberson et al., 1972). POLRMT (DNA-directed RNA polymerase, mitochondrial) is required for the synthesis of short RNA sequences at O_H and O_L, in order to prime the respective strands for subsequently POLγ (DNA polymerase gamma)-mediated synthesis of mtDNA (Wanrooij et al., 2008). The Twinkle DNA helicase performs unwinding of the double-stranded mtDNA. DNA synthesis of the H-strand starts at O_H and progresses continuously until O_L is reached. Until then the L-strand is not synthesized, therefore the parental H-strand is bound by mtSSB (mitochondrial single-strand binding protein) to prevent random initiation of transcription by POLRMT (Miralles Fuste et al., 2014). Hence, the SDM represents an asynchronous mode of replication. As soon as O_L is passed, the synthesis of the L-strand is initiated, too. Ribonuclease H1 most probably carries out primer removal. After termination of replication DNA ligase III ensures ligation of the newly synthesized strands and separation of both resulting daughter molecules mechanically linked via a hemi-catenane structure after termination of replication requires the enzymatic activity of topoisomerase 3α (Falkenberg, 2018).

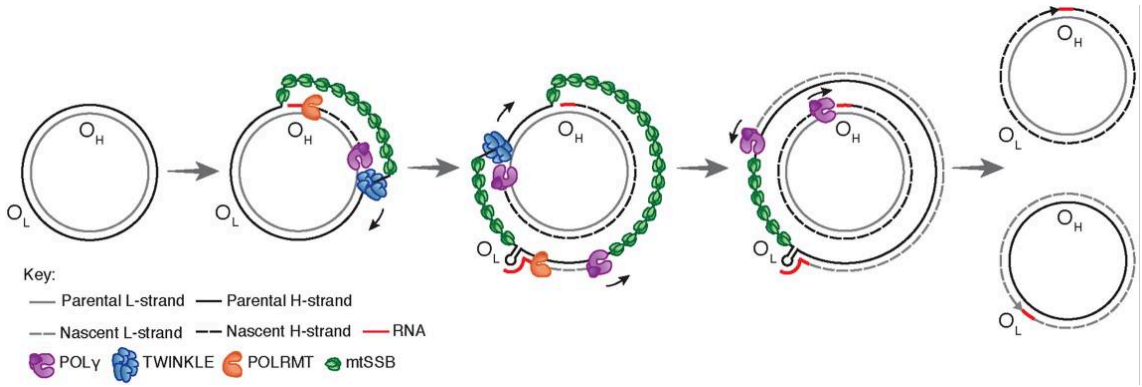

Figure 1.2: Replication of human mtDNA according to the strand displacement model (SDM).

The minimal human mitochondrial replisome is constituted of POLγ, Twinkle DNA helicase and mtSSB (Korhonen et al., 2004). POLRMT is required for primer synthesis. Reprinted from (Falkenberg, 2018).

1.1.1.2 Transcription

Besides its role in mtDNA packaging the DNA-binding protein TFAM was also shown to be a core component of the mitochondrial transcription machinery, allowing the recruitment of POLRMT during transcription initiation by inducing a sharp bend of the DNA upstream of the transcription start site at LSP and HSP (Morozov et al., 2014; Shi et al., 2012). Subsequent binding of TFB2M (mitochondrial transcription factor B2) induces promoter melting and facilitates the formation of the open initiation complex (Posse and Gustafsson, 2017). The elongation process is launched by release of TFAM and TFB2M followed by recruitment of TEFM (transcription elongation factor, mitochondrial), that enhances the processivity of POLRMT, leading to synthesis of one single polycistronic precursor mRNA molecule for each strand. The synthesis of the replication priming short RNA sequences is most probably induced by absence of TEFM resulting in premature termination after initiation of transcription (Agaronyan et al., 2015; Minczuk et al., 2011).

1.1.1.3 Translation

Even though the mitochondrial translation machinery still carries traits recalling its bacterial ancestry as illustrated by the susceptibility of mitochondrial translation to antibiotics such as aminoglycosides or tetracyclines, it harbours several mitochondria-specific characteristics neither present in conventional prokaryotic or cytoplasmic eukaryotic translation (Hutchin et al., 1993; van den Bogert and Kroon, 1981). This includes the high protein content of the 55S mitoribosome (formed by two

mtDNA-encoded rRNAs and approximately 80 nDNA-encoded proteins), a codon usage deviant form the universal code (e.g. the stop codon UGA encodes for Trp in mitochondria) or the usage of one single $tRNA^{Met}$ for both, initiation and elongation, for example (Amunts et al., 2015; Chrzanowska-Lightowlers et al., 2011; Mikelsaar, 1983).

Translation initiation (Figure 1.3) begins with the recruitment of the mRNA to the small subunit of the mitochondrial ribosome (mtSSU). During this phase mtSSU-bound mtIF (mitochondrial initiation factor) 3 prevents the premature association of the mtSSU with the large subunit of the mitochondrial ribosome (mtLSU) (Gaur et al., 2008; Haque and Spremulli, 2008; Mai et al., 2017). Subsequently, f-Met-$tRNA^{Met}$ is recruited by mtIF2:GTP to the start codon. Upon stable codon:anticondon interaction the formation of the monosome by interaction of the mtSSU with the mtLSU occurs, inducing hydrolysis of GTP and mtIF2/3 release in parallel. Elongation (Figure 1.3) requires the formation of a ternary complex comprising mtEF-Tu (mitochondrial elongation factor Tu), GTP and an aminoacylated tRNA (Mai et al., 2017; Tucker et al., 2011). As soon as a stable codon:anticondon interaction at the A-site of the ribosome forms, GTP hydrolysis allows peptide bond formation and release of mtEF-Tu. As a result, the ribosomal A-site contains a dipeptidyl tRNA and the P-site is occupied by an uncharged tRNA. A conformational change induced by mtEF-G results in release of the uncharged tRNA as well as the translocation of the dipeptidyl tRNA to the P-site (Cai et al., 2000). When the termination codon reaches the A-site, the protein mtRF1a induces the GTP-catalyzed release of the polypeptide chain from the mitoribosome in humans. The recycling of the mitoribosome for a new cycle of translation depends on mtRRF1(mitochondrial ribosomal recycling factor 1) and mtEF-G2 triggering the dissociation of mtSSU and mtLSU (Figure 1.3) (Rorbach et al., 2008; Soleimanpour-Lichaei et al., 2007; Tsuboi et al., 2009).

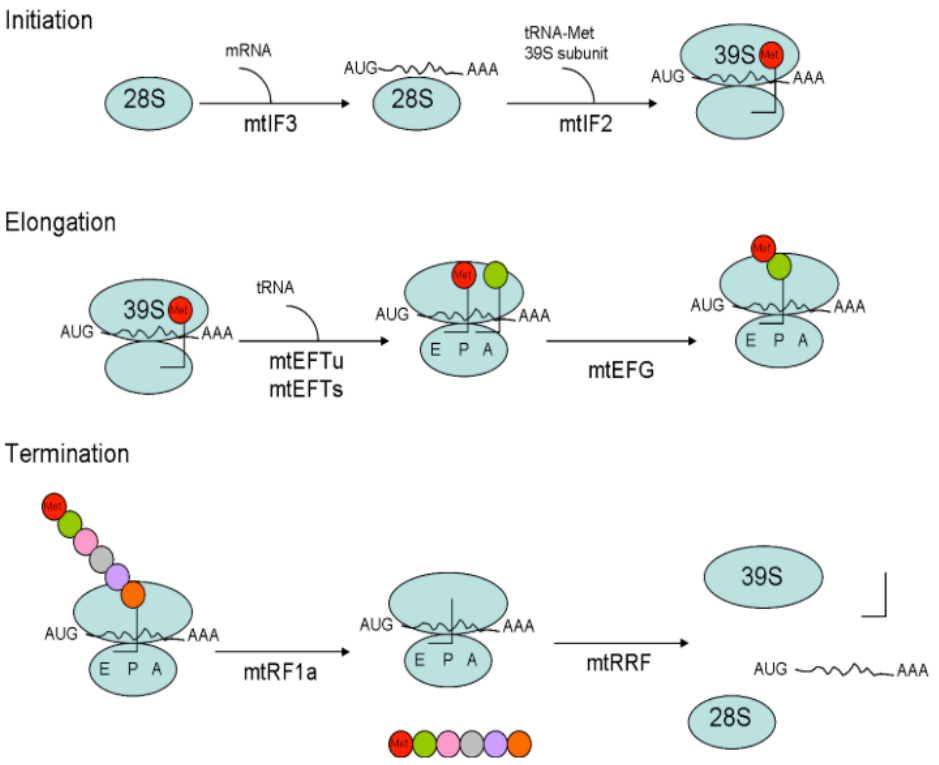

Figure 1.3: Mitochondrial translation in humans.

Main components of the translation complex in the three respective translational stages: initiation, elongation and termination. E, P and A mark the mito-ribosomal E (exit), P (peptidyl) and A (aminoacyl)-sites. Reprinted from (Jhas, 2012).

1.1.2 OXPHOS

The OXPHOS system is composed of the complexes I-IV and the two electron carriers coenzyme Q and cytochrome c, forming the electron transport chain (ETC) and building up a proton gradient in the IMS, as well as CV, utilising the proton motive force generated by the ETC to synthesise ATP (Figure 1.4). Except for the water-soluble cytochrome c located in the IMS, all components of the OXPHOS system are embedded in the IMM (Papa et al., 2012). CV (also known as F_1F_0 ATP synthase) is organised in dimer rows and thereby induces the membrane curvature at the cristae ridges required for cristae formation. The ETC complexes are located in the cristae on both sides of the CV dimer rows (Arnold et al., 1998; Davies et al., 2012; Gilkerson et al., 2003).

Briefly, the OXPHOS system has two entry points for electrons in the ETC: (i) CI, the NADH dehydrogenase, and (ii) CII, the succinate dehydrogenase. As indicated by the respective names, CI is fuelled by NADH whereas CII oxidises succinate to fumarate, using $FADH_2$ as co-factor for the electron transfer. CI subsequently transfers two

electrons from NADH to coenzyme Q. The electron transfer is coupled to the translocation of four protons (H^+) from the matrix to the IMS via four individual channels in CI. The oxidation of succinate by CII yields two more electrons. However, the transfer of those electrons from $FADH_2$ to coenzyme Q is not releasing comparable amounts of energy as it is the case for NADH. Therefore no protons are translocated by CII (Baradaran et al., 2013; Rutter et al., 2010). Following the electron transfer from CI or II, coenzyme Q is oxidised by CIII through a series of subsequent reactions called the 'Q'-cycle, culminating in reduction of cytochrome c (Al-Attar and de Vries, 2013; Mitchell, 1976). Finally, CIV (also known as the cytochrome c oxidase) oxidises four cytochrome c molecules utilising one oxygen molecule as the final electron acceptor. Per electron transferred by CIII and IV, both complexes pump one proton each into the IMS (Fontanesi et al., 2006; Kuhlbrandt, 2015). The electrochemical gradient resulting from the coupling of electron transfer and proton translocation by the ETC complexes is used for the rotatory catalysis of ATP by CV (Jonckheere et al., 2012).

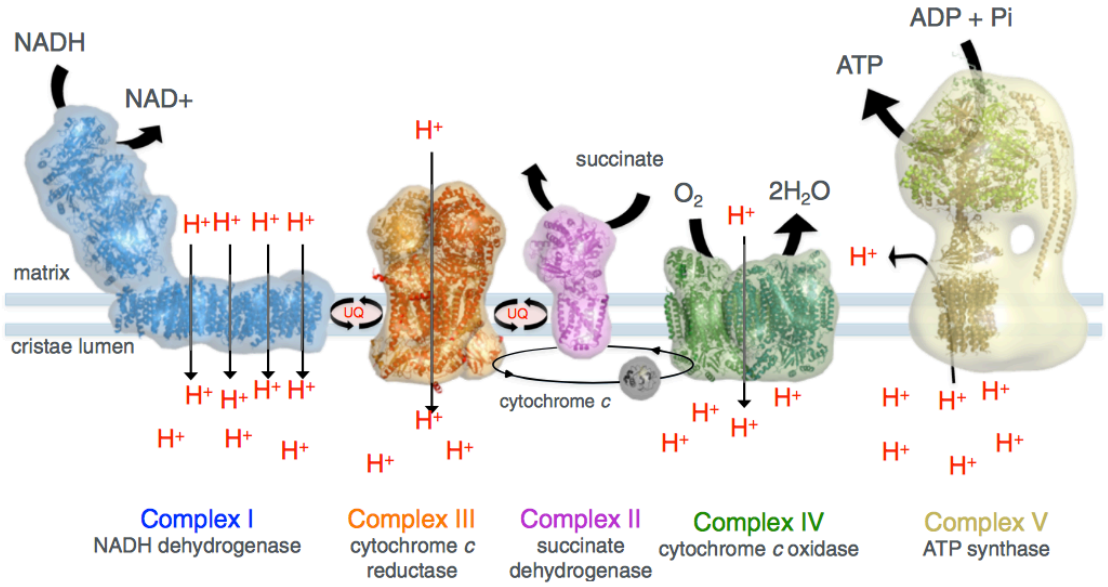

Figure 1.4: The mitochondrial OXPHOS system.
Fuelled by the TCA cycle products NADH and $FADH_2$, electron transport complexes I to IV generate an electrochemical gradient driving ATP synthesis by CV. UQ: ubiquinone (coenzyme Q). Reprinted from (Kuhlbrandt, 2015).

The assembly of multi-enzyme complexes I-V is an intricate process requiring the synergistic cooperation of the nuclear and mitochondrial genome. As discussed earlier, all 13 mtDNA-encoded proteins are subunits (SUs) of the respiratory chain (RC) complexes I, III, IV and V and synthesised in the mitochondrial matrix. CI-V, however, consist of approximately 80 additional SUs encoded by the nDNA. Those proteins are synthesised in the cytosol and subsequently imported in mitochondria, where the

assembly of the RC, promoted by numerous assembly proteins, occurs (Falkenberg et al., 2007; Ghezzi and Zeviani, 2012).

Various supra-molecular assemblies of the ETC complexes, so-called supercomplexes, have been observed. The largest one is the respirasome, constituted of one CIII dimer (III_2) along with CI and up to four copies of CIV. The close proximity of the complexes might promote an economic electron transfer. Furthermore, the dynamic supra-molecular organisation of the ETC components could support an adapted oxidation depending on the substrates used to fuel the TCA cycle, since the ratio of generated NADH to $FADH_2$ varies as a function of the TCA cycle-feeding upstream pathway (e.g. β-oxidation of fatty acids vs. glycolysis) (Lapuente-Brun et al., 2013; Schagger and Pfeiffer, 2000).

1.1.3 Mitochondrial genetics in the context of diseases

Mitochondrial disorders belong to the most common genetic disorders caused by mutations of mitochondrial genes. However, for several reasons, the diagnosis is highly challenging. First, the clinical symptoms emerge as extremely heterogeneous with regard to the affected tissues (isolated organs vs. multisystem disorders), the precise tissue-specific symptoms or the age of manifestation (neonatal phase, childhood or adulthood). Second, the phenotype-genotype correlation is very weak. Third, there is no limitation regarding the inheritance pattern: possible inheritance mechanisms comprise non-mendelian (maternal inheritance via mtDNA) and mendelian (X-linked, autosomal recessive or autosomal dominant) inheritance. Furthermore, de novo occurrence of mutations also need to be considered (Craven et al., 2017; Gorman et al., 2016; Schon et al., 2012; Vafai and Mootha, 2012).

Mutations in mitochondrial genes are either localised in the nuclear or the mitochondrial genome. The former group of mutations typically affect the stability of mtDNA, comprise mutations in structural SUs or assembly factors of the respiratory chain, impact on mitochondrial translation or has other implications for instance on the mitochondrial network dynamics (Chinnery, 1993). The latter can be divided into two classes of mtDNA mutation variants: First, mtDNA rearrangements (e.g. deletions or inversions) most often resulting from replication errors or inefficient mtDNA repair machinery. Second, mtDNA point mutations representing either (i) neutral, non-pathogenic variations of the ancestral “mitochondrial Eve’s” mtDNA that gave rise to distinct mitochondrial haplogroups common in the population, or (ii) rare, pathogenic mtDNA mutations primarily in protein-coding or tRNA genes (Chinnery, 1993; Schon et al., 2012).

Regarding pathologic mtDNA mutations, a further degree of complexity is added by the possible co-existence of two or more mtDNA genotypes within a mitochondrion, cell, tissue or organism, termed heteroplasmy (Figure 1.5a). In conclusion, the proportion of mutated mtDNA copies can vary from 0% to 100%, whereby both extremes correspond to a homoplasmic and all possible interjacent ratios to a heteroplasmic status (Craven et al., 2017; Larsson, 2010; Schon et al., 2012; Stefano et al., 2017). The phenotypic threshold effect describes the positive correlation between the percentage of mutated mtDNA and the severity of clinical symptoms observed up to a certain extent. Most often, low levels of mutations do not entail clinical symptoms. However, upon passing a certain threshold (usually 60-80% of heteroplasmy), the disease manifests as a mild disorder at an intermediate mutation level or as a severe disease at high mutation level (Figure 1.5a) (Larsson, 2010; Rossignol et al., 2003).

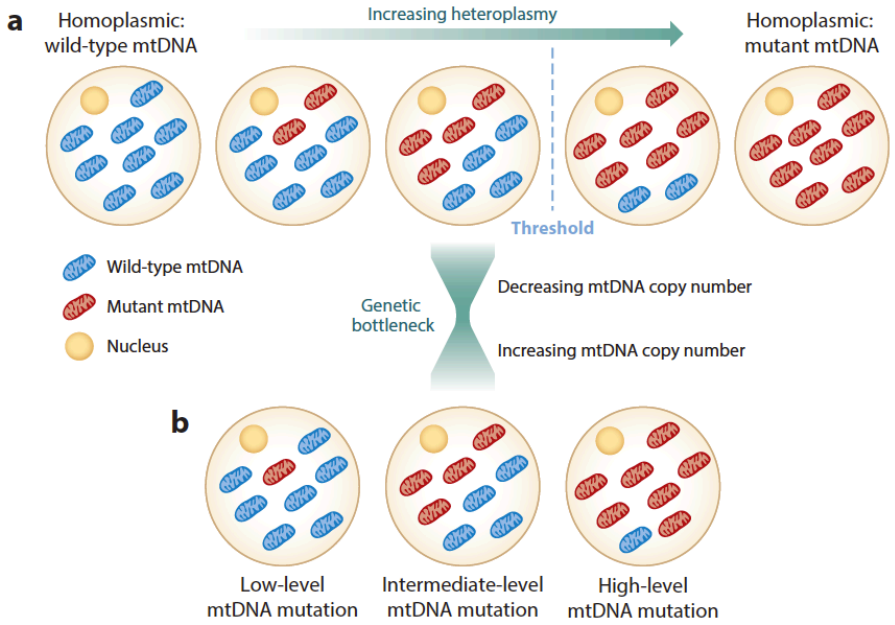

Figure 1.5: Heteroplasmy, the threshold effect and the genetic bottleneck.
(a) Disease-causing mtDNA mutations are predominantly heteroplasmic. Exceeding a certain tissue and mutation-specific threshold results in manifestation of the disease phenotype. (b) During oogenesis, only a fraction of mitochondria originating from the primary oocyte is transmitted to the mature oocyte possibly resulting, together with the subsequent mitochondrial biogenesis in the mature oocyte, in marked differences of heteroplasmy levels when comparing primary and mature oocyte. Reprinted from (Craven et al., 2017).

Furthermore, random segregation of mitochondria upon cell division, as well as mitotic or post-mitotic nature of different tissues, can result in a variation of heteroplasmy levels over time. Random segregation results inter alia in a phenomenon called the “genetic bottleneck”, where the transmission of only a fraction of the mitochondria from the primary to the mature oocyte and the subsequent amplification of those respective

mitochondria can lead to significantly different heteroplasmy levels in the mature vs. the primary oocyte (Figure 1.5b) (Gorman et al., 2016; Stewart and Larsson, 2014).

1.1.3.1 Aminoacyl-tRNA synthetase-related diseases

The cluster of mitochondrial aminoacyl-tRNA synthetase-related diseases exemplarily reflects clinical heterogeneity of mitochondrial diseases. Phenotypes resulting from mutations in aminoacyl-tRNA synthetases range, among other things, from ovarian dysfunction over hearing loss to cardiomyopathies (Nunnari 2012).

The canonical function of aminoacyl-tRNA synthetases (in the abbreviated form: ARSes or aaRSes) and a major prerequisite for protein synthesis is the charging of tRNAs with cognate amino acid residues. In the cytoplasm, one ARS per amino acid residue ensures tRNA aminoacylation for translation. Those 20 ARSes comprise two bi-functional synthetases, KARS (alternative terminology: LysRS) and GARS (GlyRS), showing dual localisation in both, cytoplasm and mitochondria. In addition to KARS and GARS, 17 mito-specific aminoacyl-tRNA synthetases (in the abbreviated form: ARS2es or mt-aaRSes) enable mitochondrial translation (Antonellis and green 2008). One worthy detail to note is that mitochondria appeared to lack the equivalent to cytoplasmic QARS (GlnRS), charging the $tRNA^{Gln}$. Instead, EARS2 (mt-GluRS) mischarges mt-$tRNA^{Gln}$ with glutamic acid that is subsequently converted to glutamine by tRNA-dependent aminotransferases (Nagao 2009).

Intriguingly, despite the essential canonical role in protein synthesis and the ubiquitous expression across all tissues, disease-causing mutations of distinct ARS-encoding genes exhibit a striking tissue-specificity (Figure 1.6).

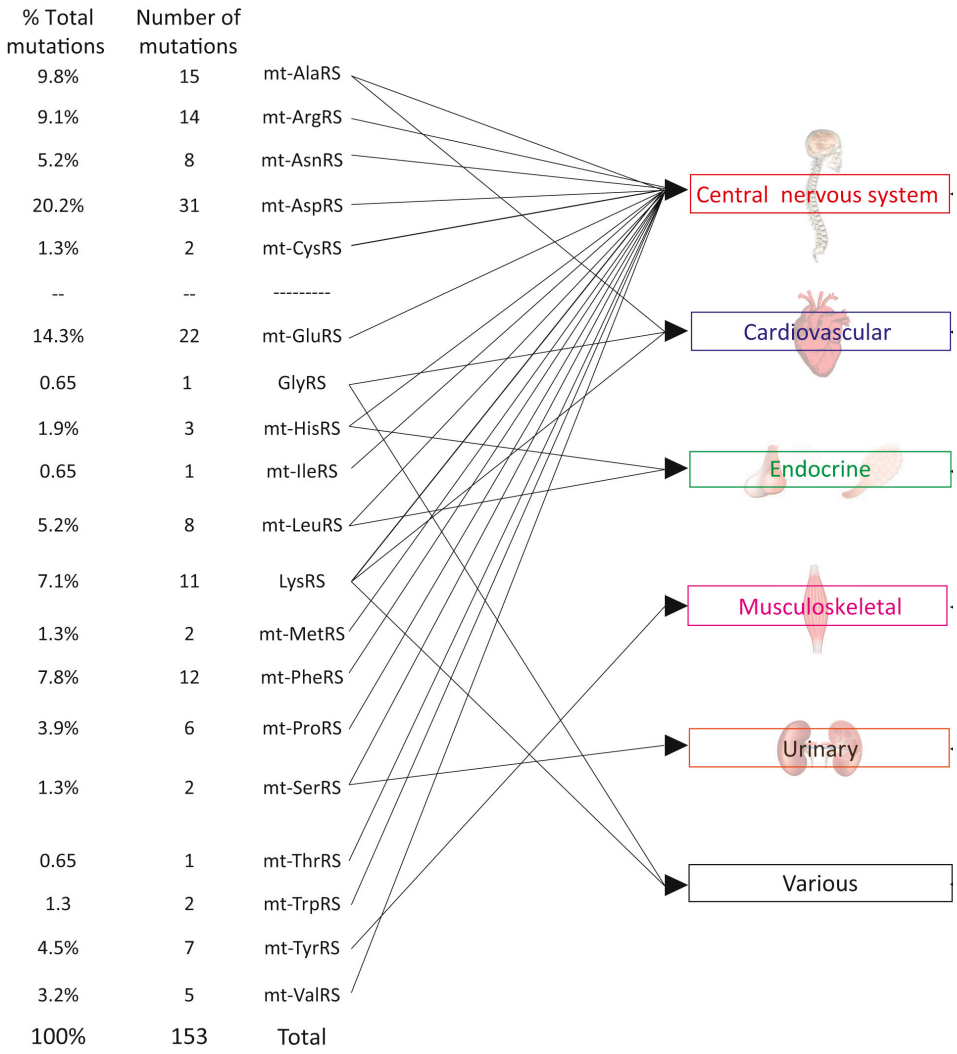

Figure 1.6: Reported mutations of mitochondrial aminoacyl-tRNA synthetase-encoding genes in humans and the corresponding organ system affected by the respective mutations.

The dashed line functions as a placeholder for the lacking mitochondrial counterpart of the cytosolic QARS (GlnRS). Modified from (Sissler et al., 2017).

ARS-mediated genetic diseases may be categorised in (i) dominant mutations, characterised by late-onset and a predominant impairment at the level of the central nervous system, and (ii) recessive, primarily loss-of-function mutations, characterised by early-onset and severe pathology affecting a wide range of tissues (Meyer-Schuman 2017). With regard to the protein architecture of ARSes, mutations either affect (i) one of the substrate-binding sites (ATP, amino acid or tRNA terminal -CCA binding site) usually resulting in impaired or disrupted catalysis, (ii) the binding interface (concerns amino acid residues essential for specific binding of the ARS to the cognate tRNA or oligomer formation essential for the activity of certain ARSes) usually resulting in mischarging of tRNAs or misfolding of ARSes leading to inactive particles/ aggregates, or (iii) regions distant from known key functional regions (Sissler 2017). The first publication

characterising mutations in mitochondrial aminoacyl-tRNA synthetases described the autosomal recessive disease LBSL (leukoencephalopathy with brain stem and spinal cord involvement and lactate elevation) caused by DARS2-deficiency (Scheper 2007).

1.2 Mitochondrial stress signalling

As one of the first mitochondrial stress signalling pathways the concept of the retrograde response was born around 30 years ago. Pioneering work of the Butow laboratory on *S. cerevisiae* provided first evidence for the influence of nuclear gene expression by the functional state of mitochondria (Liao and Butow, 1993; Parikh et al., 1989; Parikh et al., 1987). The retrograde response is a mitochondria-to-nucleus signalling pathway initiated in response to mitochondrial dysfunction by metabolic cues or straighter routes. It results in mostly adaptive rewiring of cellular metabolism or stress-related pathways, thereby representing a cellular adjustment orchestrated by the nucleus to the altered mitochondrial state in order to restore mitochondrial homeostasis (Butow and Avadhani, 2004; Giannattasio et al., 2005).

Following up on these fundamental findings, different types of retrograde communication pathways were also described in the mammalian system. One of the most straightforward examples is the signalling cascade initiated by energy deprivation. Briefly, the increase of AMP/ATP ratio activates AMPK, which in turn increases ATP production via several direct and indirect routes. Core events of AMPK signalling result in induction of mitochondrial biogenesis, and inhibition of mTOR signalling leading to reduced cell growth, lipid and protein synthesis (Bolster et al., 2002; Jäger et al., 2007). Other examples of retrograde signalling in mammals are the mitochondrial unfolded protein response (UPR^{mt}) and in a wider definition, also the integrated stress response (ISR).

1.2.1 Mitochondrial unfolded protein response (UPR^{mt})

Roughly two decades ago first experiments described transcriptional activation of the mitochondrial chaperones HSP10 and HSP60 by retrograde mitochondria-to-nucleus communication upon induction of protein folding stress in mammalian cells via loss of mtDNA (Martinus et al., 1996; Yoneda et al., 2004) or accumulation of protein aggregates in the mitochondrial compartment (Papa and Germain, 2014; Zhao et al., 2002). In analogy to the conceptually similar UPR^{ER} activated by endoplasmatic reticulum (ER)-

specific perturbation of proteostasis, the stress response was named the UPR^{mt} (Yoneda 2004, Horibe 2007).

Remarkable progress in decipherment of the UPR^{mt} was made in *C.elegans*. Precise shaping of this pathway in the mammalian system, however, still challenges numerous research groups. To name but one example, the mere definition of the pathway used in the field is still very heterogenous. This is illustrated by two recent reviews on the UPR^{mt} either limiting the definition to primary involvement of mitochondrial protein misfolding as causative agent (Münch, 2018) or extending it to a transcriptional response activated by multiple forms of mitochondrial dysfunction (Shpilka and Haynes, 2017).

The effects of the UPR^{mt} are not only limited to recovery of mitochondrial proteostasis by transcriptional activation of mitochondrial chaperones and proteases. In addition, it is commonly accepted that the UPR^{mt} also exerts an important role in inducing profound metabolic adaptations representing a cellular adjustment to the altered mitochondrial state (Jovaisaite and Auwerx, 2015; Lin and Haynes, 2016; Topf et al., 2019).

1.2.1.1 The UPR^{mt} in *C.elegans*

Over the years numerous methods triggering the UPR^{mt} in *C. elegans* were established, reaching from OXPHOS impairment (e.g. knockdown or mutation of RC subunits) to disruption of the protein quality control system consisting of mitochondrial chaperones and proteases (e.g. knockdown of chaperones *hsp-6* or *hsp-60*), among others (Baker et al., 2012; Durieux et al., 2011; Lin et al., 2016; Yoneda et al., 2004). All mentioned conditions finally culminate in the accumulation of unfolded proteins in the mitochondrial matrix that are subsequently degraded in short peptides by one of the two matrix proteases: ClpP-1 (ATP-dependent Clp protease proteolytic subunit 1, mitochondrial). Thereafter, the IMM ABC transporter HAF-1 is required for the active export of the generated peptides, presumably inhibiting the mitochondrial import of the TF ATFS-1 (stress-activated transcription factor 1). ATFS-1 is characterised by a dual localisation signal, as it harbours a nuclear localisation sequence (NLS) as well as a mitochondrial targeting sequence (MTS). Under normal conditions, the MTS of the TF predominates the signal of the NLS. This results in preferential import of the protein into mitochondria, followed by ATFS-1 degradation mediated by the second matrix protease LONP-1 (Lon protease homolog, mitochondrial) (Harbauer et al., 2014; Haynes et al., 2007; Haynes et al., 2010; Nargund et al., 2012). As mentioned before, this process is prevented by the activation of the UPR^{mt} and thus allows the NLS of ATFS-1 to take effect. ATFS-1-mediated transcriptional activation was previously related to OXPHOS recovery, restoration of mitochondrial proteostasis, ROS detoxification and mitochondrial protein

import (Figure 1.7) (Arnould et al., 2015; Shpilka and Haynes, 2017). Besides ATFS-1 another TF complex composed of DVE-1 (Homeobox domain-containing protein) and UBL-5 (Ubiquitin-like protein 5) was shown to be involved in the transcriptional regulation of the UPR^{mt} in *C.elegans* (Haynes et al., 2007).

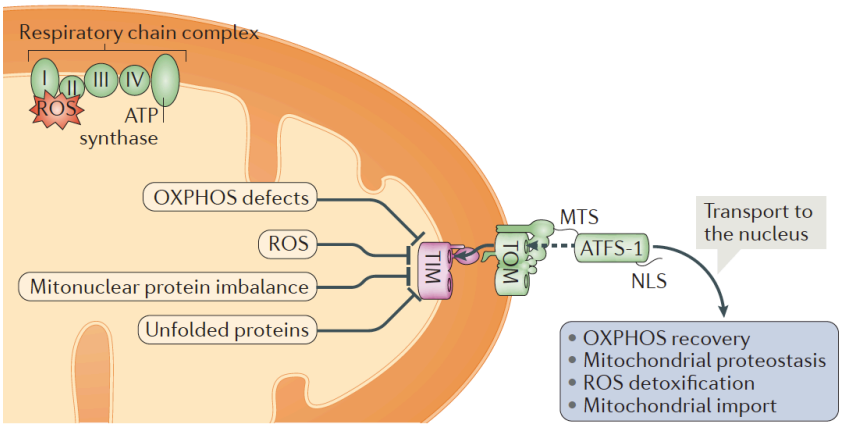

Figure 1.7: Mitochondrial dysfunction in *C.elegans* induces cytoplasmic accumulation and subsequent nuclear translocation of ATFS-1 resulting in activation of UPR^{mt} target genes. Reprinted from (Shpilka and Haynes, 2017).

1.2.1.2 The mammalian UPR^{mt}

In mammals, the situation appears to be less clear (especially regarding the upstream signalling events of the stress response) and more complicated as it is the case in the before-mentioned nematode model system. A recent review proposed the subdivision of the mammalian UPR^{mt} into four different axes (Figure 1.8): (i) The canonical UPR^{mt}, that will be discussed in greater detail below. (ii) The UPR^{mt} sirtuin axis promoting antioxidant activity. (ii) The UPR^{IMS}/ERα axis, specifically activated by accumulated proteins in the IMS. (iii) The UPR^{mt} translational axis, a local response to accumulation of unfolded proteins in the mitochondrial matrix resulting in reduced mRNA processing and thereby decreased mitochondrial protein translation (Münch, 2018).

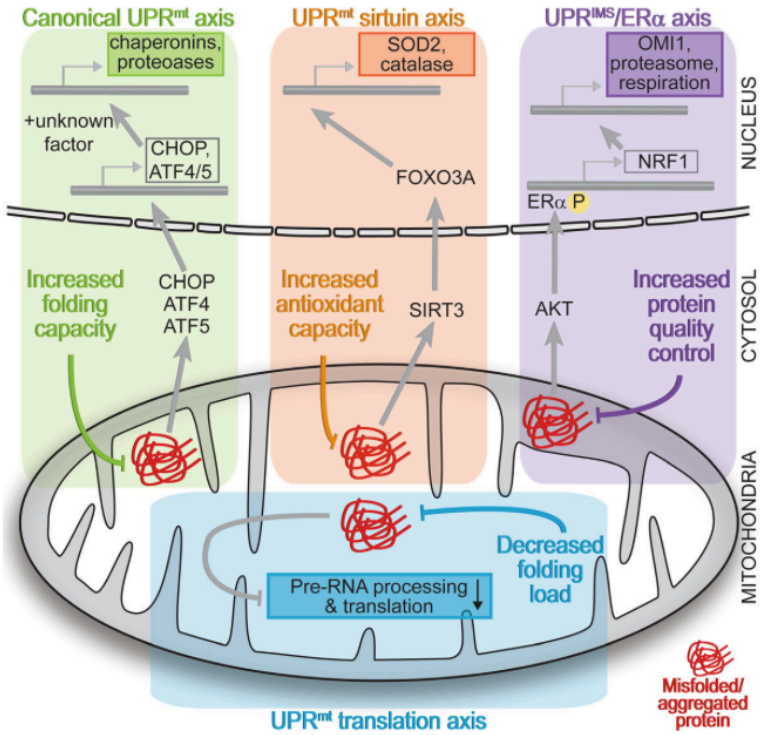

Figure 1.8: The four axes of mammalian UPR^{mt}.
Reprinted from (Münch, 2018).

Major findings of the canonical UPR^{mt} were generated by the Hoogenraad laboratory using either ρ^0 rat hepatoma H4 cells or simian kidney-derived COS-7 cells overexpressing a truncated version of the mitochondrial matrix protein ornithine carbamoyltransferase (ΔOTC) to induce the stress pathway (Martinus et al., 1996; Zhao et al., 2002). Core events of the mammalian UPR^{mt} comprise the JNK2-dependent phosphorylation of the TF c-Jun, promoting mRNA expression of the TF CHOP (C/EBP homologous protein) (Aldridge et al., 2007; Horibe and Hoogenraad, 2007). The latter one appeared to exert – in association with the TF C/EBPβ (CCAAT/enhancer-binding protein beta) – an essential role for the transcriptional activation of the chaperones HSP10 and HSP60 (Aldridge et al., 2007; Zhao et al., 2002). In the course of their work, Hoogenraad and co-workers established an extensive list of UPR^{mt} target genes, including chaperones, proteases and other mitochondrial proteins such as components of the mitochondrial import machinery (Horibe and Hoogenraad, 2007). However, only a mere fraction of these candidates mainly generated by reporter assays was confirmed as endogenous targets in the following years (Arnould et al., 2015). Still, CHOP proved to be a constant factor throughout the work of several research groups on retrograde signalling induced by mitochondrial dysfunction (Dogan et al., 2014; Forsstrom et al., 2019; Horibe and Hoogenraad, 2007; Michel et al., 2015). Nonetheless it became apparent, that the induction of mitochondrial dysfunction by other types of stress such as neuron-specific DRP1 (Dynamin-1-like protein) deletion, depletion of mtDNA,

inhibition of mitochondrial protein import, interference with mitochondrial translation or inhibition of the RC rather carry essential features of another stress response: the ISR (Ishikawa et al., 2009; Michel et al., 2015; Quirós et al., 2017; Restelli et al., 2018). Most likely, UPR^{mt} and ISR at least partially overlap and participate in a complicated crosstalk.

One of the first publications suggesting a possible interconnection of UPR^{mt} and ISR analysed a murine model of intestinal bowel disease, where the ISR was shown to mediate the UPR^{mt} via JNK phosphorylation by the ISR effector kinase PKR (Interferon-induced, double-stranded RNA-activated protein kinase) (Rath et al., 2012). Notably, activation of the ISR preceding the UPR^{mt} was also proposed in a model of arsenite-mediated inhibition of the OXPHOS system (Rainbolt et al., 2013) as well as in a recently published stress response model termed the integrated mitochondrial stress response (ISR^{mt}). In mammalian muscle, the ISR^{mt} is characterised by sequential induction of distinct stages transcriptionally mediated by the TFs ATF5, ATF3 and ATF4 and followed by mild UPR^{mt} activation during the terminal state (Forsstrom et al., 2019; Suomalainen and Battersby, 2017).

1.3 Integrated stress response (ISR)

Activation of the ISR can occur in response to a multitude of physiological and pathological conditions. Therefore, this pathway could be considered as an all-purpose response to stress aiming to aid cell survival, cell recovery and – in cases of persisting stress – execute apoptotic cell death. Extrinsic triggers are viral infection, glucose deprivation or hypoxia, among other things (Pakos-Zebrucka et al., 2016). Intrinsically the ISR is, for instance, activated by mitochondrial dysfunction or ER protein folding stress (Harding et al., 1999; Quirós et al., 2017). The specific outcome with regard to the initiating stressors is regulated inter alia at the level of (i) duration and intensity of eIF2α (eukaryotic translation initiation factor 2A) phosphorylation or (ii) the translation of ATF4 (activating transcription factor 4) and other bZIP transcription factors (Guan et al., 2014; Novoa et al., 2003; Scheuner et al., 2006). The key events of ISR signalling are summarised below (Figure 1.9).

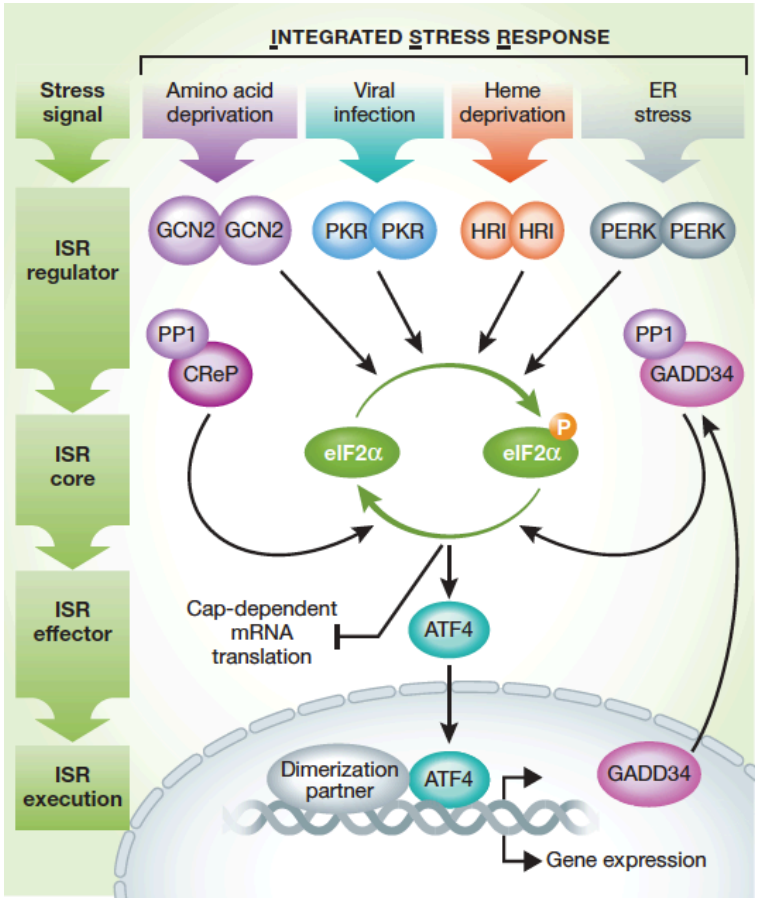

Figure 1.9: The ISR - a retrograde signalling cascade.
Integration of stress signals originating from different cellular compartments into one stress pathway is achieved via a set of four kinases at the regulatory level. The ISR core event is the phosphorylation of eIF2α, leading to inhibition of global protein synthesis and translation of stress-responsive proteins like the key effector of the ISR: ATF4. Reprinted from (Pakos-Zebrucka et al., 2016).

1.3.1 Initiation, progression and termination of the ISR

In mammals, ISR triggering events are sensed and processed by a set of four eIF2α kinases phosphorylating eIF2α at S51 (Ron, 2002). Each kinase detects a specific set of stress signals; however it was already shown for multiple conditions that the functions of these kinases partially overlap and a cooperative mode of action allows fine-tuning of the cellular response to a variety of stressors (Pakos-Zebrucka et al., 2016). All four kinases are characterised by a considerable homology of the catalytic domain and similar requirements (dimerisation followed by auto-phosphorylation) to achieve full activation (Donnelly et al., 2013).

1.3.1.1 The four eIF2α kinases

PERK (PKR-like ER kinase) is the only membrane-embedded eIF2α kinase. It senses explicitly stress in the ER lumen that can be caused e.g. by perturbations of Ca^{2+} homeostasis or accumulation of unfolded proteins (Korennykh and Walter, 2012; Wang and Kaufman, 2016). The activation mechanism resulting in kinase dimerisation is still a matter of research as currently two models are proposed. First, dissociation of the under normal conditions PERK-bound ER chaperone BiP (binding-immunoglobulin protein) was proposed as the activating signal (Bertolotti et al., 2000; Carrara et al., 2015). Second, the direct binding of unfolded proteins to the luminal domain of PERK might cause the activation of the kinase (Gardner and Walter, 2011).

PKR (double-stranded (ds) RNA-dependent protein kinase) differentiates from the other three kinases via its two N-terminal dsRNA binding domains (Saunders and Barber, 2003). Those DSDBs allows PKR to sense dsRNA, e.g. originating from viral infections or released by mitochondria (Kim et al., 2018; Lemaire et al., 2008).

HRI (heme-regulated inhibitor) exhibits a relative tissue-specific expression pattern as it is mainly expressed in erythroid cells (Han et al., 2001). Its primary function consists in the detection of iron deficiency by sensing heme levels via two heme-binding domains (Rafie-Kolpin et al., 2000). In case of low heme availability HRI inhibits the translation of globin mRNA by activation of the ISR and thereby prevents the accumulation of toxic globin aggregates in erythroid cells (Chefalo et al., 1998; Han et al., 2001). Other HRI-activating signals are NO or arsenite-induced oxidative stress (Ill-Raga et al., 2015; McEwen et al., 2005).

GCN2 (general control non-derepressible protein 2) is activated upon accumulation of uncharged tRNAs that the kinase detects via an histidyl-tRNA synthetase-related domain (Wek et al., 1995). Besides amino acid starvation, glucose deprivation and UV light are known to activate GCN2 (Deng et al., 2002; Ye et al., 2010).

1.3.1.2 eIF2α phosphorylation represents the core event of the ISR

As mentioned earlier, the activation of each eIF2α kinase cumulates in phosphorylation of eIF2α, the central hub of the ISR. As a consequence, global cytoplasmic protein synthesis is attenuated, while specific stress-responsive mRNAs are preferentially translated (Pakos-Zebrucka et al., 2016). What are the underlying mechanisms of action?

Inhibition of cytoplasmic protein synthesis is based on prevention of ternary complex (TC) assembly. The ternary complex consists of (i) the eIF2α-containing eIF2 complex,

(ii) GTP and (iii) $tRNA_i^{Met}$. Together with the 40S subunit of the ribosome as well as eIF1A and eIF1 it is forming the 43S pre-initiation complex (PIC) recognising the AUG start codon on the respective mRNA to be translated. Binding of $tRNA_i^{Met}$ to AUG triggers hydrolysis of GTP, resulting in the release of eIF2-GDP. Exchange of GDP for GTP is a prerequisite for recycling eIF2-GDP to form a new TC together with $tRNA_i^{Met}$. Phosphorylated eIF2α, however, is a competitive inhibitor of the guanine exchange factor (GEF) eIF2B required for the recycling step and thereby prevents TC formation (Figure 1.10) (Jackson et al., 2010; Lomakin and Steitz, 2013; Pain, 1996).

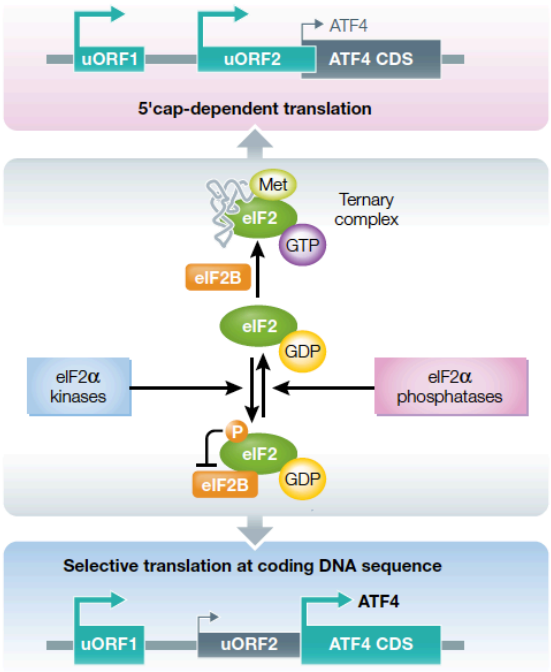

Figure 1.10: Translation initiation on murine *atf4* mRNA under regular conditions (upper part) or during eIF2B inhibition (lower part).
CDS: coding DNA sequence. Reprinted from (Pakos-Zebrucka et al., 2016).

The mechanism behind preferential translation is based on specific structural elements characterising stress-responsive mRNAs: the occurrence of inhibitory upstream open reading frames (uORFs) in the 5' untranslated region (UTR). For example ATF4, the key effector of the ISR, is encoded by a transcript harbouring two uORFs in mice (three uORF in humans) (Figure 1.10) (Harding et al., 2000). Under un-stressed conditions, the ribosome scanning the *atf4* mRNA would initiate translation at uORF1 generating only a short peptide as translation re-initiates at uORF2. Translation starting at uORF2 (uORF3 in humans, respectively) overlaps with the ATF4 coding sequence but the generation of ATF4 is prevented, as the overlap is out-of-frame. As a result, ATF4 is not synthesised under these conditions (Pakos-Zebrucka et al., 2016). In contrast to this, the re-initiation of translation at uORF2 in mice fails increasingly with decreased TC availability. This

results in an augmenting number of ribosomes correctly initiating translation at the AUG of the coding sequence and therefore augmenting ATF4 protein levels (Donnelly 2013).

1.3.1.3 Activating transcription factor 4 (ATF4)

ATF4 is the central effector of the ISR regulating gene expression either as a homodimer or in cooperation with other TFs as a heterodimer. Like CHOP and C/EBPβ it is a bZIP TF and belongs to the ATF family. Heterodimers of ATF4 and C/EBP family members recognise a consensus sequence called the C/EBP-ATF response element (CARE) (Ameri and Harris, 2008; Dey et al., 2010; Fawcett et al., 1999; Kilberg et al., 2009; Pakos-Zebrucka et al., 2016). ATF4 targets are subjected to a dynamic mode of regulation as the following example illustrates: During amino acid deprivation, a heterodimer consisting of C/EBPβ and ATF4 induces transcription of *Asns* (asparagine synthetase). Later during the stress response, however, the heterodimer bound to the *Asns* promoter sequence remodels and ATF4 is replaced by ATF3, followed by decreased *Asns* gene expression (Chen et al., 2004).

As a stress-responsive protein, it is characterised by an extremely short half-life and is tightly regulated on the transcriptional, translational and post-translational level as well as by dimerisation partners (Dey et al., 2010; Pakos-Zebrucka et al., 2016; Rutkowski et al., 2006). ATF4 mainly acts as an activator of transcription, among other things for genes involved in amino acid import and metabolism, mitochondrial 1-C metabolism or protection from oxidative stress (Harding et al., 2003; Kilberg et al., 2012; Krug et al., 2014; Nikkanen et al., 2016).

1.3.1.4 eIF2α de-phosphorylation terminates the ISR

The ISR comprises a GADD34 (growth arrest and DNA damage-inducible protein 34)-mediated negative feedback mechanism responsible for the termination of the stress response upon resolution of stress. Transcriptional activation of *Gadd34* occurs downstream of the eIF2α-ATF4-CHOP signalling cascade and is essential for the formation of the GADD34-containing PP1 (protein phosphatase 1) complex (Connor et al., 2001; Marciniak et al., 2004; Novoa et al., 2001). This complex includes GADD34 as regulatory SU as well as the catalytical SU PP1c and executes the de-phosphorylation of eIF2α that is essential for re-initiation of cytoplasmic CAP-dependent protein synthesis (Novoa et al., 2001). However, it is interesting to note that the PP1 complex also ensures the maintenance of low eIF2α phosphorylation levels under un-stressed conditions. In this context, a second regulatory SU, CReP (constitutive repressor of eIF2α

phosphorylation), supplements GADD34 for the formation of the PP1 complex together with PP1c (Jousse et al., 2003).

1.3.2 Outcome of the ISR

Under optimal conditions, the ISR is active only for a limited time and represents an adaptive and pro-survival response. The inhibition of protein synthesis in the cytoplasm can reduce the protein load under conditions of increased protein folding stress, as it is the case during activation of the UPR^{ER}. Reduction of protein synthesis is ultimately reducing the number of proteins entering the ER, thereby allowing the organelle to process the currently present proteins first. Furthermore, beside re-routing metabolic flows in accordance to the specific condition, stress-responsive translation also provides the cell with the necessary tools to increase protein folding capacity, for instance by increased chaperone and protease levels (Ron, 2002). Another condition under which the cell benefits from temporary inhibition of translation is infection by viral particles, as the replication and propagation of viral particles requires the cellular protein synthesis machinery (Balachandran et al., 2000).

Should the ISR not successfully alleviate cellular stress and be active over a prolonged period, apoptotic cell death signalling is initiated. Apoptosis can be activated via several pathways; the best-studied however is the ATF4-mediated activation of CHOP. As a TF, CHOP has several possibilities to promote apoptosis: For instance it is a known regulator of the BCL2 (B cell lymphoma 2) family, harbouring pro- and anti-apoptotic proteins (Iurlaro and Muñoz-Pinedo, 2016; McCullough et al., 2001). Furthermore, CHOP acts as an activator of DR5 (death receptor 5), the latter promoting the assembly of the death-inducing signalling complex (DISC) necessary for initiation of the caspase cleavage cascade starting with cleavage of pro-caspase 8 (Lu et al., 2014). In addition, CHOP indirectly facilitates apoptosis by increasing *Ero1α* transcription. ERO1α (endoplasmic reticulum oxidoreductase alpha) mediates di-sulfide bond formation in the ER and produces ROS as a by-product of the reaction, thereby destabilising the oxidising environment of this cellular compartment by promoting hyper-oxidation (Marciniak et al., 2004).

1.3.3 CCAAT/enhancer-binding protein family (C/EBP)

The C/EBP family consists of six distinct members, C/EBPα, β, γ, δ, ε, and ζ (Cao et al., 1991). Structurally, a highly conserved C-terminal bZIP domain characterises the C/EBP family. The bZIP domain comprises a basic (b) DNA-binding domain (DBD) and a leucine zipper (ZIP) multimerisation domain. In order to bind target DNA sequences, C/EBP family members form Y-shaped homo- or homotypic hetero-dimers. The coiled-coil association of the respective bZIP domains stabilises the interaction of the DBDs on opposite sides of the major groove of the DNA double helix (Glover and Harrison, 1995; Landschulz et al., 1989; Miller et al., 2003). Heterodimerisation occurs predominantly within the C/EBP family or alternatively with members of the ATF (activation transcription factor) family, thereby resulting in a considerable expansion of the repertoire of DNA-binding specificities. Furthermore, four out of six C/EBP family members harbour N-terminal *trans*-activation domains (TAD) (Tsukada et al., 2011).

1.3.3.1 C/EBP-homologous protein (CHOP)

CHOP (C/EBPζ according to the nomenclature of the C/EBP family) is a stress-responsive TF induced by pathways such as the UPR^{ER}, UPR^{mt} or the ISR (Oyadomari and Mori, 2004; Shpilka and Haynes, 2017). Other common names for the protein are GADD153 (growth arrest and damage associated protein 153) or DDIT3 (DNA damage-inducible transcript 3). Its stress-specific relevance is emphasised by the fact that CHOP-deficient mice do not display substantial phenotypes under stress-free conditions. Upon activation, this multifunctional TF regulates major cellular processes ranging from inflammation, via differentiation to apoptosis (Yang et al., 2017). In the context of disorders, the major functional association of CHOP seems to be apoptosis. As an example, β-cell apoptosis – a hallmark of type 2 diabetes – was proven to depend on the expression of CHOP (Song et al., 2008). On the other hand, several new preclinical models of cancer treatment aim to selectively activate CHOP-mediated apoptosis in malignant cells (Fribley et al., 2015; He et al., 2016a; Rosilio et al., 2015).

From a structural point of view, CHOP is by far the most uncommon TF within the C/EBP family. First, it is fully devoid of a TAD. Second, CHOP exhibits a disrupted helical structure in the DBD due to several substitutions of conserved residues for the helix destabilising residues Pro and Gly. In addition to the resulting defective NLS that is localised in the DBD of bZIP TFs, those structural particularities result in obligatory heterodimer formation for CHOP. As a consequence of the divergent characteristics of the CHOP DBD, CHOP-containing heterodimers with other C/EBP family members do not recognise the classical palindromic C/EBP consensus sequence (Ron and Habener,

1992; Williams et al., 1997). Among the C/EBP TFs, CHOP preferentially associates with LIP (liver inhibitory protein), the inhibitory C/EBPβ isoform (Hattori et al., 2003).

1.4 Objectives

Maintenance of mitochondrial homeostasis is essential for a broad spectrum of signalling, metabolic and energetic processes. To maintain mitochondrial function under conditions of disturbed organelle homeostasis, an elaborated network of stress pathways signalling the dysfunction and inducing adaptive nuclear responses evolved (Arnould et al., 2015; Bohovych and Khalimonchuk, 2016; Spinelli and Haigis, 2018).

One of the most contentious mammalian mitochondrial stress pathways of the past two decades is the UPR^{mt}. The scientific community struggles for a precise definition of the conditions under which this stress pathway is activated. Another current matter of debate is the relationship between the UPR^{mt} with one of the cell's global responses to stress: the ISR. Both stress responses can be activated by mitochondrial dysfunction and show a certain degree of overlap, e.g. regarding the set of TFs activated downstream of the respective signalling cascades (Forsstrom et al., 2019; Münch, 2018; Shpilka and Haynes, 2017).

Our research group previously described a murine model of severe mitochondrial dysfunction induced by heart and skeletal muscle-specific deletion of *Dars2* (DARS2 KO). The deficiency caused (with increasing severity of mitochondrial dysfunction) up-regulation of *bona fide* UPR^{mt} markers (Dogan et al., 2014). However, this up-regulation was preceded by the increase of several TFs (ATF4, ATF5 and CHOP) previously associated with both, the UPR^{mt} and the ISR (Fiorese et al., 2016; Horibe and Hoogenraad, 2007; Pakos-Zebrucka et al., 2016; Quirós et al., 2017; Shpilka and Haynes, 2017).

Since CHOP was the first TF proposed to play a fundamental role in the UPR^{mt} and due to the fact that CHOP is an important effector of the ISR (Horibe and Hoogenraad, 2007; Oyadomari and Mori, 2004; Zinszner et al., 1998), the TF was selected as the leverage point of the present study to further disentangle the stress signalling cascades triggered by mitochondrial dysfunction in the previously described DARS2 KO mouse (Dogan et al., 2014).

The following three research aims were defined: First, to assess whether the activation of CHOP has a beneficial or detrimental impact on the pathological changes induced by

mitochondrial dysfunction. Second, to identify the pathway CHOP is operating in under the given conditions. Third, to understand the function CHOP exerts within the pathway. In order to address the before-mentioned research aims a newly generated mouse model deficient for DARS2 (heart and skeletal-muscle specific) and CHOP (whole-body) along with well-directed cell-cultural treatments were combined in a targeted approach.

2 Materials and Methods

2.1 Mouse experiments

2.1.1 Animal care and breeding

All mice (C57BL/6N) analysed during the course of this study were bred and raised in the CECAD in vivo research facility. Housing of the animals was carried out in individually ventilated cages (IVC) under the following conditions:

- Ambient temperature: 22-24°C
- 12h light/dark cycle, the light cycle starting at 6am
- *Ad libitum* access to water and normal chow diet (R/M-H-V1554, sniff Spezialdiäten GmbH)
- Specific pathogen-free (SPF)

For breeding one male was housed with 1-2 females of a similar age, 8 weeks of age being the earliest time point to start a mating. After weaning animals were kept in groups of three to five animals of the same sex. Sacrifice of animals until 10 days of age was carried out by decapitation with sharp scissors. Older animals were sacrificed by cervical dislocation. Housing conditions and experimental procedures were consistent with NIH guidelines and conducted following protocols approved by the local governmental

authorities (Landesamt für Natur, Umwelt und Verbraucherschutz Nordrhein-Westfalen, LANUV).

2.1.2 Experimental mouse models

Aiming to investigate the *in vivo* function of the stress-responsive transcription factor CHOP in the context of the heart and skeletal muscle-specific DARS2 KO, following mouse strains were used:

Chop$^{-/-}$

B6.129S(Cg)-Ddit3$^{tm2.1Dron}$/J mice were obtained from The Jackson Laboratory. Those mice are characterzied by a *Chop*::LacZ knock-out allele, resulting in the whole body knock-out of *Chop*.

Dars2$^{fl/fl}$

Dars2 conditional gene targeting was performed within the framework of the International Knockout Mouse Consortium (KOMP). *Dars2*$^{fl/fl}$ animals were generated as previously reported (Dogan et al., 2014).

CkmmCre$^{tg/+}$

Heterozygous CkmmCre transgenic mice were provided by Prof. Dr. Nils Larson (Wang et al., 1999). Those animals harbour one copy of the Cre-recombinase under control of the striated muscle creatine kinase (Ckmm) promoter, the latter getting activated after embryonic day 13.0 (E13.0) (Lyons et al., 1991).

Heart and skeletal muscle-specific DARS2-deficient mice (*CkmmCre*$^{tg/+}$, *Dars2*$^{fl/fl}$; as from now referred to as DARS2 KO) resulted from inter-crossing of *Dars2*$^{fl/fl}$ mice with *CkmmCre*$^{tg/+}$ mice. *CkmmCre*$^{tg/+}$, *Dars2*$^{fl/+}$ mice generated from this first breeding were then mated to *Dars2*$^{fl/fl}$ mice. In addition to DARS2 KO mice, wild-type littermates (*CkmmCre*$^{+/+}$, *Dars2*$^{fl/fl}$ or *CkmmCre*$^{+/+}$, *Dars2*$^{fl/+}$) resulting from this mating were used as controls, as from now referred to as WT mice.

In order to obtain mice harbouring a heart and skeletal muscle-specific deletion of *Dars2* in addition to a whole body knock-out of *Chop*, several subsequent breedings were necessary:

First, *Dars2*$^{fl/fl}$ mice were inter-crossed with *Chop*$^{-/-}$ mice. Resulting animals heterozygous for both genetic loci were mated, to obtain *Dars2*$^{fl/fl}$, *Chop*$^{-/-}$ mice. Secondly, *CkmmCre*$^{tg/+}$, *Dars2*$^{fl/+}$, *Chop*$^{-/-}$ mice were generated by breeding *Dars2*$^{fl/fl}$, *Chop*$^{-/-}$ mice with *CkmmCre*$^{tg/+}$, *Dars2*$^{fl/fl}$ mice. Resulting *CkmmCre*$^{tg/+}$, *Dars2*$^{fl/+}$, *Chop*$^{-/+}$ mice were again inter-crossed with *Dars2*$^{fl/fl}$, *Chop*$^{-/-}$. Finally, double transgenic *Dars2*$^{fl/fl}$, *Chop*$^{-/-}$ mice were inter-crossed with triple transgenic *CkmmCre*$^{tg/+}$, *Dars2*$^{fl/+}$, *Chop*$^{-/-}$ mice, resulting in animals devoid of transgenic Cre but deficient for CHOP (*CkmmCre*$^{+/+}$, *Dars2*$^{fl/+}$, *Chop*$^{-/-}$ or *CkmmCre*$^{+/+}$, *Dars2*$^{fl/fl}$, *Chop*$^{-/-}$; as from now referred to as CHOP KO mice) as well as animals harbouring a heart and skeletal muscle-specific deletion of *Dars2* in addition to a whole body knock-out of *Chop* (*CkmmCre*$^{tg/+}$, *Dars2*$^{fl/fl}$, *Chop*$^{-/-}$; as from now referred to as DKO mice).

2.1.3 Phenotyping

2.1.3.1 Sampling

Immediately following the sacrifice of mice organ sampling was performed. Harvested organs were either snap-frozen in liquid nitrogen or embedded in Tissue-Tek (Sakura Finetek) and placed on dry ice for freezing. Snap-frozen or embeded organs were subsequently stored at -80°C.

2.1.3.2 Body weight determination

Body weight of individual animals was determined at p17 (±2).

2.1.3.3 Blood glucose measurement

Glucose levels in the blood were assessed with a reflectance meter (ACCU-CHEK AVIVA, Roche) using glucose strips and following the manufacturer's instructions. Blood glucose levels of individual animals were determined at p17 (±2) from whole venous tail blood. Due to the critical health status of DKO^{L} mice at this time point, blood glucose was only determined in the fed state.

2.1.3.4 In vivo protein translation assessment

Protein translation was determined using the nonradioactive technique called surface sensing of translation (SUnSET) described in (Goodman and Hornberger, 2013). This

assay is based on the incorporation of the structural analogue of tyrosyl-tRNA called puromycin in nascent polypeptide chains and subsequent detection of puromycylated proteins using an anti-puromycin-specific antibody.

Briefly, mice were injected at the indicated time points *intraperitoneally* with 0.04 µmol of puromycin dissolved in PBS per g of body weight. 30 min after injection the animals were sacrificed and collected tissues snap-frozen in liquid nitrogen. Subsequently, protein lysates of the collected tissues were prepared as described in 2.4.1.1 and processed by SDS-PAGE and Western blot (2.4.2). The relative signal intensity of the anti-puromycin-specific antibody is proportional to the relative protein synthesis rates at the time point of the puromycin injection.

2.2 Cell Culture

2.2.1 Maintenance of cultured cells

Culture of immortalised mouse embryonic fibroblasts (MEFs) and fibroblasts was performed in a humidified atmosphere at 37°C and 5% CO2. The cell culture medium was composed of DMEM (4.5g/L glucose, GlutaMAX, sodium pyruvate; Gibco Life Technologies) supplemented with 10% 'Fetal Bovine Serum Premium, South American Origin' (Biowest) and Pen Strep (Gibco Life Technologies) and re-newed every second day. Upon conditions of mitochondrial dysfunction (induced either genetically or by treatment) the medium was additionally supplemented with 50µg/mL of uridine. At 90% confluency cells were split cell type-dependently in ratios ranging from 1:4 to 1:20.

2.2.2 Cryopreservation

Cryopreservation of cells was achieved by re-suspension of cells collected from a 90% confluent plate in 4mL freezing medium (cell culture medium supplemented with 10% fetal bovine serum and 10% DMSO). Subsequently, 1mL aliquots of the cells were stored at -80°C in a 'Cryo 1°C Freezing Container' (Nalgene) overnight, before being transferred to -145°C. For thawing, cryovials were rapidly warmed in a 37°C water bath. The liquid cell suspension was poured in 9mL of culture medium and pelleted to remove DMSO.

After re-suspension in 10mL culture medium, the cells were transferred to cell culture plates.

2.2.3 Cellular treatments

For induction of mitochondrial dysfunction by actinonin treatment, 80% confluent cells were treated for 48h with 100µM Actinonin (Sima-Aldrich). Inhibition of the ISR was achieved by 4h, 24h and 48h 1µM ISRIB (Sima-Aldrich) treatments of 90% confluent cells. Both compounds were solubilised in DMSO. Untreated cells were supplemented with corresponding amounts of the solvent. Treatments were renewed on a daily basis.

2.2.4 Transfection and selection of stably-transfected cells

Transfection of plasmids conferring hygromycin resistance was performed with Lipofectamine 2000 (Invitrogen) according to the manufacturer's instructions using the forward transfection procedure. 72h post transfection the culture medium was replaced by hygromycin-supplemented (100µg/mL) medium for negative selection of un-transfected cells.

2.3 Molecular biology

2.3.1 Isolation of genomic DNA

2.3.1.1 Isolation of crude DNA

Crude DNA preparations were used for genotyping of animals or mouse embryonic fibroblasts (MEFs). Ear biopsies or cell pellets were lysed in 500µL of DNA lysis buffer (100mM Tris-HCl, 5mM EDTA, 200mM NaCl, 0.2% SDS (w/v), 0.2 mg/mL Proteinase K, pH 7.4) at 55°C, respectively. DNA of fully digested samples was precipitated with 500µL of 2-propanol (20min centrifugation at maximum speed) and washed once with 70% ethanol (15min centrifugation at maximum speed). The DNA pellet was subsequently resolved in 150µL dH_2O and stored at 4°C.

2.3.1.2 Isolation of purified DNA

DNA of high purity was required for quantification of mtDNA levels by qPCR. Therefore, approximately 1mm3 of cardiac tissue per sample was lysed in 600µL DNA lysis buffer (20mM Tris-HCl, 10mM EDTA, 100mM NaCl, 0.5% SDS (w/v), 0.2 mg/mL Proteinase K, pH 7.4) at 55°C. RNA was degraded by the addition of RNase A (100µg/mL) and 30min of incubation at 30°C. 600µL of a mixture of cold phenol:chloroform:isoamyl alcohol (25:24:1) was added. After centrifugation (10min at maximum speed), the aqueous layer was collected. DNA was precipitated by addition of 2-3 volumes of 100%, 1/10 volume of 3M NaOAc and incubation at -80°C for 30min. The DNA pellet obtained after centrifugation (30min, maximum speed, 4°C) was washed once with 500µL of 70% ethanol. Finally, the dry pellet was dissolved in 100µL ultra-pure H_2O and stored at 4°C overnight for complete dissolving prior determination of the DNA concentration (see 2.3.3).

2.3.2 Isolation of total RNA

For isolation of total RNA cell pellets were resuspended or approximately 25mg of tissue were homogenised in 1mL TRIzol reagent (Life Technologies) using a Precellys CK 14 (Bertin Technologies) (5000rpm, 30sec). After 5min at RT, 200µL of chloroform were added and mixed vigorously for 15sec before a second incubation step at RT for 3min. Phase separation was completed by centrifugation (12.000g, 15min, 4°C). The aqueous upper phase was collected and containing RNA precipitated with 500µL 2-propanol (10min incubation at RT followed by 10min centrifugation at 12.000g and 4°C). The resulting RNA pellet was washed with 1mL of 75% ethanol (5min centrifugation at 7500g, 4°C) and briefly dried before resuspension in 50µL ultra-pure H_2O. After determination of RNA concentration (see 2.3.3), the residual DNA was digested by DNase I (New England Biolabs) treatment. The digestion mix (up to 10µg RNA, diluted 10X digestion buffer and 1µL DNase I in a total volume of 20µL) was incubated for 10min at 37°C. 0.2µL of 0.5M EDTA were added to the reaction, to protect the RNA during the heat inactivation of DNaseI (75°C, 10min). After re-determination of RNA concentration, the samples were stored at -80°C.

2.3.3 Quantification of nucleic acids

Nucleic acids were quantified using a NanoDrop ND-1000 UV-Vis spectrophotometer (Peqlab). Purity of DNA and RNA was estimated utilising the ratio of absorbance between 260nm (absorbance maximum of nucleic acids) and 280nm (absorbance maximum of proteins). A ratio of ~1.8 corresponds to “pure” DNA, whereas “pure” RNA has a ratio of ~2.0.

2.3.4 Polymerase chain reaction (PCR)

2.3.4.1 Genotyping PCR

To determine the genotype of mutant mice or cells isolated from mutant mice embryos, PCR reactions with specific primers distinguishing between WT, floxed or KO alleles of the respective genes were performed. All genotyping reactions were performed with the DreamTaq polymerase (Thermo Fisher Scientific).

PCR mix composition:

1µL	DNA
0.5-1µL	per Primer (10µM) [2-4 primer per reaction, depending on the specific PCR]
1µL	dNTP mix (1.25mM each)
2µL	DreamTaq buffer (10X)
0.05µL	DreamTaq polymerase
Up to 20µL	H_2O

Reaction-specific primers and conditions:

Dars2 PCR: Primer 1: 5' ATGAATTCTAGGCCAGCCAC 3'
Primer 2: 5' TGGCAATCTCTTAGGACTAAG 3'

$V(primer)_{per\ reaction}$=0.8µL

$T_{Annealing}$=60°C

$t_{Annealing}$=30sec

$t_{Elongation}$=45sec

Chop PCR: Primer 1: 5' ATGCCCTTACCTATCGTG 3'
Primer 2: 5' AACGCCAGGGTTTTCCCAGTCA 3'
Primer 3: 5' GCAGGGTCAAGAGTAGTG 3'

$V(primer)_{per\ reaction}$=1µL

$T_{Annealing}$=61°C

$t_{Annealing}$=1min

$t_{Elongation}$=30sec

CkmmCre PCR: Primer 1: 5' GTGAAACAGCATTGCTGTCACTT 3'
Primer 2: 5' TAAGTCTGAACCCGGTCTGC 3'
Primer 3: 5' CAAATGTTGCTTGTCTGGTG 3'
Primer 4: 5' GTCAGTCGAGTGCACAGTTT 3'

$V(primer1\&2)_{per\ reaction}$=1µL

$V(primer3\&4)_{per\ reaction}$=0.5µL

$T_{Annealing}$=63°C

$t_{Annealing}$=30sec

$t_{Elongation}$=30sec

PCR programme:

1) Initial denaturation at 95°C for 5min

For 35 cycles:

2) Denaturation at 95°C for 30sec
3) Annealing at 60 to 63°C for 30sec to 1min (see reaction-specific conditions)
4) Elongation at 72°C for 30sec to 45sec (see reaction-specific conditions)

5) Final extension: 5min at 72°C
6) Hold 4°C

2.3.4.2 Reverse transcriptase PCR (RT-PCR)

For cDNA synthesis from RNA utilising the 'High capacity reverse transcription kit' (Applied Biosystems) the following reaction mix was prepared:

2µL	RT buffer (10X)
0.8µL	dNTP mix (25X)
2µL	Random primer (10X)
1µL	Reverse transcriptase
2µg	RNA
Up to 20µL	H_2O

PCR programme:

1) Annealing 10min at 25°C

2) Elongation 120min at 37°C
3) Denaturation 5sec at 85°C
4) Hold 4°C

Synthesised cDNA was stored at -20°C.

2.3.4.3 Quantitative real-time PCR (qPCR)

qPCR reactions were performed on 96 well and 384 well plates using the 'Brilliant III Ultra-Fast SYBR Green qPCR Master Mix (Agilent Technologies) following the manufacturer's instructions. Per reaction 50ng of cDNA were employed. The cycling reaction was performed in the 'Applied Biosystems QuantStudio 7 Flex Real-Time PCR System' (Fisher Scientific). Relative target gene expression was determined by normalisation to endogenous control genes (*tbp* or *hprt*, respectively) using the comparative ($2^{-\Delta\Delta C}{}_t$).

PCR programme:

1) Initial denaturation at 95°C for 3min

For 40 cycles:

2) Denaturation at 95°C for 5sec
3) Annealing and Elongation at 60 for 15sec

Dissociation curve:

4) Denaturation at 95°C for 15sec
5) Annealing at 60°C for 1min
6) Step-wise increase of temperature until 95°C (ramp time 20min)

Table 2.1: Primers used for qPCR

Transcript	Forward Primer 5'-3'	Reverse Primer 5'-3'
afg3l2	GTTGATGGGCAATACGTCTGG	GACCCGGTTCTCCCCTTCT
atf4	AACATCCAATCTGTCCCGG	GTTCTCCAGCGACAAGGC
bip	GACTGCTGAGGCGTATTTGG	ATCTTTGGTTGCTTGTCGCTGG
cebpb	CAACCTGGAGACGCAGCACAA	TTGAACAAGTTCCGCAGGGTG
chop	TGCCTTTCACCTTGGAGACGG	CGCAGGGTCAAGAGTAGTGAAGG
clpp	CAGTCTGAAAGCAACAAGAAGC	ACTGCATTGTGTCGTAGATGG
cth	GGGTTTTGAATACAGCCGC	CTGTTGGTGCCTCCATACACT
gadd34	GAGGGACGCCCACAACTTC	TTACCAGAGACAGGGGTAGGT
hprt	GCCCCAAAATGGTTAAGGTT	TTGCGCTCATCTTAGGCTTT
hsp60	GCCTTAATGCTTCAAGGTGTAGA	CCCCATCTTTTGTTACTTTGGGA
lonp1	ATGACCGTCCCGGATGTGT	CCTCCACGATCTTGATAAAGCG
mthfd2	CCACTCCCAGAGCACATTGAT	GTTGGAATGCCTGTTCGCTT

Transcript	Forward Primer 5'-3'	Reverse Primer 5'-3'
mthsp70	ATGGCTGGAATGGCCTTAGC	ACCCAAATCAATACCAACCACTG
pycr1	GATGCTCTGGCTGACGGTGGTGT	GCTGGCTGGGATGCTGTTCTGAG
shmt2	CCACCACCACTCACAAGACACTGCG	TGTAGGGATGGGAACACAGCGAAGTTG
tbp	GGGAGAATCATGGACCAGAA	TTGCTGCTGCTGTCTTTGTT
yme1l1	ATTCTGCGGTAGACCCTGTC	CAACCACTTCCTGTAACTCTTGT

2.3.4.4 mtDNA quantification

Following DNA isolation as described in 2.3.1.2 mtDNA levels were determined by qPCR (Quiros et al., 2017). Relative mtDNA levels were estimated by normalisation of *Nd1* (mtDNA-encoded) to *Hk2* (nDNA-encoded) DNA levels.

Table 2.2: Primers used for mtDNA quantification

Gene	Forward Primer 5'-3'	Reverse Primer 5'-3'
Nd1	CTAGCAGAAACAAACCGGGC	CCGGCTGCGTATTCTACGTT
Hk2	GCCAGCCTCTCCTGATTTTAGTGT	GGGAACACAAAAGACCTCTTCTGG

2.3.5 Transformation of chemically compentent E. coli

If not stated differently, transformations were performed with 'Subcloning Efficiency DH5α Competent Cells' (Thermo Fisher Scientific). A 50µL aliquot of competent cells was thawed on ice for 15min before adding 1-10ng of DNA in a volume of maximal 5µL. Following 30min of incubation on ice, the cells were subjected to a heat shock (20sec, 42°C) and immediately put back on ice for 2min. After addition of 950µL of pre-warmed medium, cells were grown for 1h at 37°C and 800rpm. Finally, cells were pelleted (1min, 1300rpm), resuspended in 50µL of medium and plated on selective LB agar plates. After incubation overnight at 37°C plates were stored at 4°C to prevent overgrowth of the colonies.

2.3.6 Preparative and analytical scale plasmid DNA purification from E. coli

Small amounts of plasmid DNA were recovered from overnight liquid cultures (37°C, 120rpm) of 4mL LB selection medium inoculated with a colony picked from an LB agar plate in the evening before. For plasmid preparation, the 'ZymoPURE Plasmid Miniprep Kit' (Zymo Research) was used according to the manufacturer's instructions.

Large amounts of plasmid DNA were recovered from overnight liquid cultures (37°C, 120rpm) of 200mL LB selection medium inoculated in the evening before. Inoculation was performed with 500µL of a 4mL overnight pre-culture prepared the day before, as described above. For plasmid preparation, the 'ZymoPURE II Plasmid Maxiprep Kit' (Zymo Research) was used according to the manufacturer's instructions.

2.3.7 Agarose gel electrophoresis

Size-dependent separation of DNA was achieved by agarose gel electrophoresis. Agarose concentration was adapted to the fragment size and ranged between 0.5% to 2%. For the preparation of agarose gels, agarose was boiled in 0.5X TBE buffer. Subsequently, ethidium bromide (4µL per 100mL of agarose solution) was added, and the solution briefly stirred, before the agarose gel was poured into a gel chamber with slot combs. After completed polymerisation, the gel was transferred into an electrophoresis chamber and covered with 0.5X TBE. The 'GeneRuler 1kb Plus DNA Ladder (Thermo Fisher Scientific) was used for size estimation of DNA fragments. DNA samples were diluted with an agarose gel loading buffer before loading into the gel pockets. Electrophoresis was performed at 80–150V until sufficient separation of the DNA fragments. For visualisation, the GelDoc system (BioRad) was utilised.

2.3.8 DNA gel extraction

Extraction of DNA fragments form agarose gels were performed with the 'Zymoclean Gel DNA Recovery Kit' (Zymo Research) according to the manufacturer's instructions.

2.3.9 DNA sequencing

For sequencing, plasmids were send to Eurofins were they were processed via Sanger sequencing.

2.3.10 Q5 site directed mutagenesis

The 'Q5 Site-Directed Mutagenesis Kit' (New England Biolabs) was used to introduce a point mutation (L120D) in the LIP plasmid provided by Maria Hatzoglou (Chiribau et al., 2010). For primer design, the NEB online design software 'NEBaseChanger' was utilised. All three steps described in the protocol (exponential amplification, KLD reaction and transformation) were performed as indicated in the manual.

Primer LIP L120D F: 5' GGTGGAGCAGACGTCGCGAGAG 3'

Primer LIP L120D R: 5' TTCTTCTGCAGCCGCTCG 3'

$T_{Annealing}$=65°C

2.3.11 Northern blot analysis for mitochondrial mRNA quantification

2µg of RNA supplemented with 'RNA Sample Loading Buffer' (Sigma-Aldrich) were heated for 10min at 65°C prior to loading on a 1.2% agarose-formaldehyde gel. Separation of RNA was performed for 2.5h at 130V in 1X MOPS running buffer. After visualisation of the gel with the GelDoc system (BioRad), an extensive washing step followed (3X 15min in nuclease-free H2O). Subsequently, the gel and the Hybond N+ membrane (GE Healthcare) were soaked in 20X SSC for 20min, before setting up the alkaline capillary transfer of the RNA to the membrane overnight. Crosslinking of the RNA was performed at 80°C for 15min. Mitochondrial probes (ND1, ND5, COX3, 16S) and the 18S nuclear probe (70ng each) were radioactively labelled (50µCi α32P-dCTP) utilising the 'Random Primer DNA labelling Kit' (Invitrogen). Following 1h of membrane pre-hybridisation at 65°C with 'Rapid-Hyb Buffer' (GE Healthcare) the labelled probe was added for 2h of hybridisation. Subsequently, three washing steps of 20min each were performed at 65°C (A: 2X SSC/ 0.1%SDS; B: 1X SSC/ 0.1%SDS; C: 0.5X SSC/ 0.1%SDS). For detection of the radioactive signals, Amersham Hyperfilms MP (GE Healthcare) were exposed to the membrane. 18S rRNA levels served for normalisation of mitochondrial transcript levels.

2.4 Biochemistry

2.4.1 Isolation of proteins

2.4.1.1 Protein extraction from cardiac tissue

Homogenisation of 25mg of cardiac tissue samples in 400µL cold organ lysis buffer (50mM HEPES pH 7.4, 50mM NaCl, 1% Triton X-100 (v/v), 0.1M NaF, 10mM EDTA, 0.1% SDS (w/v), 10mM Na-orthovanadate, 2mM PMSF, 1X protease inhibitor cocktail (Sigma-Aldrich), 1X PhosSTOP phosphatase inhibitor cocktail (Roche)) was performed with the Precellys CK 14 (Bertin Technologies) (5000rpm, 30sec). Cleared protein lysates (45min, 13000rpm, 4°C) were transferred into fresh tubes. Subsequent determination of protein concentration was performed with Bradford reagent (Sigma-Aldrich) according to the manufacturer's instructions. Protein lysates were stored at -80°C.

2.4.1.2 RIPA lysis of cultured cells

Washed cell pellets were resuspended in 80-200µL cold RIPA buffer (150mM NaCl, 1% Triton X-100 (v/v), 0.5% Na-deoxycholate (w/v), 0.1% SDS (w/v), 50mM Tris-HCl pH 7.4, 50mM NaF, 2mM EDTA) supplemented with 1X protease inhibitor cocktail (Sigma-Aldrich) and 1X PhosSTOP phosphatase inhibitor cocktail (Roche). Next, cells were incubated 30min on ice with brief vortexing every 10min. Following 2X 45sec sonication the lysates were cleared (10min, 13000rpm, 4°C) and transferred into fresh tubes. Subsequent determination of protein concentration was performed with Bradford reagent (Sigma-Aldrich) according to the manufacturer's instructions. Protein lysates were stored at -80°C.

2.4.2 SDS polyacrylamide gel electrophoresis (SDS-PAGE) and Western blot

SDS-PAGE was conducted using the 'Mini-PROTEAN Tetra Cell' (BioRad) system as indicated by the manufacturer. Protein samples were dissolved in SDS-PAGE loading buffer (50mM Tris-HCl pH 6.8, 2% SDS (w/v), 10% Glycerol (v/v), 1% β-

mercaptoethanol, 12.5 mM EDTA, 0.02% Bromophenol blue) prior boiling for 5min at 95°C. Next, lysates were loaded next to a protein ladder ('PageRuler Prestained Protein Ladder', Thermo Fisher Scientific) on 8% to 15% acrylamide gels (stacking gel: 5% Acrylamide-bisacrylamide (37.5:1), 12.5 mM Tris-HCl, 0.1% SDS (w/v), 0.25% APS, 0.25% TEMED, pH 6.8; separating gel: 8-15% Acrylamide-bisacrylamide (37.5:1), 37.5mM Tris-HCl, 0.1% SDS (w/v), 0.1% APS, 0.1% TEMED, pH 8.8), depending on the required range of protein sizes to separate. To begin with, electrophoresis was performed at 80V for 15min in running buffer (25mM Tris-HCl, 250mM Glycine, 0.1% SDS (w/v), pH 8.3). Later, voltage was increased to 140V. Protein separation was stopped, as soon as the loading dye reached the end of the separating gel.

For wet transfer, the 'Criterion Blotter' (BioRad) was used according to the manufacturer's instructions. Transfer of proteins on a nitrocellulose membrane was conducted in transfer buffer (30mM Tris-HCl, 240mM Glycine, 0.037% SDS, 20% Methanol) at 400mA for 2h at 4°C. For a first evaluation of the transfer, shortly washed membranes (dH2O) were stained with Ponceau S solution (Sigma-Aldrich). Depending on the antibody requirements, de-staining and blocking of membranes was performed for 1h either in 5% milk-PBST or 3% BSA-TBST on a gently shaking platform. Subsequently, primary and secondary antibodies were incubated as indicated by the manufacturers. Inbetween primary and secondary antibody incubation, as well as prior detection, membranes were washed (3X, 5min) in PBST or TBST, respectively. For the visualisation of detected proteins, ECL solution (GE Healthcare) was applied to the membrane. Next, the membranes were exposed to 'Super RX' films (Fujifilm). The latter ones were developed using an automatic developer (Kodac) and scanned with a 'V800 Transparency Scanner' (Epson) at 800dpi 16Bit colour depth.

Table 2.3: Antibodies, suppliers and catalogue numbers of antibodies used for Western blot

Antibody	Supplier	Catalogue Number
4EB-P1	CST	9644
AFG3L2	Polyclonal antisera made by Prof. Dr. Elena I. Rugarli	-
AKT	CST	9272
AMPK	CST	2532
ASC	Abcam	ab175449
ASNS	Santa Cruz	sc-365809
ATF4	CST	11815
ATP5A1	Abcam	ab14748
BECLIN-1	CST	3738
BiP	Santa Cruz	sc-376768
CEBPB	Bioloegend	606203
CHOP	CST	2895S
Cleaved Caspase 3	CST	9661S
CLPP	Sigma	WH0008192M1
COXI	Molecular Probes	459600
COXIV	Molecular Probes	A21348
DARS2	Proteintech	13807-1-AP
eIF2a	Abcam	ab26197
GLUT-4	Millipore	07-1404
HSC70	Santa Cruz	sc-7298
HSP60	ATCC	HSP60
IRE1a	Santa Cruz	sc-390960
LC-3	CST	2775
LONP1	Abcam	ab103809
MRPS12	Proteintech	15225-1-AP
MTHFD2	Abcam	ab56772
mtHSP70	Abcam	82591
mTOR	CST	2972
NDUFA9	Molecular Probes	459100
NLRP3	CST	15101
OXPHOS cocktail	Abcam	ab110413
p- 4EB-P1	CST	2855
p-AKT	CST	4060
p-EIF2a	Abcam	ab32157
p-mTOR	CST	2971
p62	Abnova	H00008878-M01
p-AMPK	CST	2535
PARP	CST	9542
Puromycin	Merck	#MABE343
PYCR1	Abcam	ab94780
SDHA	Mitosciences	MS204
SDHB	Abcam	ab110413
SHMT2	Abcam	ab224428
UQCRC1	Molecular Probes	459140

2.4.3 Isolation of cardiac mitochondria

Freshly collected hearts were immediately transferred into 10mL of pre-chilled mito-isolation buffer (MIB) (100mM Sucrose, 50mM KCl, 1mM EDTA, 20mM TES, 0.2% BSA free from fatty acids, pH adjusted to 7.2) supplemented with 1µg subtilisin (Sigma-Aldrich) per mg of tissue. Approximately 20 long strokes of a Potter S (Sartorius) homogeniser at 1000rpm were required for homogenisation. After centrifugation (800g, 5min, 4°C), the mitochondria-containing supernatant was transferred into a fresh tube. Pelleted mitochondria (8500g, 5min, 4°C) were resuspended in 30mL MIB and subjected to a third centrifugation step (700g, 5min, 4°C). Finally, mitochondria were pelted (8500g, 5min, 4°C) and resuspended in 100µL MIP without BSA. Protein concentration of mitochondria was determined using Bradford reagent (Sigma-Aldrich) according to the manufacturer's instructions. Mitochondria were either immediately used (respirometry or *in* organello translation) or snap-frozen and stored at -80°C.

2.4.4 Mitochondrial respiration

High-resolution respirometry utilising an Oxygraph-2k (OROBOROS Instruments) and a carbohydrate substrate uncoupler inhibitor titration (SUIT) protocol was conducted to determine mitochondrial oxygen consumption rates. First, the respiration medium (120mM Sucrose, 50mM KCl, 20mM Tris-HCl, 1mM EGTA, 4mM KH2PO4, 2mM MgCl2, 0.1% BSA) was added to the oxygraph chamber and air equilibration was performed. Next, 25µg of freshly-isolated cardiac mitochondria were added. The respiration medium was supplemented with 2mM pyruvate, 0.8mM malate, 2mM glutamate and 2mM ADP to assess CI-dependent respiration. By providing 4mM of succinate, convergent CI and CII-dependent respiration was determined. Inhibition of CV by addition of 1.5 µg/mL of oligomycin allowed to evaluate the coupling efficiency. The maximal capacity of the electron transfer system (ETS) was assessed by titration of FCCP (0.5µM increments). Maximal capacity of the ETS of CII solely could be determined by inhibition of CI through addition of 0.5µM rotenone. Finally, inhibition of CIII by supplementation of 2.5µM antimycin A allowed the determination of the residual oxygen consumption (ROX).

2.4.5 Blue native polyacrylamide gel electrophoresis (BN-PAGE)

BN-PAGE was performed based on the 'NativePage Novex Bis-Tris Gel System' (Life Technologies) according to the manufacturer's instructions. For analysis of mitochondrial

super-complexes, 10µg mitochondria were lysed with 4% of digitonin. Analysis of individual mitochondrial complexes was conducted post lysis of 10µg mitochondria in 1% DDM. After completion of lysis (15min on ice), lysates were cleared (30min, 13000rpm, 4°C) and the resulting supernatant loaded on a 4-16% Bis-Tris gradient gel. Subsequently, proteins were transferred to an Amersham Hybond PVDF membrane (GE Healthcare) by Western blot (2.4.2).

2.4.6 *In organello* translation

De novo mitochondrial translation was assessed by incubation (1h, 37°C, on rotating wheel) of 1.5mg of freshly-isolated mitochondria in 1mL 35S-translation buffer (100mM Mannitol, 10mM Na-succinate, 80mM KCl, 5mM MgCl2, 1mM KH2PO4, 25mM HEPES pH 7.4, 5mM ATP, 200µM GTP, 6mM Creatine phosphate, 60µg/mL Creatine kinase, 60µg/mL Cysteine, 60µg/mL tyrosine, 60µg/mL Amino acids [Ala, Arg, Asp, Asn, Glu, Gln, Gly, His, Ile, Leu, Lys, Phe, Pro, Ser, Thr, Trp, Val], 7µL/mL 35S-methionine). Subsequently, mitochondria were pelleted (12000g, 2min) and resuspended in 1mL non-radioactive translation buffer containing methionine instead of 35S-methionine. Half of the sample ('pulse fraction') was pelleted again, resuspended in 100µL SDS-PAGE loading buffer (50mM Tris-HCl pH 6.8, 2% SDS (w/v), 10% Glycerol (v/v), 1% β-mercaptoethanol, 12.5 mM EDTA, 0.02% Bromophenol blue) and lysed (30min, RT) before transfer at -20°C. For the 'cold chase' allowing to estimate the protein turnover, the remaining 500µL of resuspended mitochondria were incubated for 3h at 37°C on a rotating wheel. Subsequently, the 'chase fraction' was pelleted, resuspended in 100µL SDS-PAGE loading buffer and lysed as the 'pulse sample' before.

Separation of mitochondrial proteins was achieved by SDS-PAGE. 10µL per sample were loaded on a 15cm long, 15% polyacrylamide gel and run in a 'SE600X Chroma Deluxe Dual Cooled Vertical Protein Electrophoresis Unit' (Hoefer) overnight at 80V continuously. After fixing (50% Methanol, 10% Acetic acid) for 30min, staining in Coomassie solution and de-staining (20% Methanol, 10% Acetic acid) of the polyacrylamide gel the latter one was placed on Whatman paper (GE Healthcare) and dried (2h, 80°C) in a gel dryer. For detection of radioactive signals of *de novo* synthetised proteins, Amersham Hyperfilms MP (GE Healthcare) were exposed to the membrane and developed using an automatic developer (Kodac). Digitalisation was performed using a ‘V800 Transparency Scanner’ (Epson) at 800dpi 16Bit colour depth. The scanned gel was used as loading control.

In organello translation experiments were performed together with Dr. Alexandra Kukat.

2.5 Histology

2.5.1 Cryostat sections

Tissue-Tek (Sakura)-embedded cardiac samples were sectioned utilising a 'CM1850 cryostat' (Leica). Tissue sections were immediately transferred onto poly-L-lysine glass slides and stored at -20°C.

2.5.2 Hematoxilin and eosin (H&E) staining

H&E staining was performed on 7µm cryosections. Following 1min incubation in tap water, the sections were placed in Hematoxylin solution (Sigma-Aldrich) (4min) and tap water again (15min). Subsequently, the sections were placed in dH_2O (1min), Eosin (Sigma-Aldrich) (1min) and washed several times with tap water. Next, dehydration was performed by incubation in 75% ethanol (1min), 96% ethanol (1min), 100% ethanol (1min) and xylene (1min). For mounting of cover-slips Entellan (Millipore) was used. Imaging was conducted using a ‘SCN400 Slide Scanner’ (Leica) at 40X magnification.

2.5.3 COX/ SDH staining

COX/SDH staining was performed on dried (10min, RT), 7µm cryosections surrounded with a 'Super PAP Pen' (Daido Sangyo). First, sections were incubated (40min, 37°C, humidified chamber) in COX solution (0.8mL Diaminobenzidine tetrahydrochloride, 0.2mL Cytochrome c (500µM), a few grains of catalase). After three washing steps in tap water, SDH solution (0.8mL Nitroblue tetrazolium (1.875mM), 0.1mL Succinate (1.3M) 0.1mL 2mM Phenazine methosulphate and 0.01mL Sodium azide (100mM)) was applied (12min, 37°C, humidified chamber). Subsequently, the sections were washed (3X, tap water), and dehydrated: 75% ethanol (2min), 95% ethanol (2min), 100% ethanol (10min). Finally, dried slides were mounted with Entellan (Millipore). Imaging was conducted using a ‘SCN400 Slide Scanner’ (Leica) at 40X magnification.

2.5.4 Transmission electron microscopy

Acquisition of TEM pictures was largely performed by Beatrix Martiniy of the CECAD imaging facility. Tissue were dissected in 2 x 2 x 2mm cubes with a sharp razor blade and fixed in 2% glutaraldehyde / 2% formaldehyde in 0.1M cacodylate buffer (pH 7.3) for 48h at 4°C. Afterwards, samples were rinsed in 0.1M cacodylate buffer (Applichem) and post-fixed with 2% osmiumtetroxid (Science Services) in 0.1M cacodylate buffer for 2h at 4°C. Samples were dehydrated through an ascending ethanol series (Applichem), transferred to propylene oxide (Merck) and embedded in epoxy resin (Sigma-Aldrich).

Ultrathin sections (70nm) were cut with a diamond knife (Diatome) on an ultramicrotome (EM-UC6, Leica Microsystems) and placed on copper grids (Science Services, 100mesh). The sections were contrasted with 1.5% uranyl acetate (Plano) and lead citrate (Sigma-Aldrich).

Images were acquired with a transmission electron microscope (JEM 2100 Plus, JEOL), a OneView 4K camera (Gatan) with DigitalMicrograph software at 80 KV at room temperature.

2.6 Omic Analyses

2.6.1 Label-free quantification of the cardiac proteome

For whole-tissue proteomics protein lysates of cardiac tissue samples were prepared based on a finely ground tissue powder obtained by grinding the samples in liquid nitrogen. The ten-fold amount (v/w) of RIPA (150mM NaCl, 1% Triton X-100 (v/v), 0.5% Na-deoxycholate (w/v), 0.1% SDS (w/v), 50mM Tris-HCl pH 7.4, 50mM NaF, 2mM EDTA) supplemented with 1X protease inhibitor cocktail (Sigma-Aldrich) was added to the tissue powder, vortexed and passed several times through a cannula for lysis and chromatin shearing. After incubation (30min, 4°C, on a rotating wheel) lysates were cleared (15min, 4°C, full speed) and protein concentration was determined with Bradford reagent (Sigma-Aldrich) according to the manufacturer's instructions.

Next, 50µg protein per sample were precipitated with the four-fold volume of cold 100% acetone (60min, -80°C), pelleted (15min, 4°C, full speed) and washed twice with cold 90% acetone (5min, 4°C, full speed). The air-dried pellet was subsequently resuspended in 300µL 8M urea buffer.

In solution digest was performed by addition of DTT to a final concentration of 5mM (1h, 37°C), addition of chloracetamid to a final concentration of 40mM (20min, protect from light), addition of endoproteinase Lys-C at an enzyme-substrate ration of 1:75 (4h, 37°C) and dilution with 50mM TEAB to a urea concentration of 2M before adding trypsin at an enzyme-substrate ration of 1:75 (overnight, 37°C, protect from light). Digest was stopped with formic acid (1% final concentration).

Digested protein lysates were loaded on SDB-RPS stage tips provided by the CECAD/CMMC proteomics core facility according to the standard procedure of the facility. The core facility further processed the samples using a 'Q Exactive Plus Orbitrap' (Thermo Fisher Scientific) coupled with an 'EASY nLC LC' (Thermo Fisher Scientific). Raw data were analysed with Maxquant (version 1.5.3.8).

2.6.2 CHOP co-immunoprecipitation (co-IP) and subsequent mass-spectrometrical quantification of purified proteins

For CHOP co-IP one heart per sample was homogenised in 500µL modified RIPA (150mM NaCl, 1% NP-40 (v/v), 0.25% Na-deoxycholate (w/v), 0.1% SDS (w/v), 50mM Tris-HCl pH 7.4) supplemented with 1X protease inhibitor cocktail (Sigma-Aldrich) using a Precellys CK 14 (Bertin Technologies) (5000rpm, 30sec) and lysed 20min on ice. Chromatin was sheared by sonication in a pre-cooled Bioruptor (Diagenode) (10 cycles: 30sec ON, 30sec OFF). The cleared lysate (15min, 4°C, full speed) was transferred into a fresh tube, and protein concentration was determined with Bradford reagent (Sigma-Aldrich) according to the manufacturer's instructions. The protein lysate was incubated overnight with 5µL of CHOP antibody (#2895, CST) at 4°C on a rotating wheel.

Precipitation was performed by incubation (1h, 4°C) of the lysate-antibody mixture with 50µL equilibrated, magnetic 'Dynabeads Protein G' (Invitrogen). Following consecutive washing steps were performed: 1X with cold lysis buffer, 2X using cold wash buffer 1 (50mM Tris-HCl pH 7.4, 150mM NaCl, 5% Glycerol (v/v), 0.05% NP-40), 2X utilising wash buffer 2 (50mM Tris-HCl pH 7.4). After the last washing step, the beads were resuspended in elution buffer (2M Urea, 50mM HEPES pH 8, 5mM DTT).

On-bead digest was performed by addition of 50ng trypsin (30min, RT, gentle shaking) and subsequent addition of 50µL digestion buffer (2M urea, 50mM HEPES pH 8, 50mM Chloracetamid) (30min, RT, gentle shaking). The supernatant was transferred to a new tube, while the beads were resuspended once more in 50µL elution buffer. Finally, both supernatants were combined and supplemented with 50ng LysC and 100ng trypsin for

overnight digest (37°C, shaking at 1000rpm). The digest was stopped with formic acid (1% final concentration).

Digested protein lysates were loaded on SDB-RPS stage tips provided by the CECAD/CMMC proteomics core facility according to the standard procedure of the facility. The core facility further processed the samples using a ‘Q Exactive Plus Orbitrap’ (Thermo Fisher Scientific) coupled with an ‘EASY nLC LC’ (Thermo Fisher Scientific). Raw data were analysed with Maxquant (version 1.5.3.8).

2.6.3 RNA sequencing (RNAseq) of cardiac total mRNA

RNA isolation for RNAseq was performed using the 'Direct-zol RNA MiniPrep Kit' (Zymo Research) according to the manufacturer’s instruction. Purified RNA was submitted to the Cologne Centre for Genomics for further processing. Libraries were prepared using the 'TruSeq mRNA Stranded Sample Preparation Kit' (Illumina) and validated on a tape station (Agilent). Equimolar amounts of libraries were pooled, quantified (Peqlab KAPA Library Quantification Kit, Applied Biosystems 7900HT Sequence Detection System) and finally sequenced on a 'HiSeq4000 sequencer' (Illumina). Subsequently, the RNAseq data set was analysed by the CECAD Bioinformatic facility utilising the QuickNGS pipeline (Wagle et al., 2015), ensembl version 93(mm10).

2.6.4 Amino acid quantification

Amino acid quantification was performed by Dr. Susanne Brodesser and Christina Lucas from the CECAD Lipidomics facility. Amino acid levels in mouse heart were determined by 'Liquid Chromatography coupled to Electrospray Ionisation Tandem Mass Spectrometry' (LC-ESI-MS/MS) using a 'QTRAP 6500 triple quadrupole/linear ion trap mass spectrometer' (SCIEX) coupled to a '1260 Infinity Binary LC System' (Agilent). Amino acids were derivatised with 6-aminoquinolyl-N-hydroxysuccinimidyl carbamate using the 'AccQ-Tag Ultra Derivatisation Kit' (Waters).

2.6.5 Metabolomics

Metabolomic analyses were performed by Dr. Susanne Brodesser and Christina Lucas from the CECAD Lipidomics facility. Levels of nucleotides and intermediates (organic

acids, sugar phosphates) of the glycolysis and the citric acid cycle in mouse heart were determined by 'Anion-Exchange Chromatography coupled to Electrospray Ionisation High-Resolution Mass Spectrometry' (IC-ESI-HRMS) using a 'Q Exactive HF quadrupole-orbitrap mass spectrometer' coupled to a 'Dionex Integrion RFIC system' (Thermo Scientific).

2.7 Software

'Adobe Photoshop' (Adobe) was used to adjust contrast of scanned films globally and to excise relevant areas for further processing. Densitometric analyses were performed with 'Image Studio Lite' (Licor). Figures and model illustrations were generated utilising 'Adobe Illustrator' (Adobe). For model illustrations selected medical images licensed under a Creative Commons Attribution 3.0 Unported License from 'Servier Medical Art' (Servier) were used. 'Prism 8' (GraphPad) served to generate graphs, charts and statistical analyses.

2.8 Nomenclature

In general, genes and transcripts are italicised. For genes, only the first letter is written in uppercase, whereas transcripts are entirely written in lowercase. Protein names are not italicised and fully written in uppercase.

2.9 Chemicals

Name	Supplier
Acetic Acid	AppliChem
Acetone	AppliChem
Acetyl-L-Carnitine hydrochloride	Sigma Aldrich
Acetyl-L-Cysteine	Sigma Aldrich
Adenine	Sigma Aldrich
Adenosin-Tri-Phosphate ATP	Sigma Aldrich
ADP Adenosine 5’-diphosphate sodium Salt	Sigma Aldrich
Agar bacteriology grade	AppliChem
Agarose ultra pure	Invitrogen

Name	Supplier
Alanine (L-)	Sigma Aldrich
Aminobenzaldehyde	Sigma Aldrich
Ammonia Solution 25%	AppliChem
Ammoniumpersulfat APS	Sigma Aldrich
Ampicillin sodium salt	AppliChem
Antimycin A	Sigma Aldrich
Arginine mono-hydrochloride (L-)	Sigma Aldrich
Ascorbic Acid	Sigma Aldrich Life Sc.
Asparagine monohydrate (L-)	Sigma Aldrich
Aspartic Acid (L-)	Sigma Aldrich
Benzamidin-Hydrochloride	AppliChem
Bis Tris	Santa Cruz
Blue Native Marker	GE
Boric acid	Sigma Aldrich
Bromophenol Blue	MERCK
BSA (Albumin from bovine serum) fatty acid free	Sigma Aldrich
Calcium Carbonate	AppliChem
Calcium chloride dihydrate	MERCK
Carnithine hydrochloride	Sigma Aldrich Life Sc.
Catalase, bovine liver	Sigma Aldrich
CCCP (Carbonyl cyanide 3-chloro-phenylhydrazon)	Sigma Aldrich
Chloro-D-Phenylalanine	Sigma Aldrich
Chloroform	AppliChem
Citrat Synthase	Sigma Aldrich
Coomassie Brilliant Blue G250	AppliChem
Creatin Monohydrate	Sigma Aldrich Life Sc.
Creatine Phosphokinase Type III, bovine	Sigma Aldrich
Cyclohexamide	Sigma Aldrich
Cysteine hydrochloride monohydrate (L-)	Sigma Aldrich
Cytochrome c, bovine heart	Sigma Aldrich
DDM Dodecyl-β-maltosicyl	Roth
DEPC	AppliChem
Diethylamine	Sigma Aldrich
Digitonin (HP)	MERCK
Dimethyl malonate	Sigma Aldrich
DMSO Dimethylsulfoxide	Sigma Aldrich
DTT Dithiothreitol	Sigma Aldrich
ECL	Thermo
EDTA Ethylenediaminetetraacetic acid	Sigma Aldrich

Name	Supplier
EGTA Ethylene glycol-bis(2-aminoethylether)-N,N,N′,N′-tetraacetic acid	Sigma Aldrich
EtBr	Sigma Aldrich
Ethanol abs.	AppliChem
Ethylmethansulfonate	Sigma Aldrich
FCCP	Sigma Aldrich
Formaldehyde (mol. Biol grade)	Sigma Aldrich
Glucose	AppliChem
Glutamic Acid (L-)	Sigma Aldrich
Glutamine (L-)	Sigma Aldrich
Glutaraldehyde solution Grade I 50%	Sigma Aldrich
Glycerol	Sigma Aldrich
Glycine Molecular Biology grade	AppliChem
Glycogen	Roche
GTP Guanosine 5'triphosphate sodium salt	Sigma Aldrich
Guanindine hydrochloride	Sigma Aldrich
HCl 37%	VWR
Heparin Sodium salt	Sigma Aldrich Life Sc.
HEPES-Molecular biology grade	AppliChem
Hexane	Sigma Aldrich
Histidine mono hydrochloride monohydrate (L-)	Sigma Aldrich
Hydrogen peroxid solution	Sigma Aldrich
Iso-Pentane Methylbutanol	VWR
Isobutylmethylxanthine	Sigma Aldrich
Isoleucine (L-)	Sigma Aldrich
Isopropanol	Applichm
Ketamin hydrochloride CIIIN	Sigma Aldrich
Ketoglutaric acid disodium Sigma Aldrichlt dihydrate	Aldrich Chemistry
Ketoglutaric acid potassium Sigma-Aldrichlt	Sigma Aldrich
L-Glutathion (reduced)	Sigma Aldrich
L(+)-lactic acid	AppliChem
LB Medium - powder acc to Miller	AppliChem
LB Medium - powder according to Lennox	AppliChem
Leucine (L-)	Sigma Aldrich
Lithium acetoacetate	Sigma Aldrich
Lysine mono-hydrochloride (L-)	Sigma Aldrich
Magnesium chloride hexahydrate	Fluka Analytical
Magnesium sulfate anhydrate	AppliChem
Malic acid	Sigma Aldrich

Name	Supplier
Mannitol Biochemica	AppliChem
Mercaptoethanol 98%	Sigma Aldrich
MES	ROTH
Methionine (L-)	Sigma Aldrich
Methylbutane	Sigma Aldrich
Milk powder	AppliChem
MOPS Mol Bio grade	AppliChem
Myxothiazol	Sigma Aldrich
N-Lauroylsarcosine Sodium Salt	Sigma Aldrich Life Sc.
Nicotinamid	Sigma Aldrich Life Sc.
Nitro Blue Tetrazolium	Sigma Aldrich
NP40 Nonidet P40 Biochemica	AppliChem
Oligomycin	Sigma Aldrich
Ornithine monohydrochloride	Sigma Aldrich Life Sc.
Oxaloacetic acid	Sigma Aldrich
Palmitic Acid	Sigma Aldrich Life Sc.
Paraquat Methylviologendichloride	Sigma Aldrich
PBS Buffer (10X Dulbecco's) Powder	AppliChem
PBS Tablets	Calbiochem
PEG Polyethylene glycol	Sigma Aldrich Life Sc.
Peptone from meat	MERCK
Periodic Acid	Sigma Aldrich
Phenol	AppliChem
Phenol/Chloroform/Isoamylalcohol	Roth
Phenylalanine (L-)	Sigma Aldrich
Phenylmethanesulfonylfluorid PMSF	Sigma Aldrich
PMSF	AppliChem
Poly-L-Lysine	Sigma Aldrich
Polyethylenimine	Sigma Aldrich Life Sc.
Potassium chloride	AppliChem
Potassium hydrogen phosphate	MERCK
Proline (L-)	Sigma Aldrich
Protein Standard	Sigma Aldrich
Puromycin	Sigma Aldrich
Retinoic Acid	Sigma Aldrich
RNase A	AppliChem
RNAse ZAP	Sigma Aldrich
Rotenone	Calbiochem
Rotiphorese Gel 40 (37.5:1)	ROTH

Name	Supplier
SDS granules	Sigma Aldrich Life Sc.
Serine (L-)	Sigma Aldrich
Sodium 3-hydroxybutyrate	Sigma Aldrich
Sodium acetate solution (3M, pH 5,2) Molecular Biology grade	AppliChem
Sodium azide	AppliChem
Sodium chloride for molecular biology	Sigma Aldrich Life Sc.
Sodium deoxycholate	AppliChem
Sodium fluoride	AppliChem
Sodium Hydrogen Carbonate	AppliChem
Sodium hydroxide	Sigma Aldrich
Sodium Orthovanadate	AppliChem
Sodium Phosphate dibasic	Sigma Aldrich Life Sc.
Sodium Phosphate monobasic	Sigma Aldrich
Sodium pyruvate	Sigma Aldrich
Sodium succinate dibasic hexhydrate	Sigma Aldrich
Sodium tetraborate	Sigma Aldrich
Sodium Thiosulfate	Sigma Aldrich Life Sc.
Sodium- L- Lactate	Sigma Aldrich
Sorbitol	AppliChem
Succinic Acid	Sigma Aldrich
Sucrose	Sigma Aldrich Life Sc.
Sulfuric Acid	Fluka
Superoxide Dismutase	Sigma Aldrich
TCEP HCl	Thermo
TEMED	Sigma Aldrich
TES Buffer grade	AppliChem
Thapsigargin	Sigma Aldrich
Threonine (L-)	Sigma Aldrich
TMPD Tetramethyl-p-phenylenediamin	Sigma Aldrich
Tri-sodium citrate dihydrate	AppliChem
Tricine	ROTH
Triton X-100, molecular biology grade	AppliChem
Trizma Base	Sigma Aldrich Life Sc.
TrypanBlue	Sigma Aldrich
Trypsin from bovine pancreas	VWR
Tryptophan (L-)	Sigma Aldrich
Tween 20	VWR
Tyrosine (L-)	Sigma Aldrich
Uracil	Sigma Aldrich Life Sc.

Name	Supplier
Urea	Fluka Analytical
Uridine	Sigma Aldrich Life Sc.
Valine (L-)	Sigma Aldrich
Valinomycin	Sigma Aldrich
Xylazine Hydrochloride	Sigma Aldrich
Xylol	ROTH
Yeast extract granulate for Microbiology	MERCK
Zinc Sulfate Heptahydrate	Aldrich

3 Results

3.1.1 Generation of DARS2/CHOP double knock-out mice

Initial studies on DARS2 KO mice (heart and skeletal muscle-specific deletion of the mitochondrial aspartyl-tRNA synthetase) revealed a trend towards up-regulation of the stress-responsive TFs ATF5 and CHOP already from one week of age on. The present study aims to investigate further the stress response triggered by mitochondrial dysfunction in DARS2 KO mice in general, and to understand the function of the TF CHOP, as known effector of the ISR and first UPR^{mt} associated TF, in detail (Dogan et al., 2014; Horibe and Hoogenraad, 2007; Pakos-Zebrucka et al., 2016). For this purpose, DKO mice deficient for DARS2 (heart and skeletal muscle-specific) and CHOP (whole-body) were generated. Detailed information regarding the used mouse strains, the breeding procedure and genotypes of the animals used are given under 2.1.2 and summarised in the scheme below (Figure 3.1):

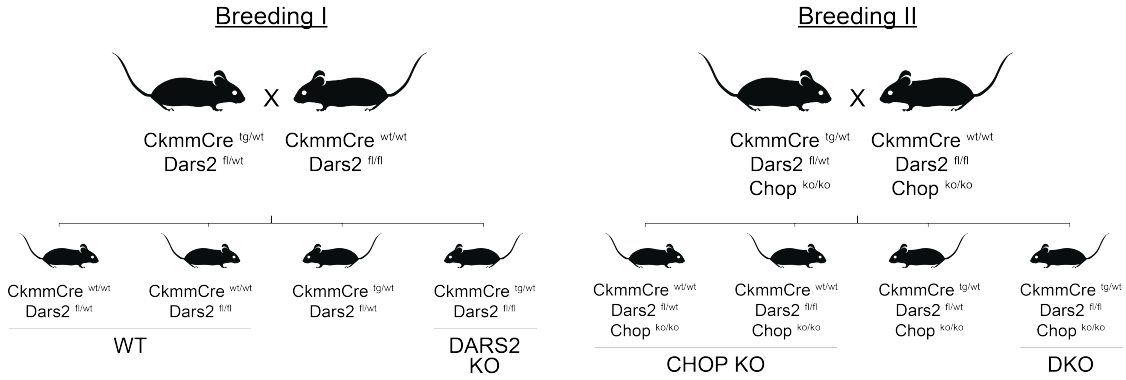

Figure 3.1: Breeding scheme for generation of WT, DARS2 KO, CHOP KO and DKO mice. Note that deletion of *Chop* applies to the whole body whereas D*ars2* deletion only concerns heart and skeletal muscle. Allele nomenclature: wild type (wt), transgene (tg), flowed (fl) and knock-out (ko).

To generate the *Chop* deletion-comprising mouse line (breeding II Figure 3.1), the newly acquired mouse strain B6.129S(Cg)-Ddit3$^{tm2.1Dron}$/J from the Jackson Laboratory was employed. Disruption of *Chop* in the animals used for this study was verified by PCR (Figure 3.2A), and RNAseq (Figure 3.2B). Further validation by Western blot on the protein level failed, as all tested CHOP-detecting antibody did not work (data not shown).

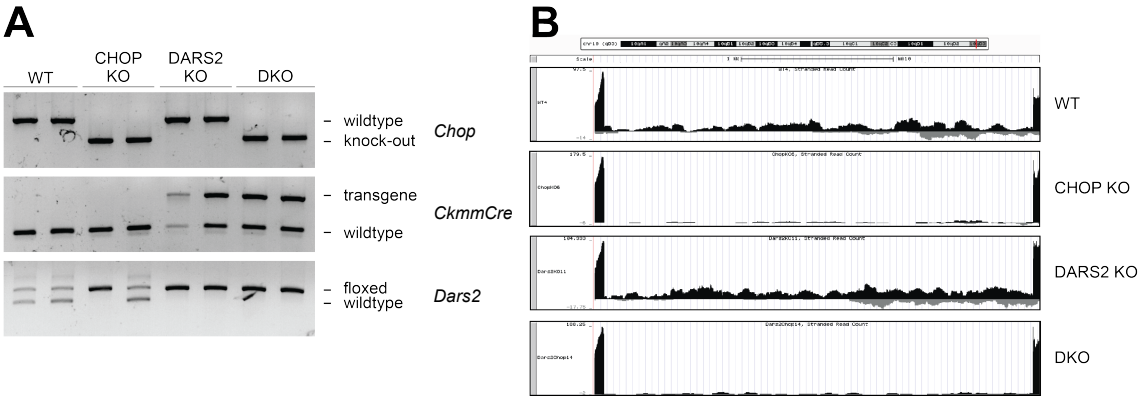

Figure 3.2: Genotypic validation of WT, CHOP KO, DARS2 KO and DKO mice.
(A) Genotyping agarose gel electrophoresis of WT, CHOP KO, DARS2 KO and DKO mice. PCR products were generated from DNA isolated from ear biopsies using gene-specific primer pairs for *Chop, CkmmCre* and *Dars2*. (B) Exemplary RNAseq data track visualisation of the *chop* mRNA by UCSC genome browser of one animal per genotype. RNAseq was performed on cardiac samples of animals at p17 (±2) (n=4).

3.1.2 Phenotypic changes caused by deletion of *Dars2* develop prematurely upon loss of *Chop*

The dedicated aim of the present study was to decipher the role of the stress-responsive TF CHOP, which is up-regulated from early-on in DARS2 KO animals developing mitochondrial dysfunction later in life but also in the muscles of human patients came down with the mitochondrial disease of progressive external ophthalmoplegia (PEO) (Dogan et al., 2014; Forsstrom et al., 2019). Loss of aspartyl-tRNA synthetase DARS2 in heart and skeletal muscle was characterised by progressively impaired mitochondrial translation and followed by reduced levels of fully assembled respiratory chain complexes I, IV and (to a lesser extent) III from the age of three weeks on. As a result of this, DARS2 KO animals displayed severe OXPHOS deficiency as well as a massively increased heart to body weight ratio, indicating strong cardiomyopathy at six weeks of age. Finally, those pathological changes entailed a drastic reduction of lifespan to only 6-7 weeks. Up-regulated mRNA levels of stress-responsive TFs such as *chop, atf4* and *atf5* as well as increased protein levels of further stress-associated markers (e.g. p62, LONP1 or HSP60) were predominantly detected in hearts but not in skeletal muscle of DARS2 KO animals (Dogan et al., 2014). Due to the prominent stress response activation primarily observed in the heart, all analyses of the present study were performed exclusively on cardiac samples.

To predict the impact of depleting CHOP in this system turned out to be difficult, as published studies revealed very context-specific beneficial or unfavourable effects of the TF in different disease models (Yang et al., 2017). It appeared very quickly that CHOP deficiency, contrarily to the situation in the WT background, entails deleterious consequences in the DARS2 KO background. The already considerably shortened lifespan of DARS2 KO mice was further reduced by more than 50% to less than three weeks. In contrast, CHOP KO animals did not display any physical or behavioural abnormalities up to an age of one year in accordance with information provided by the Jackson Laboratory (Figure 3.3A).

The distribution of genotypes in the litters followed Mendel's laws (data not shown), and as no sex-specific differences were observed, male and female animals were analysed together. Aiming to distinguish between early initiated adaptations and late pathological changes, animals were analysed at following average time points: One week after birth (p6), two weeks after birth (p13) and after the visible manifestation of the phenotype (p17 (±2)). Since the vast majority of analyses were performed on animals at p13 and p17 (±2) constituting the 'early' and 'late' stage of the phenotype in DKO mice, the latter will be referred to as DKO^{E} (p13) and DKO^{L} (p17 (±2)), respectively.

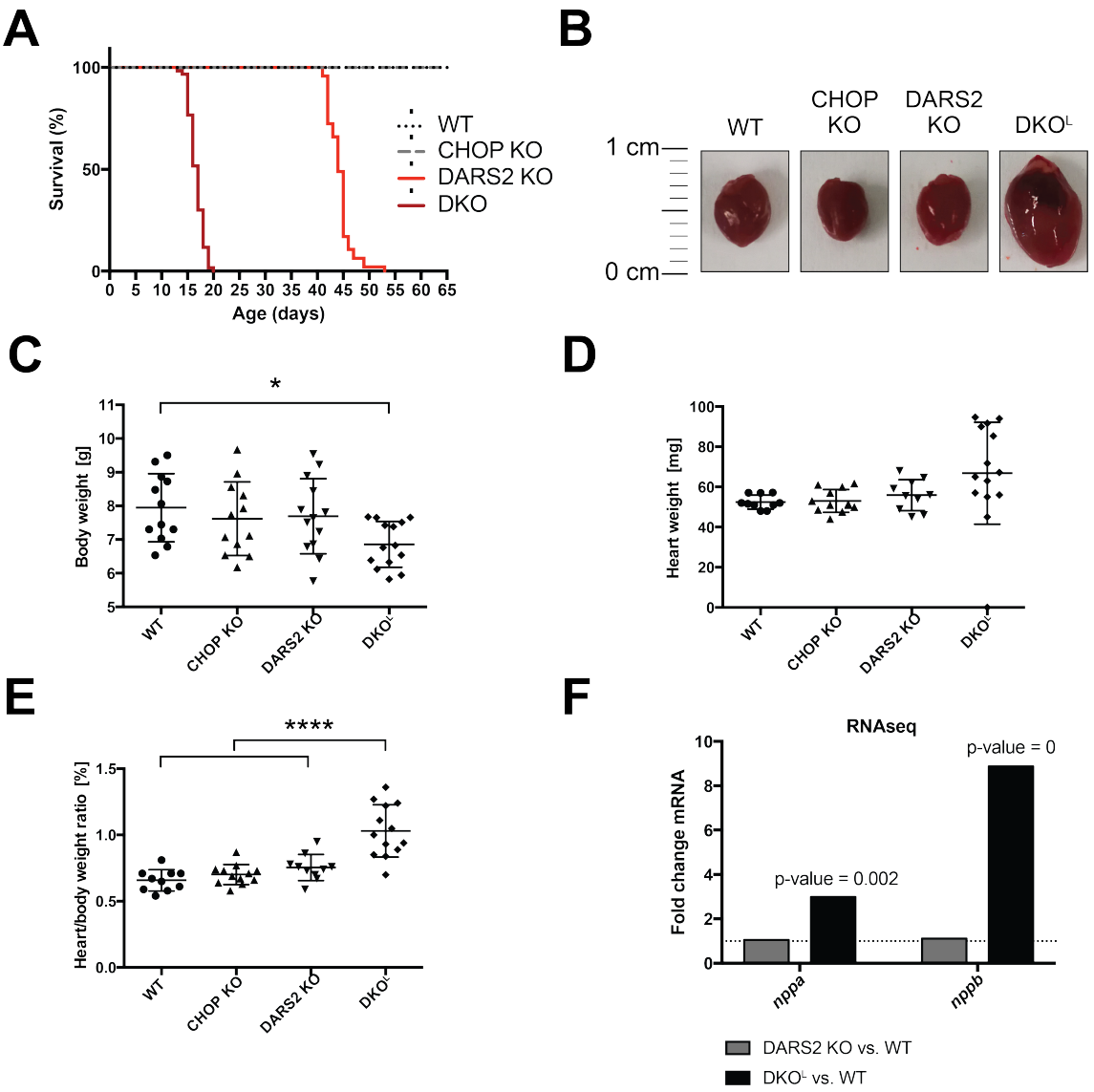

Figure 3.3: Phenotypic characterisation of DKO animals.

(A) Kaplan-Meyer survival curves for WT (n=36), CHOP KO (n=35), DARS2 KO (n=47) and DKO animals (n= 60). Lifespan of DKO in comparison to DARS2 KO mice is significantly decreased (****). Viability of CHOP KO mice was WT-like in 12-month follow-up. (B) Heart gross morphology. (C) Bodyweight (n=12-14). (D) Heart weight (n=10-14) and (E) heart-to-body weight ratio (n=10-13) of animals at p17 (±2). Bars represent mean ± SD (One-way ANOVA; *p<0.05, **p<0.01, ***p<0.001, ****p<0.0001). (F) Fold changes of the cardiac hypertrophy markers *nppa* and *nppb* obtained from the RNAseq data set of DARS2 KO and DKO^{L} mice in comparison to WT mice at p17 (±2) (n=4).

During the first two weeks of life, no obvious phenotypic differences between DKO mice and their respective controls were visible. However, shortly after this age, DKO mice appeared to develop high stress sensitivity. Simple handling of those animals to punch ear tags necessary for identification, caused several DKOs to die during the procedure.

Usually, this routine is performed when animals are older than two weeks of age. Shifting ear clipping to postnatal day 13 (p13) latest, however, prevented loss of animals due to stress induced by the procedure. At p17 (±2) a phenotype characterised by inactivity, bent posture and unsteady gait manifested. Once those symptoms appeared, most of the affected animals died within 24 hours, calling for close monitoring of the litters from the age of approximately two weeks on. During this terminal stage, DKO^{L} mice display a markedly reduced body weight combined with a severe dilated cardiomyopathy shown by a highly significant increase of the heart to body weight ratio (Figure 3.3B-E). The significant increase of natriuretic peptide A and B transcript levels (*nppa* and *nppb*, respectively) provide further evidence for degeneration of the cardiac tissue (Figure 3.3F). Strikingly, all previously mentioned morphological changes, namely reduced lifespan, decreased body weight and progressing degeneration of the heart recapitulate the DARS2 KO phenotype. However, at the age DKO^{L} display the described changes, none of them manifested in DARS2 KO mice, yet. CHOP KO mice generally did not exhibit differences to WT animals.

At the histological level first pathological changes at p17 (±2) not only appeared in DKO^{L} but also in DARS2 KO samples. Hematoxylin and eosin (H&E) staining were without pathological findings. In contrast, cytochrome c oxidase/ succinate dehydrogenase (COX/ SDH) staining, visualising the functionality of the respiratory chain by the respective enzymatic activities, uncovered anomalies in DARS2 KO and DKO^{L} mice. While DARS2 KOs presented first signs of COX deficiency, characterised by weakened brown staining, DKO^{L} mice developed a deficiency for both, COX and SDH. As frequently observed in mito-deficient mutants (Trifunovic et al., 2004), transmission electron microscopic (TEM) pictures visualised a mosaic distribution of mitochondria with structural defects in DKO^{L} mice. Structural defects ranged from loss of cristae to disturbed organellar integrity. Furthermore, the structural arrangement of sarcomeres was compromised (Figure 3.4). Collectively, the data clearly demonstrated that loss of CHOP in the context of disturbed mitochondrial proteostasis intensifies pathological changes in the heart. In comparison to DARS2 KO mice OXPHOS deficiency assessed by COX/SDH staining as well as degeneration of the cardiac tissue developed prematurely.

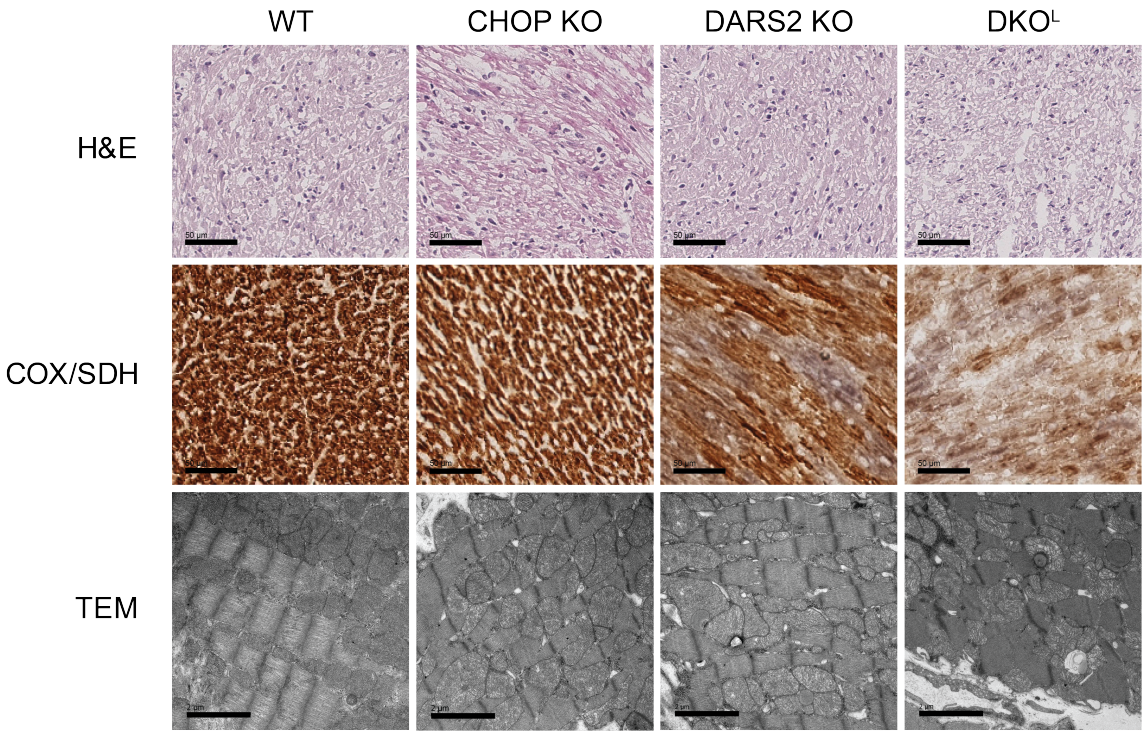

Figure 3.4: DARS2 KO and DKO^{L} hearts display pathological changes.
Histological, enzymatic and transmission electron microscopy (TEM)-based analyses of cardiac tissue sections (haematoxylin and eosin (H&E) and cytochrome c oxidase/ succinate dehydrogenase (COX/SDH) staining; scale bars: 50µm) (n=3) and biopsies (TEM, scale bars: 2µm) (n=1) at p17 (±2).

To perform an unbiased analysis of the consequences triggered by CHOP deficiency in the DARS2 KO background, whole tissue proteomics of mice at p6 and p17 (±2) were performed. While gene ontology enrichment analysis did not result in any significantly enriched terms at p6 (data not shown) the situation was different at p17 (±2). At that time, DKO^{L} mice exhibit robust enrichment of many metabolically associated terms in contrast to the respective controls (WT, CHOP KO and DARS2 KO). Besides categories related to oxidative phosphorylation, biological processes concerning amino acid metabolism were immensely represented (Figure 3.5).

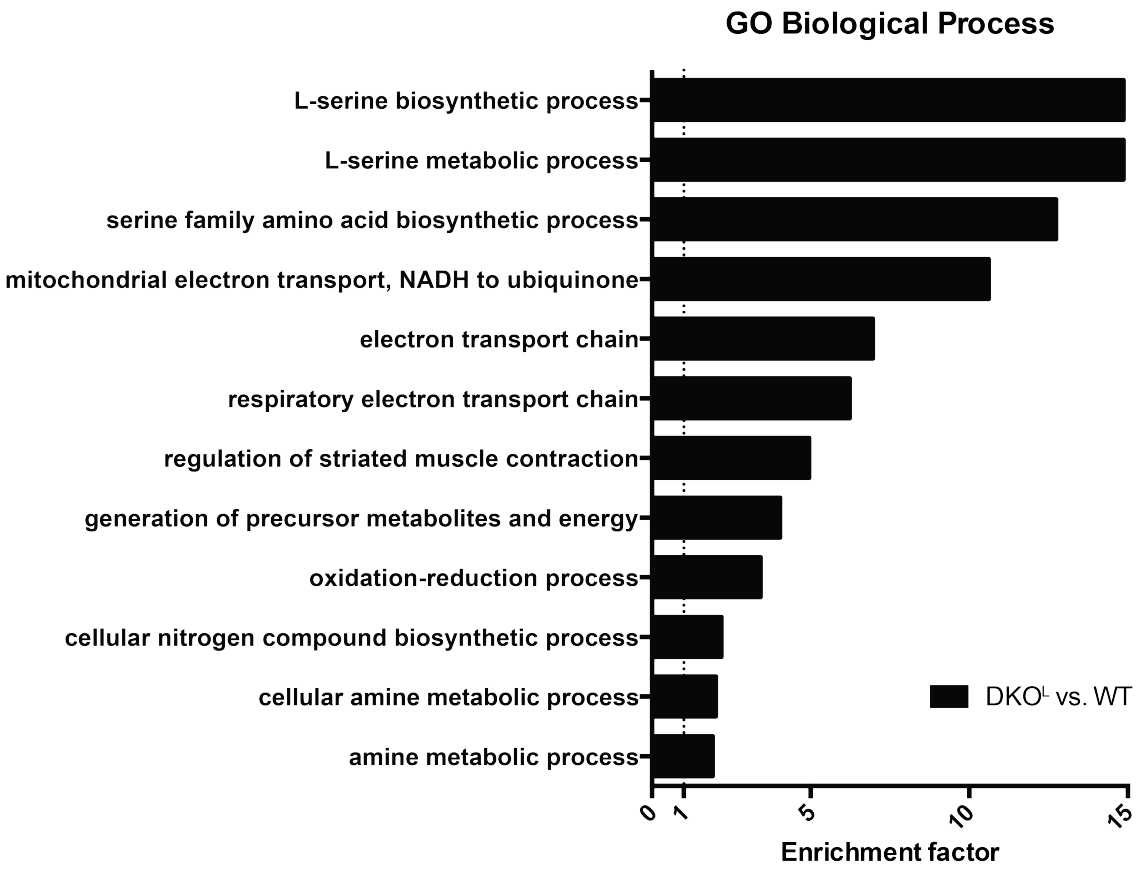

Figure 3.5: GO term analysis revealed strong enrichment of amino acid-related categories in DKO^{L} mice.

Gene enrichment analysis using gene ontology (GO) terms for biological pathways evaluating significant changes in the proteomic data set (FDR<0.05; Enrichment factor>1) of DKO^{L} vs. WT mice at p17 (±2). CHOP KO and DARS2 KO in comparison to WT mice did not display any significantly enriched GO terms.

With respect to the significant enrichment of amino acid metabolism-related GO terms in DKO^{L} mice, amino acid levels were additionally quantified by mass-spectrometry (Figure 3.6). Except for cysteine, all amino acids were successfully detected. In DARS2 KOs only two amino acids were changed: threonine (increased) and histidine (decreased). Consistent with the results from the proteomic analysis, 13 out of 19 amino acid species showed significant increases in DKO^{L} mice. Serine, glutamine, glutamate and aspartate levels were not changed. Considering the different serine-related GO terms enriched in DKO^{L} (Figure 3.5), the unaltered serine levels suggest an increased flux of serine into the one-carbon (1-C) cycle.

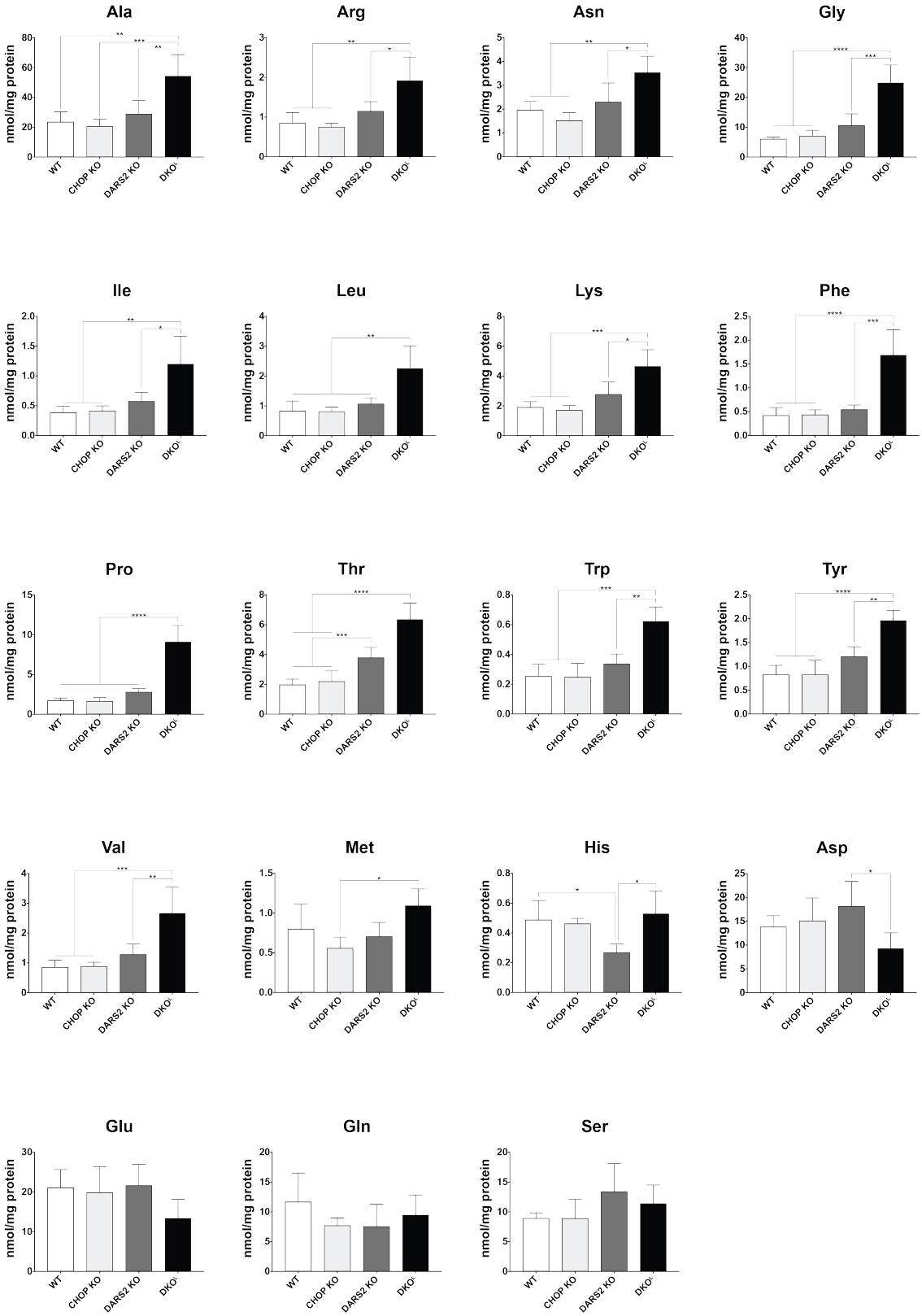

Figure 3.6: Metabolic alterations induced by loss of DARS2 and CHOP result in overall elevated amino acid levels in DKO^{L} mice.

Amino acid levels determined by liquid chromatography coupled to electrospray ionisation tandem mass spectrometry (n=4-5). Bars represent mean ± SD (One-way ANOVA, *p<0.05, **p<0.01, ***p<0.001, ****p<0.0001).

Similar to the amino acid-related results, the proteomic data set revealed only a few significant changes of individual RC subunits in DARS2 KO mice. In DKO^{L}s, the tendency towards reduced RC subunits was exacerbated with 43 significantly decreased RC subunits. No significant changes were observed in CHOP KO mice (Figure 3.7A). Surprisingly, super-complex (SC) assembly appeared to be affected in comparable proportions in DARS2 and DKO^{L} mice, suggesting an impairment at the assembly level despite less pronounced reduction of individual RC subunits in DARS2 KOs (Figure 3.7B). Northern blot analysis revealed significant increases of selected RC subunit-encoding transcripts (*cox3*, *nd1*) in DKO^{L} and DARS2 KO mice. Compared to DKO^{L} mice, increases of *cox3* and *nd1* levels in DARS2 KOs occurred to a lesser extent. In addition, the 12S mito-ribosomal RNA was up-regulated in DKO^{L} animals (Figure 3.7C, D). Based on those results and along with unaltered mtDNA levels (Figure 3.7E), potential causes of the strong alterations on the protein level in DKO^{L} animals most likely originating from the post-transcriptional level.

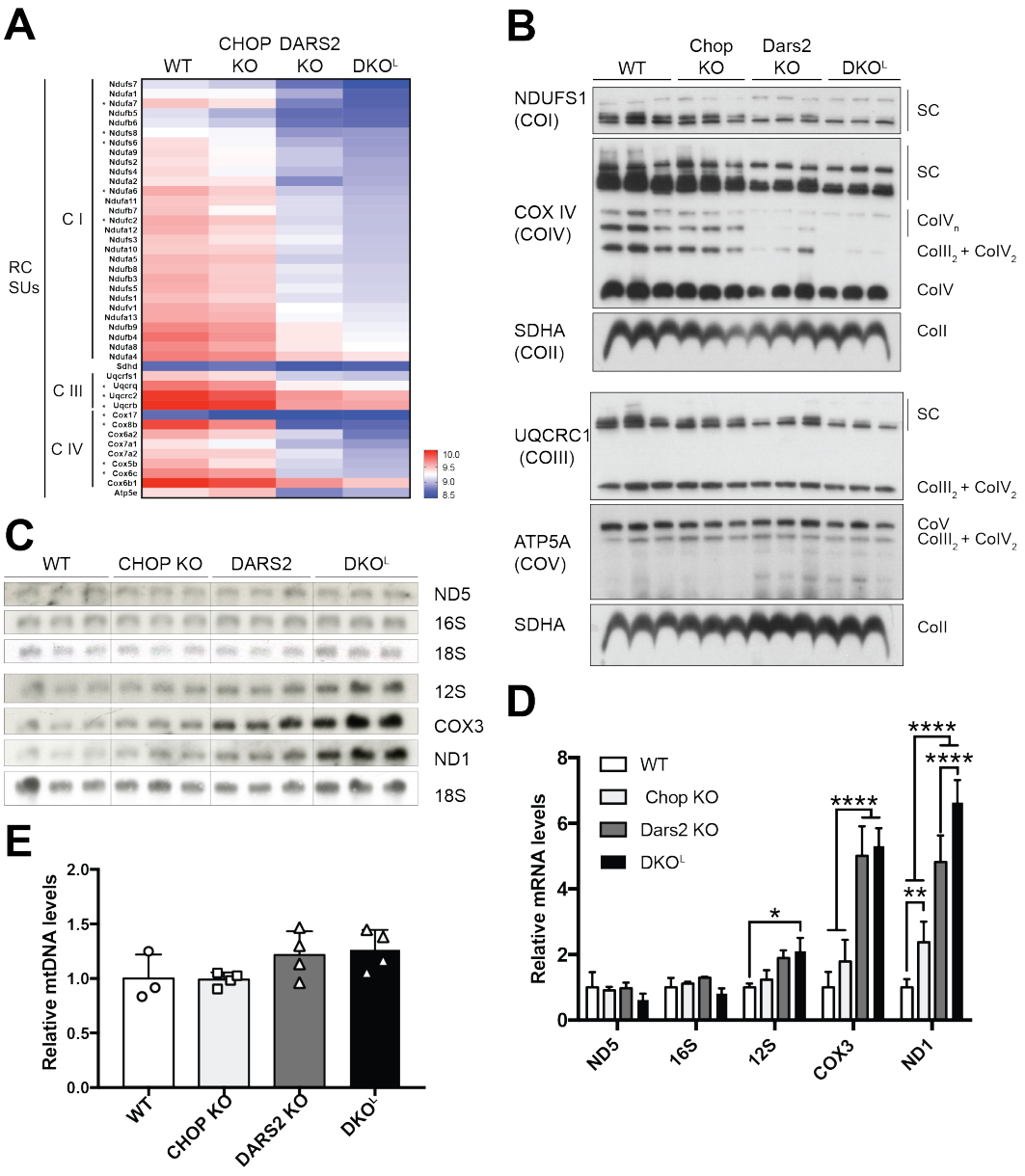

Figure 3.7: Lack of CHOP in DARS2-deficient hearts promotes loss of the respiratory chain. (A) Heatmap displaying the iBaq values of all significantly changed respiratory chain (RC) subunits (SUs) in the DKO^{L} background ($q<0.05$, $\log_2(FC)>|1|$) along with the according iBaq values in WT, CHOP KO and DARS2 KO mice. iBaq values were determined by label-free quantitative proteomics of the heart (n=4). RC SUs with significant changes in the DARS2 KO background are labelled with an asterisk. No significant changes occurred in CHOP KO compared to WT mice. (B) BN-PAGE and subsequent Western blot analysis of OXPHOS complexes and super-complexes (SCs) in isolated mitochondria (n=3). Subunit-specific antibodies (left) were used to detect respective subunit-containing complexes and SCs (right). (C) Northern blot analysis and (D) relative quantification of mitochondrial transcript levels. mRNA levels were normalised to 18S rRNA. (E) Relative mtDNA levels determined by qPCR of isolated DNA using an *Nd1*-specific primer pair. Results were normalised to hexokinase-2 expression. No significant

changes were detected. Bars represent mean ± SD (One-way ANOVA, *p<0.05, **p<0.01, ***p<0.001, ****p<0.0001).

DARS2 deficiency results in a primary defect in mitochondrial translation, which is the expected leading cause for the observed perturbations of the mitochondrial proteome. However, the mitochondrial proteome of DKO mice showed larger changes as the one of DARS2 KO animals (Figure 3.7A). In order to assess mitochondrial translation in DARS2 KO and DKO^{L} mice, *in organello* translation was performed with freshly isolated cardiac mitochondria. Although the overall synthesis rate of total mitochondrial proteins was not changed at p17 (±2) in DARS2 KO mice, individual proteins presented altered synthesis rates compared to CHOP KO and WT samples. Synthesis of mitochondria-encoded proteins was reduced, with the exception of five proteins (see bold labelling on the left side of Figure 3.8A) compensating on the level of overall synthesis rate (Figure 3.8A-C). Those proteins (namely ND2, ND1, ATP6, ATP8 and ND4L) contain low amount of aspartate residues, thus translation can occur more easily under conditions of a translation machinery devoid of aspartyl residues-charged tRNAs. Surprisingly, loss of CHOP in DARS2 KO animals additionally affected mitochondrial protein synthesis. The overall protein synthesis rate in DKO^{L} mitochondria was reduced by 20% (Figure 3.8C). Whereas the five above-mentioned RC SUs with low aspartate levels displayed the same synthesis pattern in DKO^{L} mitochondria, the reduction of the synthesis rate for all the other proteins was much stronger than in DARS2 KO mice (Figure 3.8A-B). Subsequently, the bioenergetic consequences of reduced RC subunit availability (at least partially) caused by diminished mitochondrial translation rates were assessed by high-resolution respirometry following a SUIT protocol (Figure 3.8D) (Lemieux et al., 2011). Therefore, freshly isolated cardiac mitochondria were provided with pyruvate, glutamate and malate as well as succinate, feeding electrons in complex I and II, respectively. Oxygen consumption rates were recorded in parallel. Oxygen consumption is correlating with the proportion of on-going ADP phosphorylation, hence state 3 is also called the phosphorylating state. Coupling efficiency was monitored by addition of the complex V inhibitor oligomycin (state 4, also called the non-phosphorylating state). To finally determine the maximum capacity of the electron transfer system (ETS) of complex I and II, mitochondria were uncoupled by FCCP (carbonyl cyanide 4-(trifluoromethoxy)phenylhydrazone) treatment. By additionally inhibiting complex I with rotenone, the maximum ETC capacity of complex II was determined. Complex I-mediated respiration as well as combined respiration of complex I and II proved to be significantly decreased in DKO^{L} mice compared to WT, CHOP KO and DARS2 KO mice. Additionally, proton leak characterised by reduced state 4 respiration was elevated in DKO^{L}. In line with complex I-based state 3 respiration being

mainly affected in DKO^{L} mice, the combined maximum capacity of the ETS for complex I and II was significantly reduced in those mice (Figure 3.8D).

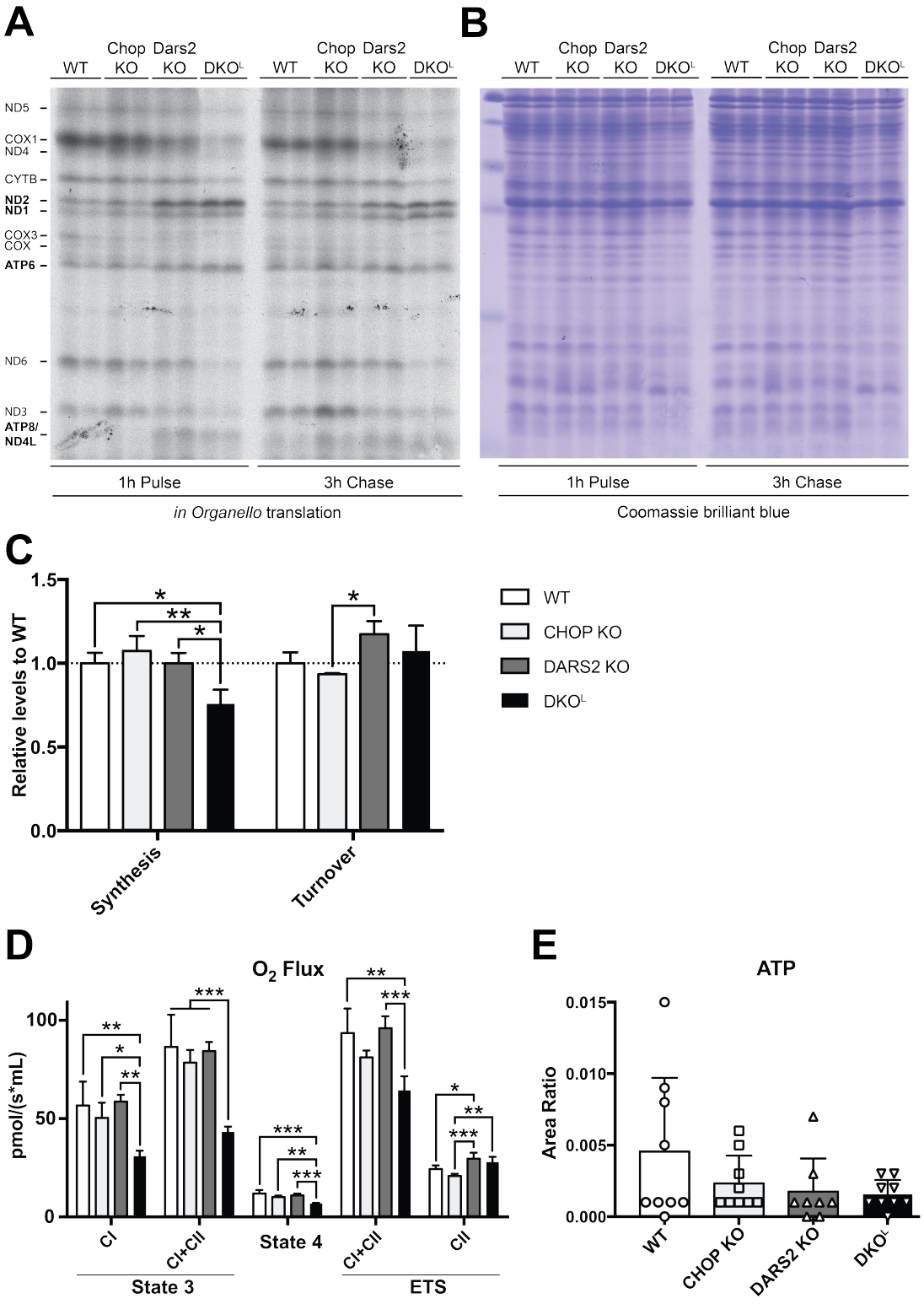

Figure 3.8: Mitochondrial translation defect in DKO^{L} results in a respiratory defect at the organelle level.

(A) *In organello* translation assay of cardiac mitochondria at p17 (±2). *De novo* protein synthesis was determined after one hour of ^{35}S-methionine pulse labelling; protein turnover was assessed

after three hours of cold chase. Subsequently, isolated proteins were separated by SDS-PAGE. Individual proteins exhibiting increased synthesis rates in DKO^{L} mice are labelled in bold. (B) Coomassie brilliant blue stained gels served as loading control for (A). (C) Relative protein synthesis and turnover rates calculated from the experiment shown in (A-B) and a second independent assay (n=3). (D) Oxygen consumption of intact cardiac mitochondria at p17 (±2) determined by oxygraph measurement. State 3: ADP-stimulated respiration of complex I (CI) and complex I and II (CI+CII) fed with the respective substrates (CI: pyruvate, malate, glutamate; CII: succinate). State 4: Determination of leak respiration by oligomycin-driven inhibition of CV. ETS: Maximum capacity of the ETS determined by titration with FCCP to uncouple mitochondria. Subsequent inhibition of CI by rotenone allowed determination of the maximal CII ETS capacity (n=3-4). (E) Cardiac ATP levels at p17 (±2) determined by metabolomic analyses: anion exchange chromatography followed by electrospray ionisation high-resolution mass spectrometry (n=8-9). Bars represent mean ± SD (One-way ANOVA; *p<0.05, **p<0.01, ***p<0.001, ****p<0.0001).

Finally, cardiac ATP levels were determined (Figure 3.8E). A possible trend towards decreased ATP levels in DKO^{L} mice was detected by mass spectrometry, suggesting that the previously detected respiratory defect impacts on ATP availability in the heart. However, those results have to be interpreted with caution, as the analysis could not be performed under ideal conditions.

Taken together, those results are raising novel issues. First, similar complex assembly defects in DARS2 KO and DKO^{L} mice are not resulting in similar respiratory defects, as DARS2 KO respiration rates are WT-like. Notably, TEM pictures revealed local accumulations of mitochondria displaying severely compromised organellar structure in DKO^{L} animals. Those defects most likely impact on the membrane potential and thereby negatively affect mitochondrial respiration. Second, mitochondrial translation is affected at a much earlier time point in DKO than in DARS2 KO mice in general, arguing for additional effects beyond loss of *Dars2* impacting on translation.

To investigate if DARS2-deficiency, the resulting respiratory chain defects and possibly induced metabolic adaptations also affect the TCA cycle, TCA cycle intermediates were quantified by metabolomic analyses (Figure 3.9). The TCA cycle is not only required to feed the respiratory chain with NADH and $FADH_2$, respectively, but also provides precursors for numerous biosynthetic pathways (Owen et al., 2002). The most prominent changes were detected for citrate. In DKO^L mice, citrate levels show a four to five-fold increase in comparison to the other three genotypes. This phenotype was described before for patient cell lines harbouring mtDNA mutations (Chen et al., 2018).

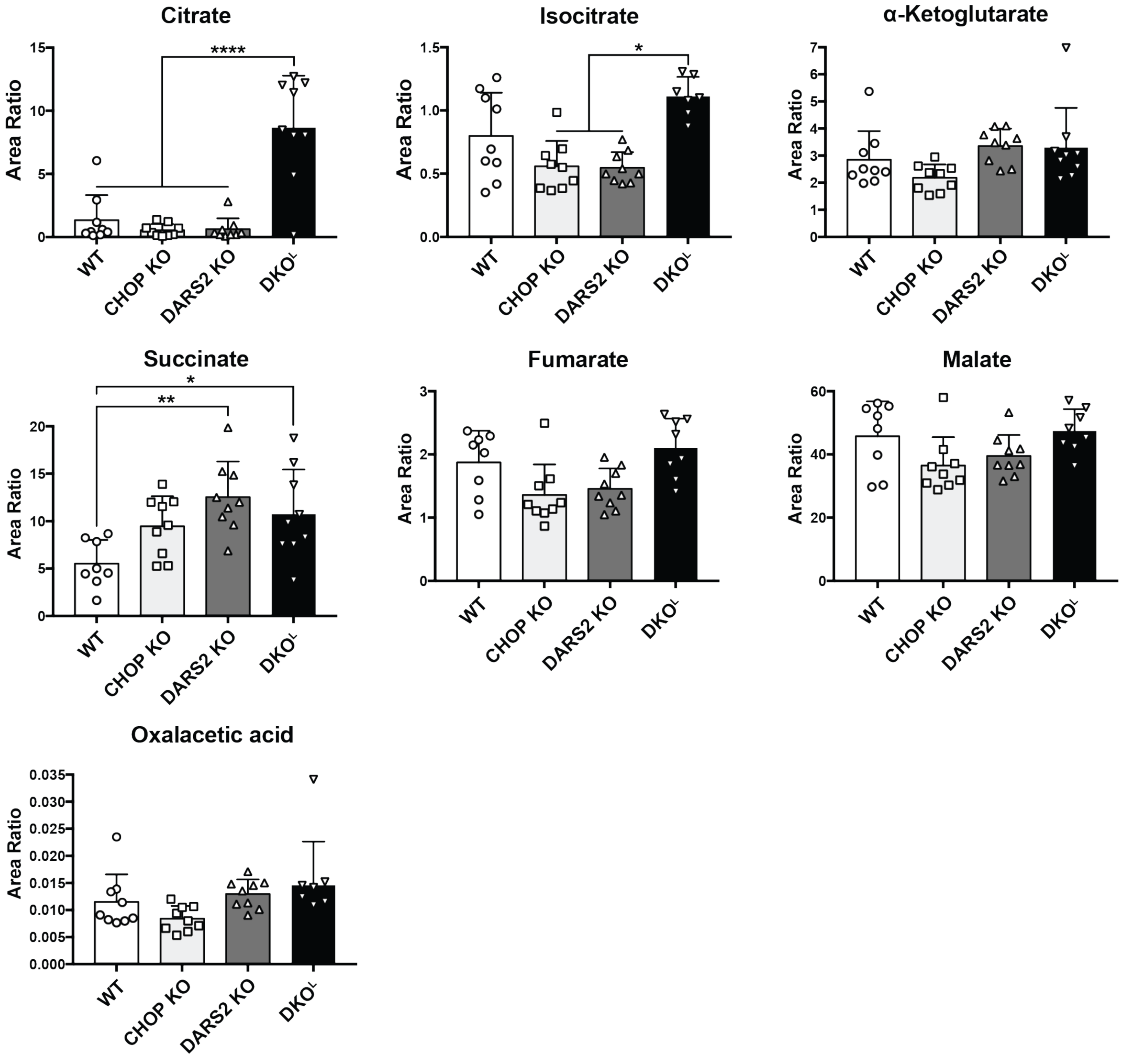

Figure 3.9: DKO^L mice accumulate high levels of citrate in cardiac tissue.

Levels of TCA cycle intermediates at p17 (±2) determined by metabolomic analyses: anion exchange chromatography followed by electrospray ionisation high-resolution mass spectrometry (n=7-9). Bars represent mean ± SD (One-way ANOVA; *p<0.05, **p<0.01, ***p<0.001, ****p<0.0001).

3.1.3 Mitochondrial and cellular stress responses activated in DARS2 KO and DKO^{L} mice

As CHOP is a stress-responsive TF, it is essential to analyse how the deficiency of this TF influences the resulting mitochondrial and cellular stress-related pathways. Therefore unbiased techniques (proteomics, transcriptomics) were combined with targeted approaches in order to identify the major driving processes and monitor pathways with possible relevance at the same time.

3.1.3.1 Omics analyses showcase transcriptional and translational changes of ATF4 targets as a central aspect of the response to mitochondrial dysfunction in DARS2 KO and DKO mice

The global approach of omics analyses can facilitate the perception of a broader context, constituted of many single changes. Aiming to understand the on-going early changes in DARS2 KO mice at p17 (±2), the RNAseq data set was filtered, selecting only significantly changed transcripts ($p<0.05$; FC larger than 1.5 or smaller than -1.5) in DARS2 KO compared to WT mice. The respective FCs of selected transcripts for CHOP KO, DARS2 KO, and DKO^{L} vs. WT mice were plotted on a heat map (Figure 3.10A). CHOP KO samples displayed no significant changes contrary to the transcript levels in DKO^{L} samples, which were all (like the DARS2 KO samples) significantly changed. The spectrum of determined FCs in DARS2 KO mice was relatively narrow, ranging from -4.7 to 4.32 vs. -2.3 to 240.47 in DKO^{L} mice. Also, the predominant number of the selected transcripts in DARS2 KO and DKO^{L} samples was up-regulated.

Interestingly, the massive increase of FC range in DKO^{L} mice was solely due to up-regulation, as changes in down-regulated transcripts were in a similar range in DARS2 KO and DKO^{L} animals. Hence, loss of *Chop* entails a general re-enforcement of transcriptional alterations already present in DARS2 KO mice. The transcriptional up-regulation of transcripts suggests a repressive effect of CHOP (Figure 3.10A). For further analysis of the RNAseq data set, the Cytoscape plug-in iRegulon, utilising large motif and track collections to predict putative regulators of a selected gene list, was used (Janky et al., 2014). ATF4 was identified with a normalised enrichment score (NES) of 18.73 as the presumed master regulator of the transcript list. For comparison: the second-best motive cluster obtained an NES of 5.29. According to this analysis, 41 of the 60 differentially expressed transcripts in DARS2 KO mice are ATF4 targets. Additionally, the transcription of the vast majority of those dedicated transcripts is further increased upon CHOP deficiency (Figure 3.10B).

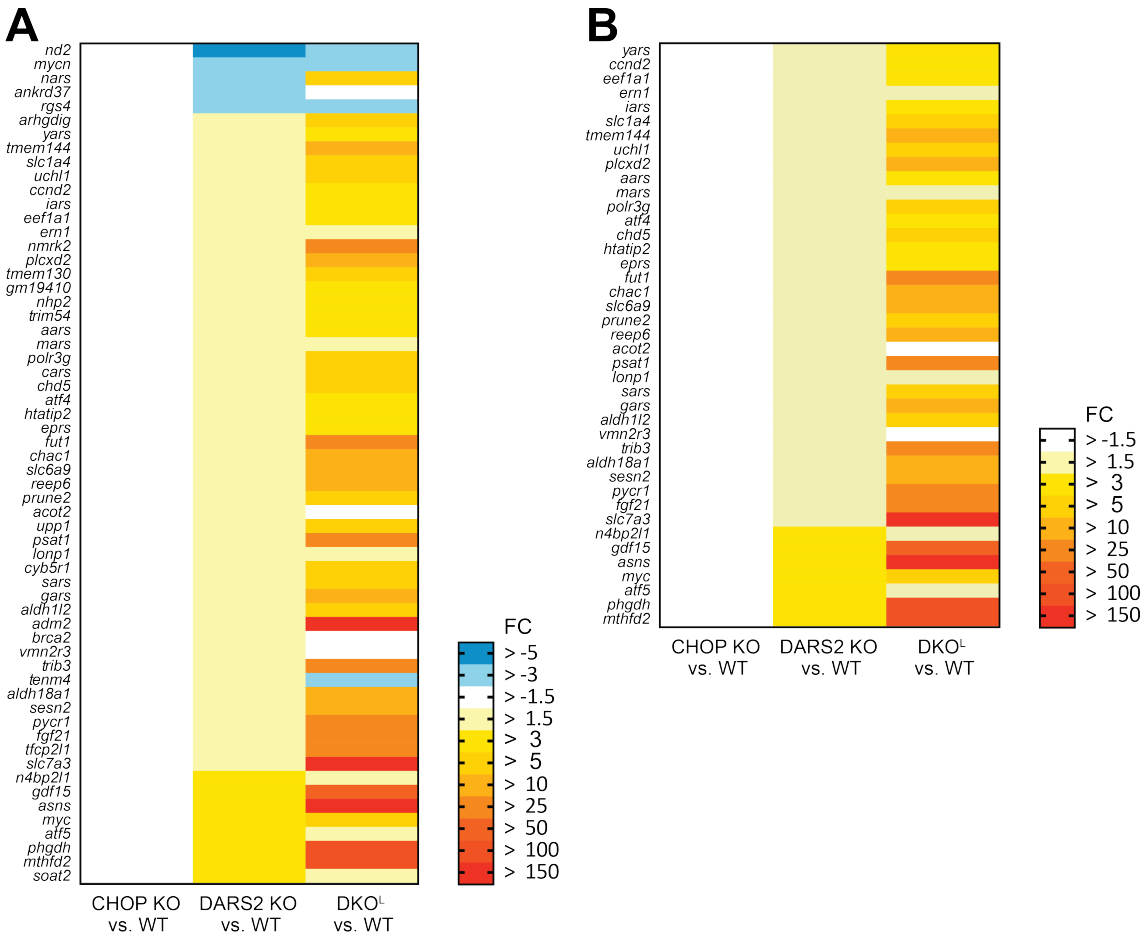

Figure 3.10: RNAseq analysis suggests ATF4-like regulation of DARS2 KO and DKO^{L} transcripts.

(A) Heat map displaying the relative FCs of all significantly changed transcripts in the DARS2 KO background ($p<0.05$, $FC>|1.5|$) along with the according FCs in CHOP KO (no significant changes) and DKO^{L} mice. FCs were determined by RNAseq of the hearts at p17 (±2) (n=4). (B) Heat map displaying the respective transcripts of (A) identified by *cis*-regulatory sequence analyses using iRegulon as potential ATF4 targets.

Often enough, the central dogma of molecular biology is not applicable one-to-one, transcriptional changes not necessarily being followed by similar changes of the proteome. To understand if the observed enhanced ATF4-like regulation in DKO^{L} compared to DARS2 KO animals on the transcript level is conveyed to the protein level as well, the proteomics data of DKO^{L} and DARS2 KO samples were directly compared. Selecting only significantly increased proteins in DKO^{L} vs. DARS2 KO samples ($q<0.05$, $FC>2$), a list of 62 proteins was generated. Further analysis of this list using iRegulon (Janky et al., 2014) affirmed a major proportion of ATF4 targets (33/62) among significantly increased proteins in the DKO^{L} vs. DARS2 KO mice (Figure 3.11). Collectively, the omics analyses provide evidence for congruent changes in the transcriptome and translatome of DARS2 KO and DKO^{L} mice. DKO^{L} samples illustrated

a reinforced intensity of the detected changes in DARS2 KO mice. Furthermore, ATF4-like regulation was identified as the most probable cause for the mentioned transcriptional and translational changes.

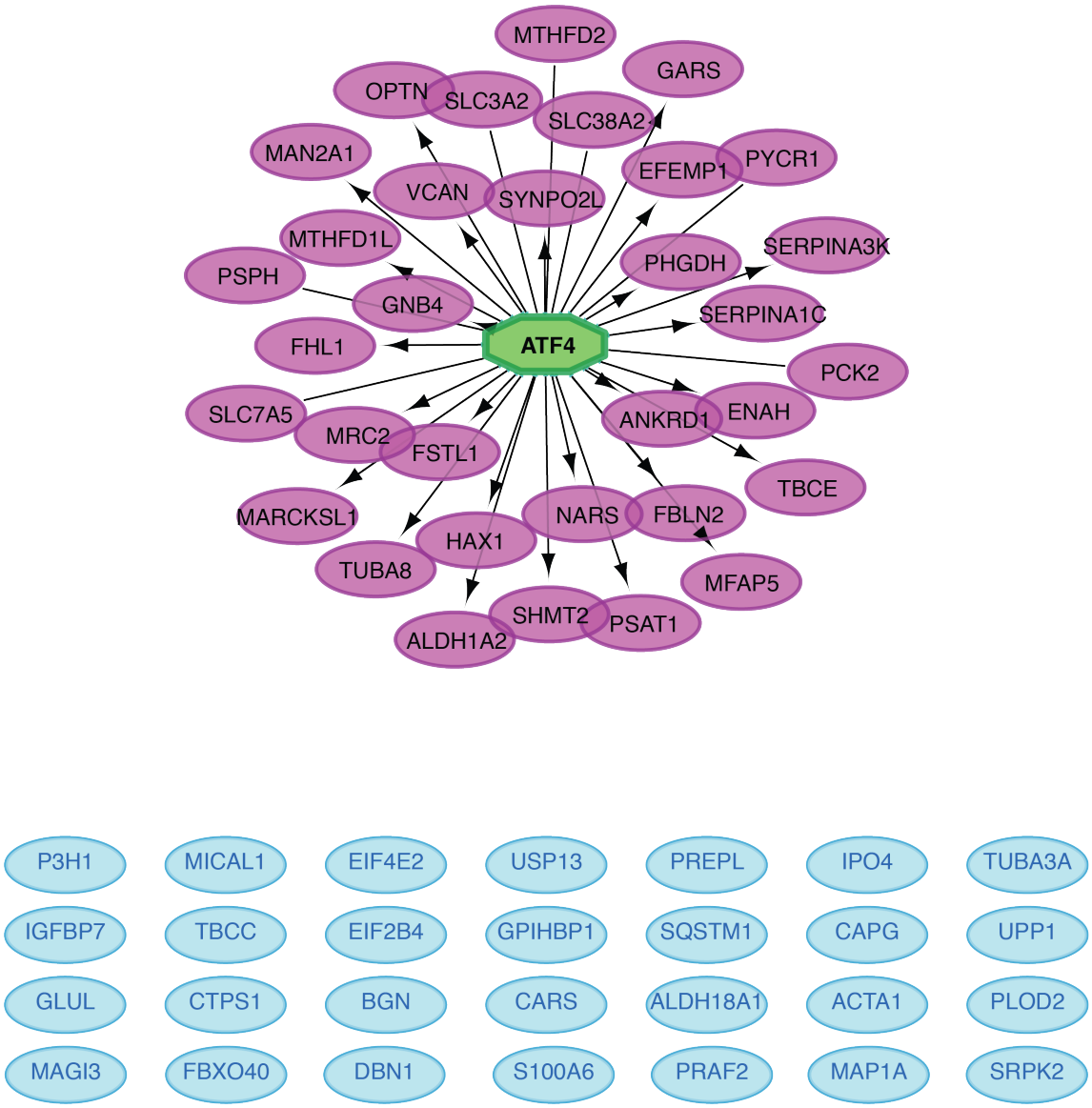

Figure 3.11: Enhanced ATF4-like regulation of the DKO^{L} proteome.

Classification of significant changes ($q<0.05$, $\log_2(FC)>|1|$) in the DKO^{L} vs. DARS2 KO proteomes determined by label-free quantitative proteomics of cardiac samples at p17 (±2) (n=4) by means of the Cytoscape plug-in iRegulon in ATF4 (violet) and non-ATF4 targets (blue).

3.1.3.2 ISR activation in DKO^{L} exceeds the degree of activation in age-matched DARS2 KO mice

The omics analyses suggested a CHOP-dependent role in phenotype progression for ATF4. Since CHOP had been previously linked to both, the UPR^{mt} and the ISR (Aldridge et al., 2007; Horibe and Hoogenraad, 2007; Michel et al., 2015; Restelli et al., 2018; Zhao et al., 2002), it seemed obvious to subject those stress responses to a general investigation. First analyses of commonly used UPR^{mt} markers such as the mitochondrial proteases LONP1 (Lon protease homolog, mitochondrial), AFG3L2 (AFG3-like protein 2) and CLPP (ATP-dependent Clp protease proteolytic subunit, mitochondrial) on the protein level did not reveal significant changes neither in DARS2 KO nor DKO^{L} mice (Figure 3.12A, B).

As mentioned in the introduction, the UPR^{mt} concept harbours deficits regarding the precise definition of the pathway (1.2.1.2). Also, the method of choice to detect UPR^{mt} activation is a matter of debate. As changes of chaperones - regularly present at high levels in the cell - are often barely visible on the protein level, the quantification of transcript levels was proposed as gold standard marker for UPR^{mt} activation (Münch, 2018). Although the biological significance of those changes are worthy of discussion, the transcript levels of three UPR^{mt}-associated chaperones and proteases each are listed below (Table 3.1). Based on the debatable criteria proposed in the publication mentioned above, it could be reasoned that the UPRmt is activated in DKO^{L} mice.

Table 3.1: RNAseq data suggest activation of the UPR^{mt} in DKO^{L} mice.
*p<0.05, **p<0.01, ***p<0.001, ****p<0.0001

Transcript	DARS2 KO vs. WT		DKO^{L} vs. WT		DKO^{L} vs. DARS2 KO	
	Fold change	P-value	Fold change	P-value	Fold change	P-value
mtHsp70	1.31	****	2.13	****	1.58	****
hsp10	1.1	0.09	1.66	****	1.49	****
hsp60	1.15	***	1.17	***		
lonp1	1.73	****	2.57	****	1.33	**
afg3l2	1.1	*	2.26	****	2.04	****
yme1l1	-1.05	0.31	1.56	****	1.63	****

Whereas ATF4 was not detectable under unstressed conditions in WT and CHOP KO samples, DKO^{L} mice exhibited significantly increased ATF4 protein levels. Also, DARS2 KO animals showed a trend towards augmented ATF4 protein levels. The spread of ATF4 protein levels most probably reflects differences in the phenotype progression of individual animals (Figure 3.12A, B). A direct measure for ISR activation is an increased proportion of phosphorylated eIF2α moieties. Both DARS2 KO and DKO^{L} mice presented explicit activation of the ISR. DKO^{L} animals, however, clearly exceeded the phosphorylated vs. un-phosphorylated eIF2α ratio of DARS2 KO mice (Figure 3.12C, D). Protein levels of the *bona fide* ATF4 targets ASNS (asparagine synthetase), MTHFD2 (mitochondrial methylenetetrahydofolate dehydrogenase), SHMT2 (mitochondrial serine hydroxymethyltransferase) and PYCR1 (pyrroline-5-carboxylate reductase) were analysed, to assess whether increased ATF4 protein levels resulted into increased activation of ATF4 targets. A vast increase ranging from 10 to 275-fold of all four ATF4 targets was detected in DKO^{L} mice (Figure 3.12E).

Collectively, the data provided minor evidence for the activation of the UPR^{mt} in DARS2 KO and DKO^{L} mice. Contrary to this, the ISR was doubtlessly activated in both DARS2-deficient mouse models. The extent of ISR activation, however, is amplified by a multiple of times upon CHOP deficiency.

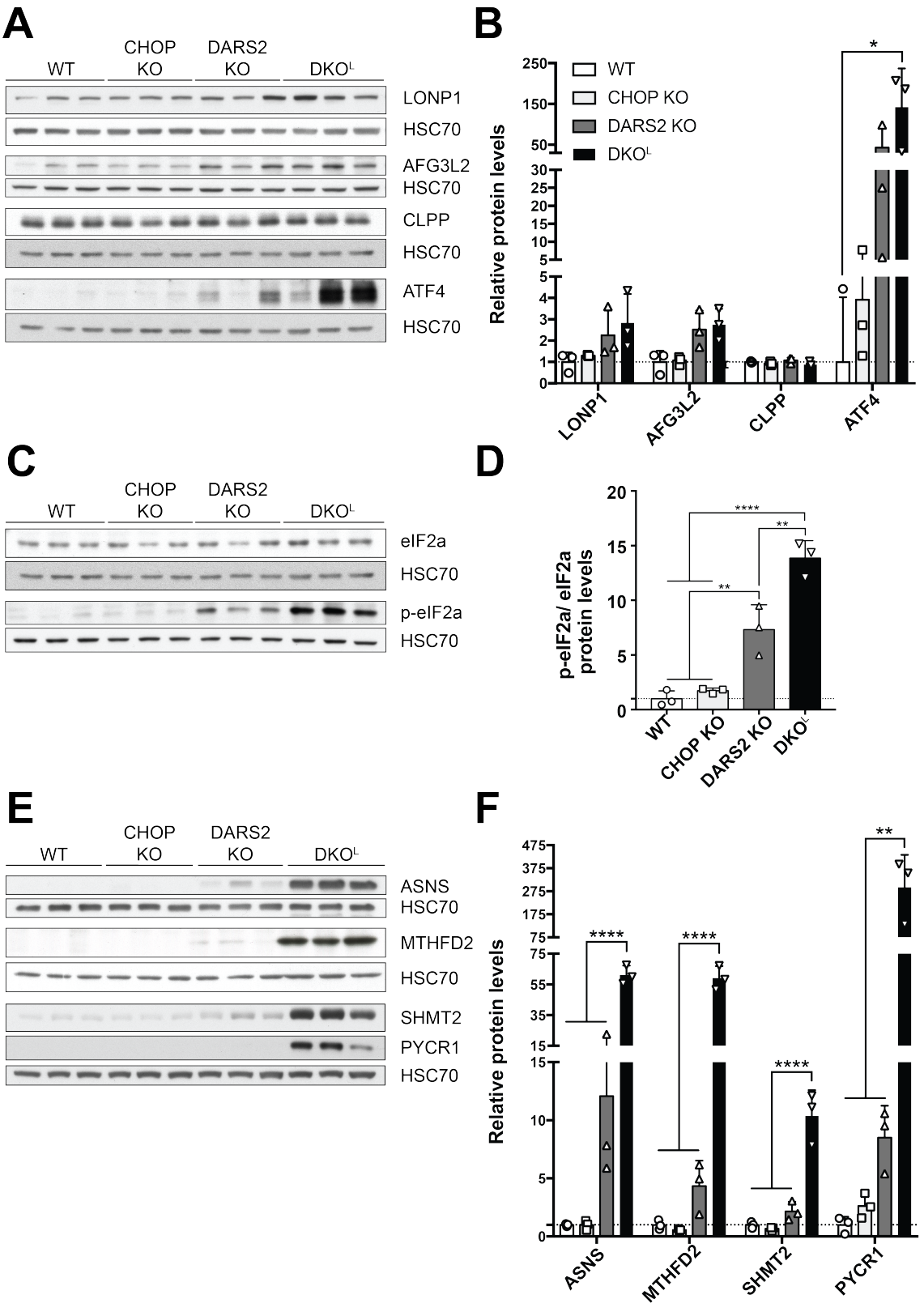

Figure 3.12: Distinct ISR activation in DARS2 KO mice is tremendously enhanced upon loss of *Chop*.

Western blot analysis of UPR^{mt} markers (A), total and pSer51 eIF2α (C) and ATF4 downstream targets (E). HSC70 serves as loading control. (B, D, F) Quantification of Western blots shown in

(A, C, E). Experiments were performed on cardiac lysates of mice at p17 (±2). Bars represent mean ± SD (One-way ANOVA, *p<0.05, **p<0.01, ***p<0.001, ****p<0.0001).

3.1.3.3 The ISR is the earliest detected activated stress pathway in DKO animals

It is commonly accepted, that during the terminal stage of a phenotype large variety of changes occur, complicating the task to separate cause and consequence. For this reason, we decided to analyse the animals not only around p17 (±2) during the terminal stage of DKO^{L} mice, but also at one week of age (p6), far before the health status of DKO mice deteriorates. The corresponding proteomic data set provided us with a list of in total six significantly changed proteins in DKO compared to WT mice (Table 3.2).

Table 3.2: Significantly changed proteins (q<0.05) determined by label-free quantitative proteomics of cardiac samples at p6 in DKO vs. WT mice.

*p<0.05, **p<0.01, ***p<0.001, ****p<0.0001, n.s.: not significant

Protein	CHOP KO vs. WT		DARS2 KO vs. WT		DKO vs. WT	
	Fold change	q-value	Fold change	q-value	Fold change	q-value
GBP5	1.84	n.s.	22.61	n.s.	21.51	*
NUDT12	18.16	****	19.59	n.s.	19.28	*
TUBA1c	10.49	****	12.57	n.s.	7.92	*
EPPK1	1.10	n.s.	-1.49	n.s.	-5	*
RPAP1	-1.96	n.s.	-4.55	n.s.	-11.11	****
ABLIM1	-2.94	n.s.	-2.78	n.s.	-11.11	*

Out of those six candidates, GBP5 (Guanylate-binding protein 5) was the only protein striking out due to a possible link to mitochondrial dysfunction. GBP5 was previously shown to be an activator of the NLRP3 (NACHT, LRR and PYD domains-containing protein 3) inflammasome assembly in mammals (Shenoy et al., 2012). The link between innate immunity and mitochondria is known for a long time. In recent years the topic attracted notice in the scientific community since mtDNA was established as a cell-intrinsic trigger of the anti-viral innate immune response (Oka et al., 2012; West et al., 2015). NLRP3 inflammasome activation was assessed indirectly by caspase-1 and interleukin-1β cleavage, in order to investigate whether inflammasome activation is playing a role in DARS2 KO or DKO animals. However, in neither case significant changes were detected (data not shown). Furthermore, the protein levels of NLRP3 and ASC, an activating adapter for the inflammasome formation (He et al., 2016b), were not affected (Figure 3.13A). In DARS2 KO mice no significant changes were detected.

Although, the RNAseq analysis around p6 did not reveal significant changes (data not shown) the mRNA levels of a few dedicated transcripts officiating as markers for the UPR^{mt} or the ISR were tested (Figure 3.13B). Because the two ATF4 targets *Cth* and *Mthfd2* showed a high level of variation, observed strong tendencies (eight-fold and 14-fold, respectively) for up-regulation in DKO mice were not significant (Figure 3.13B). As the ISR signalling cascade starts with eIF2α phosphorylation resulting in increased *atf4* translation and preceding transcriptional changes in the nucleus (Pakos-Zebrucka et al., 2016), phospho-eIF2α and ATF4 protein levels were analysed. Similarly to ATF4 target mRNA levels before, individual DKO animals exhibited increased levels of phosphorylated eIF2α and ATF4, showcasing differences in phenotype progression (Figure 3.13C-F). Taken together, analysis of one-week-old animals provided first indications for an activated ISR in DKO mice.

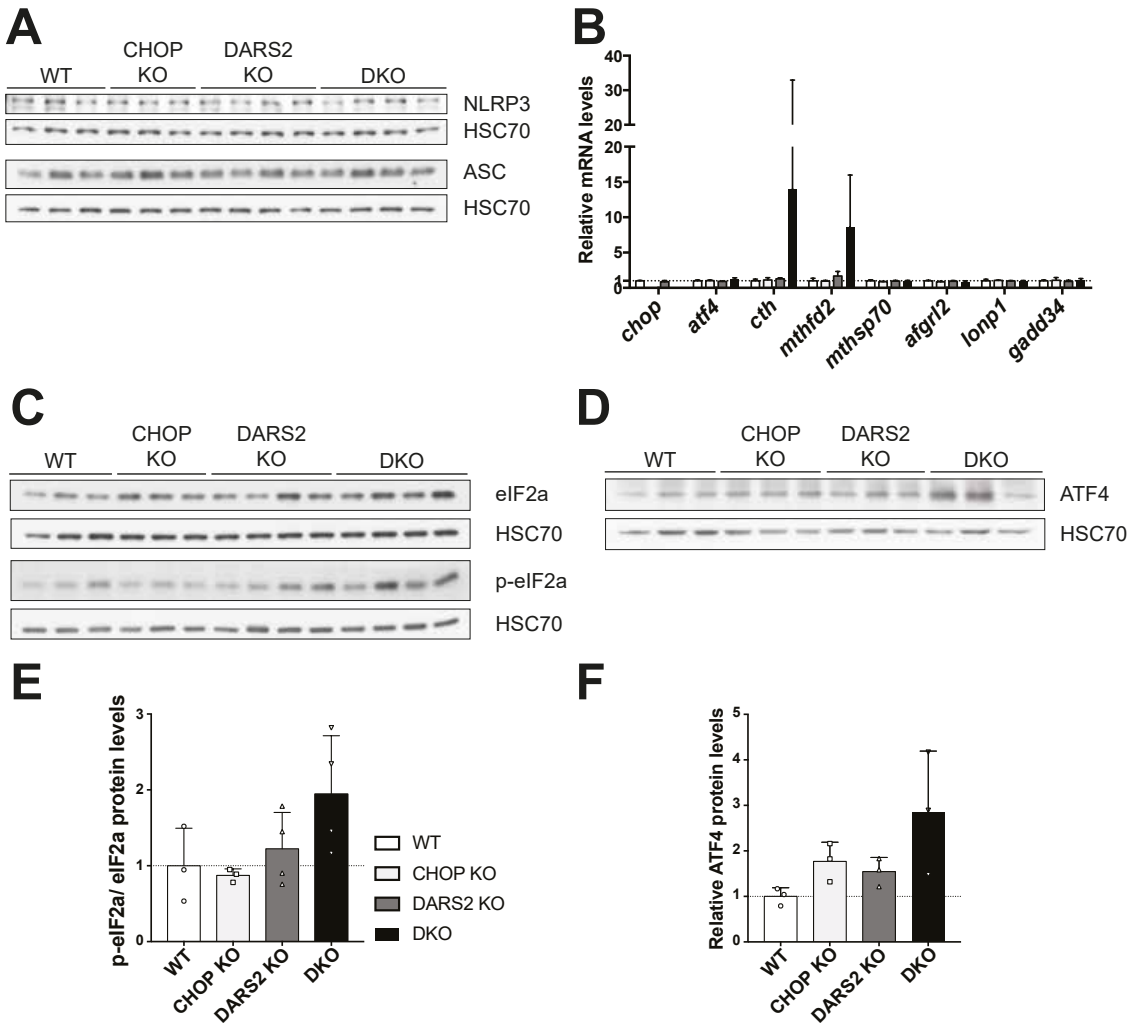

Figure 3.13: At p6 DKO animals provide first indications for ISR activation.

(A) Western blot analysis and (B) relative protein levels of NLRP3, ASC and MRPS12. (C, D) Western blot analysis and (E, F) relative protein levels of total and pSer51 eIF2α as well as ATF4, respectively. HSC70 serves as loading control. Bars represent mean ± SD (One-way ANOVA, no significant changes detected).

3.1.3.4 UPR^{mt} and ISR show different degrees of activation during the terminal stages of DARS2 KO and DKO^{L} animals, respectively

A direct comparison between the terminal stages of DKO^{L} mice around p17 (±2) and DARS2 KO mice at six weeks of age could provide further insight into the relative degree of activation of UPR^{mt} and ISR.

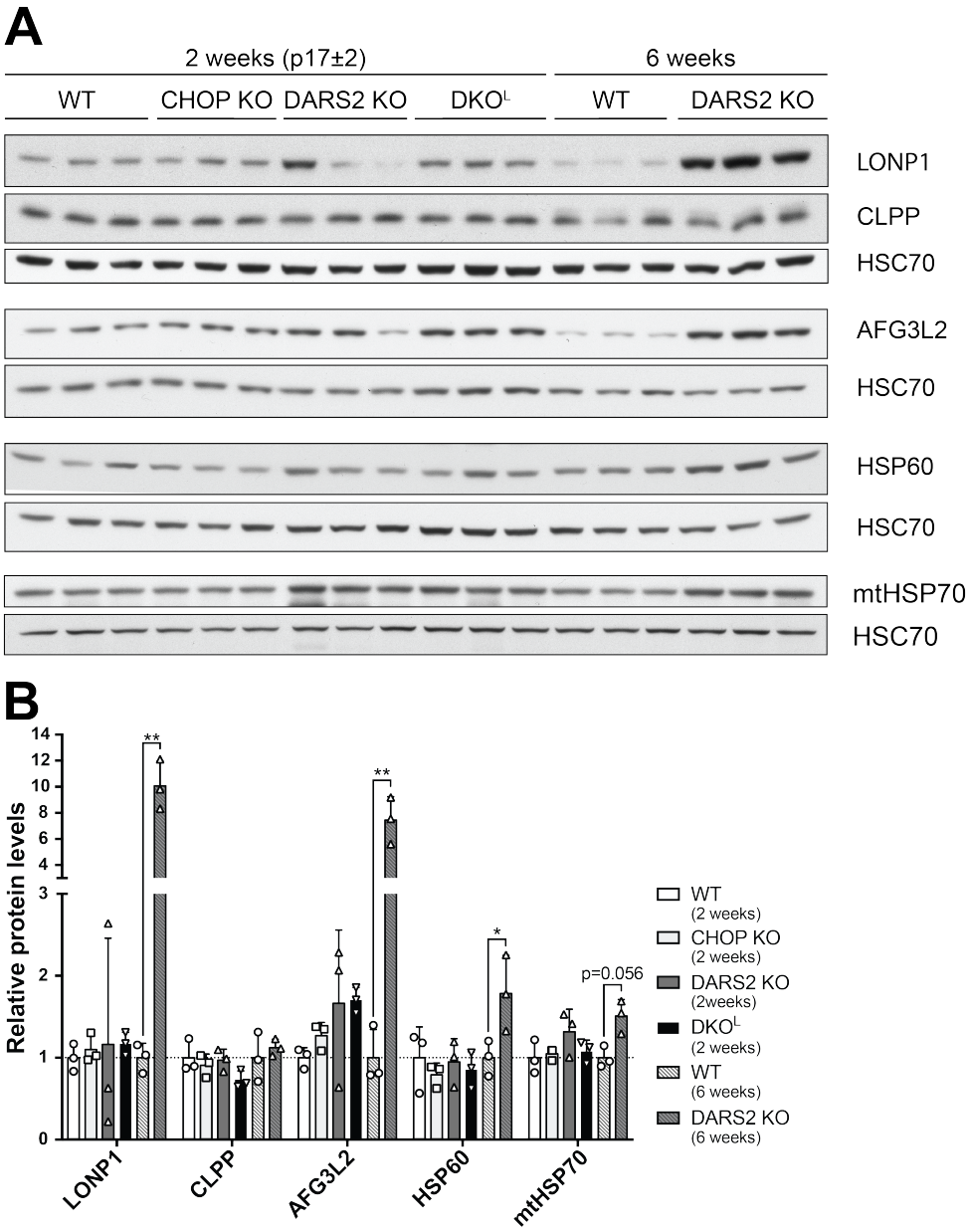

Figure 3.14: DARS2 KO mice display upregulation of UPR^{mt} markers at six weeks of age. (A) Western blot analysis and (B) relative protein levels of UPR^{mt} markers. HSC70 serves as loading control. Bars represent mean ± SD, samples were normalised to WT mice of the respective age (2 weeks (p17±2): one-way ANOVA; 6 weeks: two-tailed t-test; *p<0.05, **p<0.01).

Previous results demonstrated that UPR^{mt} activation was not detectable on the protein level neither in DARS2 KO nor DKO^{L} animals at p17 (±2) (3.1.3.2). In accordance with

previous work of the lab, up-regulation of the UPR^{mt} markers LONP1, AFG3L2, HSP60 and mtHSP70 but not CLPP were observed in DARS2 KO mice at six weeks of age (Dogan et al., 2014; Seiferling et al., 2016) (Figure 3.14). Based on those results a major role of the UPR^{mt} in the accelerated deterioration of the health status of DARS2 KO mice induced by CHOP deficiency is improbable.

Contrary to the UPRmt, first signs of ISR activation in individual DKO mice were already detected at p6 (3.1.3.3). At p17 (±2) the ISR was strongly activated in DKO^{L} mice while individual DARS2 KO mice exhibited first signs of initial activation (3.1.3.2). At six weeks of age, DARS2 KO animals displayed robust ISR activation characterised by a significantly increased phospho-eIF2α to eIF2α ratio comparable to DKO^{L} mice around p17 (±2) (Figure 3.15A, C). Moreover, increased ATF4 activity in DARS2 KO animals was determined by protein level quantification of the *bona fide* ATF4 targets SHMT2, ASNS and PYCR1 (Figure 3.15B, D). Taken together, the data suggest a time-staggered activation of the ISR initiated around p6 in DKO^{L} and around p17 (±2) in DARS2 KO mice. Direct comparison of the p-eIF2α to eIF2α ratios of DKO^{L} and DARS2 KO during the respective terminal stages (Figure 3.15C) might indicate a stronger activation of the stress pathway in DKO^{L} mice.

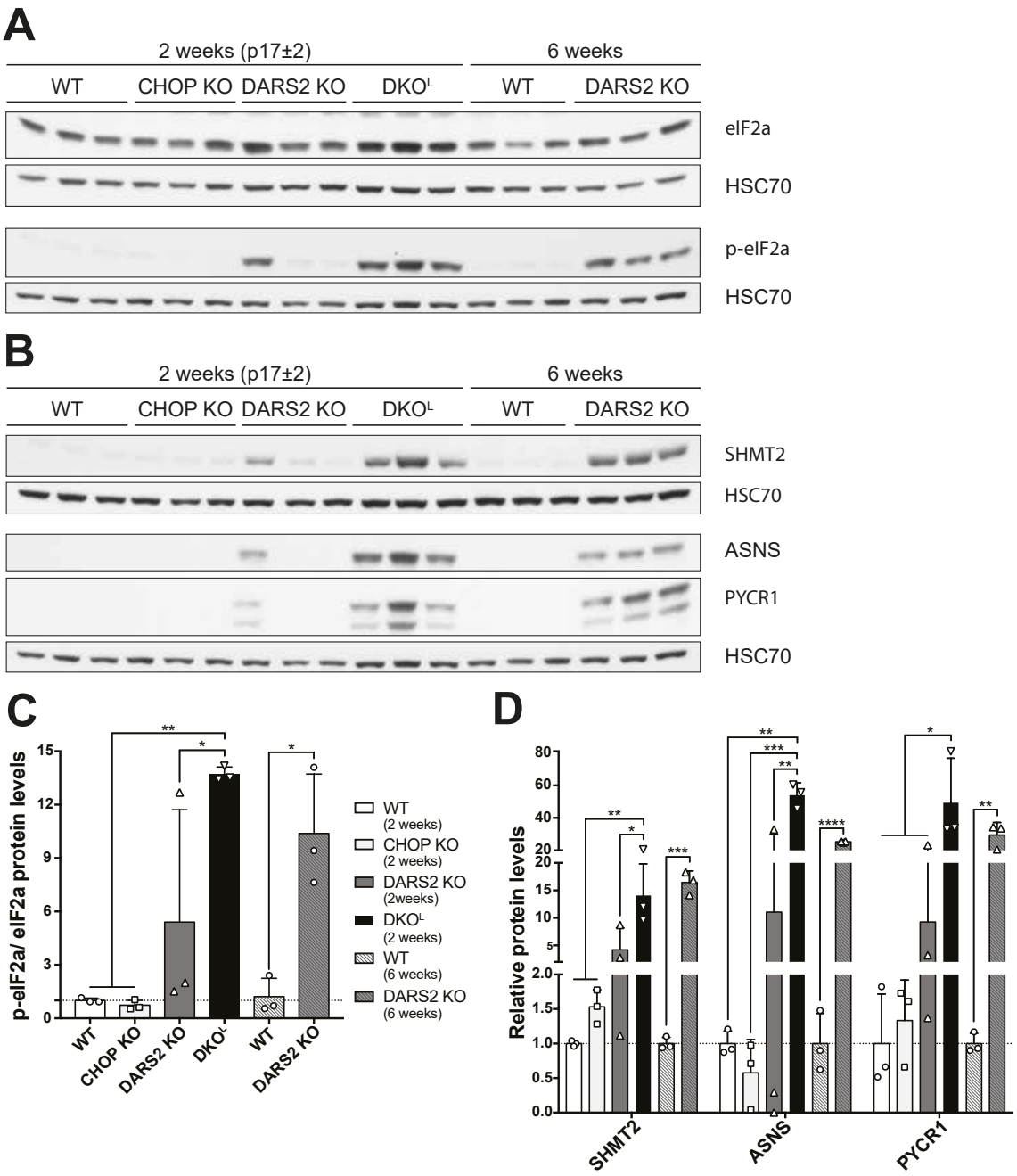

Figure 3.15: Loss of *Chop* precedes ISR activation caused by DARS2 deficiency from six to less than three weeks of age.

Western blot analysis of total and pSer51 eIF2α (A) and ATF4 downstream targets (B). HSC70 serves as loading control. (C, D) Quantification of Western blots shown in (A, B). Bars represent mean ± SD, samples were normalised to WT mice of the respective age (2 weeks (p17±2): one-way ANOVA; 6 weeks: two-tailed t-test; *p<0.05, **p<0.01, ***p<0.001, ****p<0.0001).

3.1.3.5 Activation of the ISR results in inhibition of cytoplasmic protein synthesis in DKO^{E} mice

The ISR pathway acts through two distinct effects: (i) preferential translation of stress-responsive mRNAs like the *atf4* transcript and (ii) global inhibition of CAP-dependent protein synthesis (Pakos-Zebrucka et al., 2016). Given the high relevance of the ISR for the mouse models in this study (3.1.3.1 - 3.1.3.4), relative protein synthesis rates were assessed (Figure 3.16). During the ISR a shift in translational programmes occurs, as the formation of the pre-initiation complex (PIC) for translation is inhibited by phosphorylation of eIF2α. The resulting inhibition of cytoplasmic protein synthesis is accomplished by eIF2α-independent translation of a specific subset of mRNAs, like the *atf4* transcript (Guan et al., 2017; Krishnamoorthy et al., 2001; Pakos-Zebrucka et al., 2016). *In vivo* protein synthesis rates were determined by the SUnSET assay. This assay is based on intraperitoneal puromycin injection in mice and subsequent detection of puromycin incorporation in nascent protein chains by Western blot (Schmidt et al., 2009). Cytoplasmic protein synthesis rates were equal among all four genotypes at one week of age (Figure 3.16A, C), in line with only mild changes on the molecular level in DKO mice at p6 (3.1.3.3).

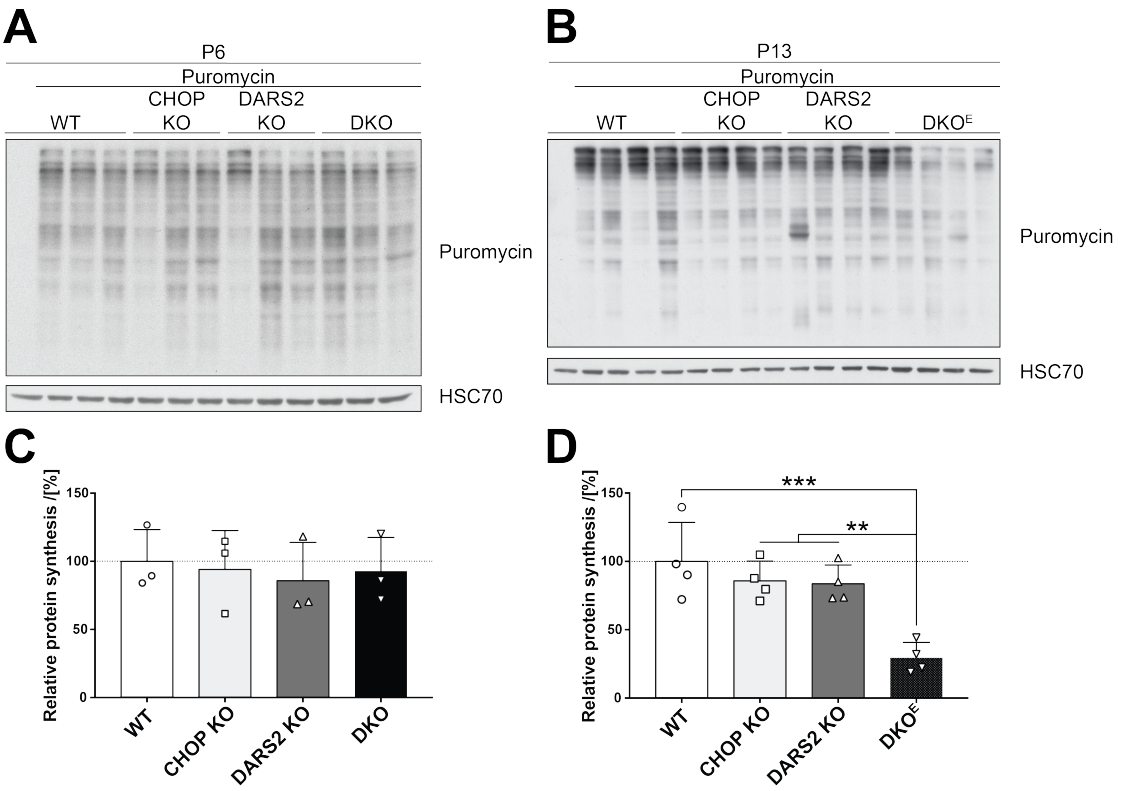

Figure 3.16: DKO^{E} animals exhibit inhibition of protein synthesis and up-regulation of *gadd34* mRNA levels, two hallmarks of the ISR.

Western blot analysis of puromycin-injected animals at p6 (A) and p13 (±1) (B) for determination of relative protein synthesis rates (C, D). HSC70 serves as loading control.

However, around p13 a striking reduction down to 30% of residual protein synthesis was observed in DKO^{E} mice (Figure 3.16B, D), indicating full ISR activation in DARS2/CHOP double-deficient animals at two weeks of age.

3.1.3.6 Re-initiation of cytoplasmic protein synthesis in DKO^{L} animals coincides with further reinforced pathological changes

Previous findings revealed a reduction of global protein synthesis in DKO^{E} mice to 30% of the WT level (3.1.3.5). This raised the question, how protein synthesis-deficient DKO^{E} mice can survive three to five more days before reaching the final stage of the phenotype. For this reason, the SUnSET assay (Schmidt et al., 2009) was repeated with animals of all genotypes at p17 (±2). Surprisingly, the inhibition of protein synthesis, a hallmark of the ISR, is entirely reversed in DKO^{L} mice (Figure 3.17A, B). This finding implies that translation in DKO^{L} animals was not limited to mainly stress-responsive mRNAs anymore. Whereas control mice exhibited no changes in the protein levels of ISR markers from p13 to p17 (±2) (data not shown), DKO^{E} and DKO^{L} mice did. A rising trend for phospho-eIF2α to eIF2α ratios, similar to ATF4 and ATF4 target protein levels (ASNS, SHMT2, PYCR1), was observed (Figure 3.17C-E). This suggests that stress-specific and standard protein syntheses are both simultaneously performed. In conclusion, several high-energy demanding processes such as re-initiation of protein synthesis and enhanced ATF4-driven amino acid synthesis (Figure 3.5 and Figure 3.6) concur with loss of mitochondrial respiration in the heart (Figure 3.8), an organ covering its high energy demand under normal conditions to 90% by oxidative phosphorylation (Mootha et al., 1997). As a consequence, the heart of DKO^{L} mice undergoes an energy crisis during which it is not surprising to observe systemic changes like hypoglycemia (Figure 3.17F) besides pathological changes in the organ itself (Figure 3.3, Figure 3.4).

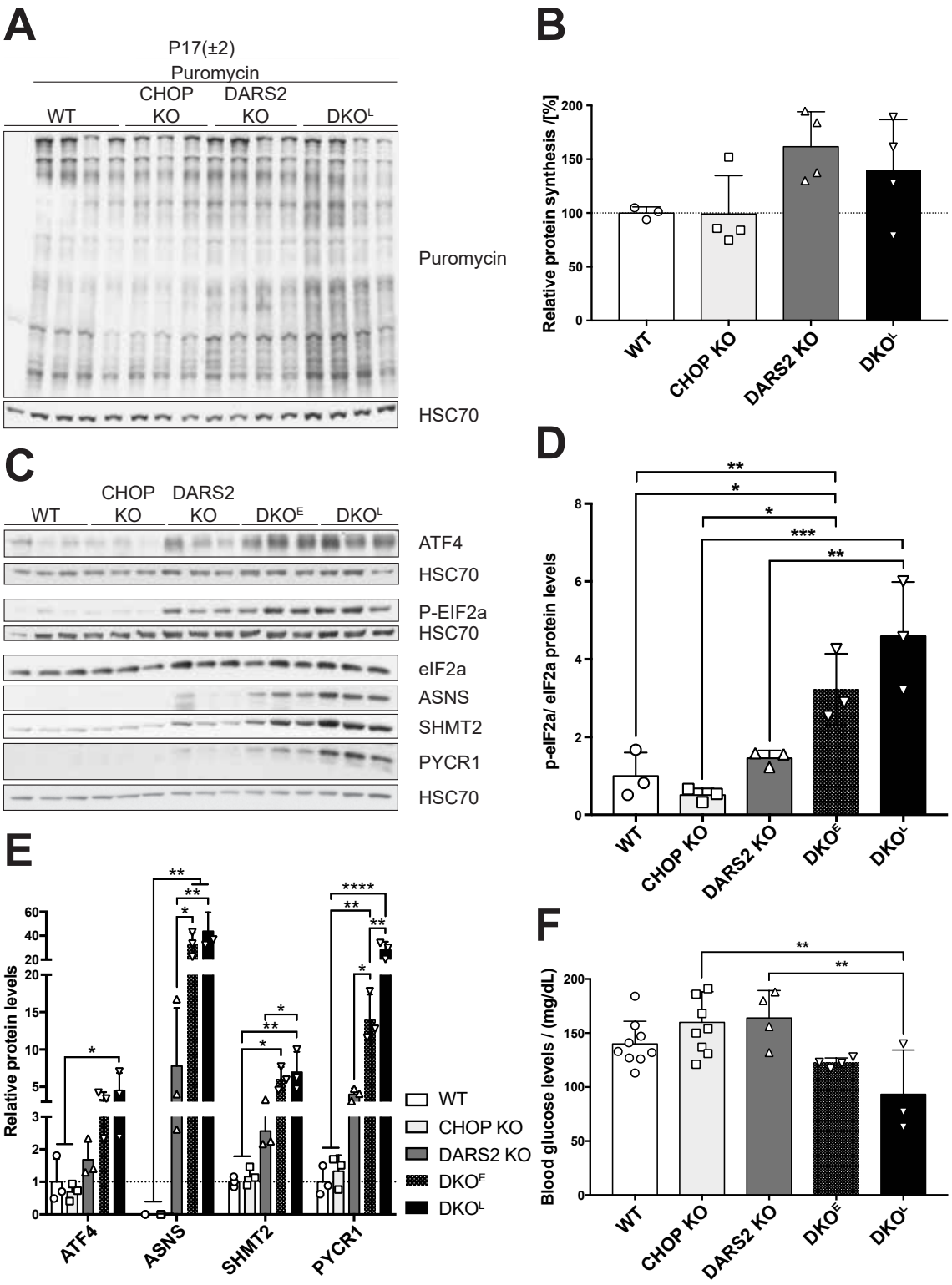

Figure 3.17: In contrast to the current model of the ISR, protein synthesis in DKO^L mice is re-initiated during the ISR.

Western blot analysis of puromycin-injected animals at p17 (±2) to determine relative protein synthesis rates (B). (C) Western blot analysis and (D, E) relative protein levels of ISR markers. HSC70 serves as loading control. (F) Blood glucose levels determined in non-fasted animals. (C-F) Direct comparison of early (DKO^E) and late stage (DKO^L) DKO mice. Bars represent mean ± SD (One-way ANOVA; *p<0.05, **p<0.01, ***p<0.001, ****p<0.0001).

In addition to the re-initiation of global protein synthesis and the deterioration of the health status, DKO^{L} mice displayed further differences in comparison to DKO^{E} animals. Also, on the level of mitochondrial translation (Figure 3.18A) and RC complex assembly (Figure 3.18B) a striking difference between early and late stage of the phenotype was observed. Whereas DKO^{E} did not differ from WT animals, DKO^{L} mice were characterised by loss of mitochondrial translation and RC complex assembly (Figure 3.18B), as already described earlier (Figure 3.8). It seems particularly conspicuous that DARS2 KO mice displaying first changes, e.g. at the level of RC complex assembly (Figure 3.18B) without a measurable impact on respiration (Figure 3.8A, D) exhibit stronger changes in comparison to WT than DKO^{E} mice.

Hence, although DARS2 KO animals display early changes on the molecular level delayed for a brief period by CHOP deficiency, DARS2 KO animals can maintain their state of health over an extended period, recognizable by a lifespan of six to seven weeks in contrast to less than three weeks for DKO^{L} mice.

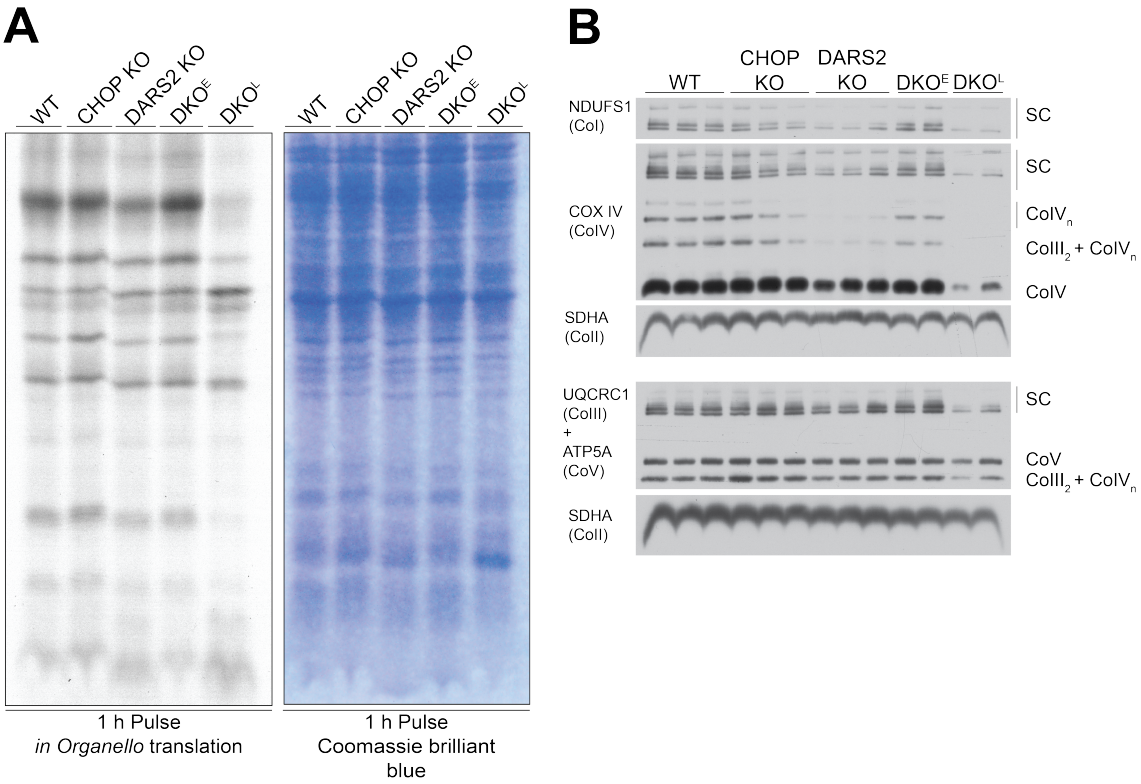

Figure 3.18: Mitochondrial translation and RC complex assembly of DKO^{E} mice is comparable to WT mice.

(A) *In organello* translation assay of cardiac mitochondria. *De novo* protein synthesis was determined after one hour ^{35}S-methinonine pulse labelling. Coomassie brilliant blue stained gel serves as loading control. DKO mice were littermates, phenotype progression however occurred faster in the DKO^{L} animals. The observed results were reproduced in additional experiments resulting in a total number of replicates of 3 (n=3). (B) BN-PAGE and subsequent Western blot

analysis of OXPHOS complexes and super-complexes (SCs) in isolated mitochondria directly comparing early (DKO^E) and late stage (DKO^L) DKO mice (n=2-3). Subunit-specific antibodies (left) were used to detect respective subunit-containing complexes and super-complexes (right).

3.1.3.7 Despite CHOP deficiency the negative feedback loop of the ISR is activated in DKO^L mice

The last uninvestigated ISR hallmark in the context of this work was the GADD34 controlled negative feedback loop. GADD34 is essential for de-phosphorylation of eIF2a and results in de-activation of the ISR (Novoa et al., 2001; Novoa et al., 2003). Transcriptional activation of *Gadd34* in the course of the ISR was shown to depend on CHOP (Marciniak et al., 2004). Therefore, it was surprising to detect the sharpest increase of *gadd34* transcripts at p17 (±2) in DKO^L mice. Since those mRNA levels ranged in a comparable order of magnitude as *gadd34* levels in DARS2 KO mice at six weeks, an impairment of the ISR's negative feedback mechanism in DKO mice is implausible (Figure 3.19).

Hence, the hallmarks of the ISR, namely (i) increased levels of phosphorylated eIF2α, (ii) ATF4 activation, (iii) inhibition of cytoplasmic protein synthesis and (iv) activation of the negative feedback loop, were fully recapitulated by DKO animals.

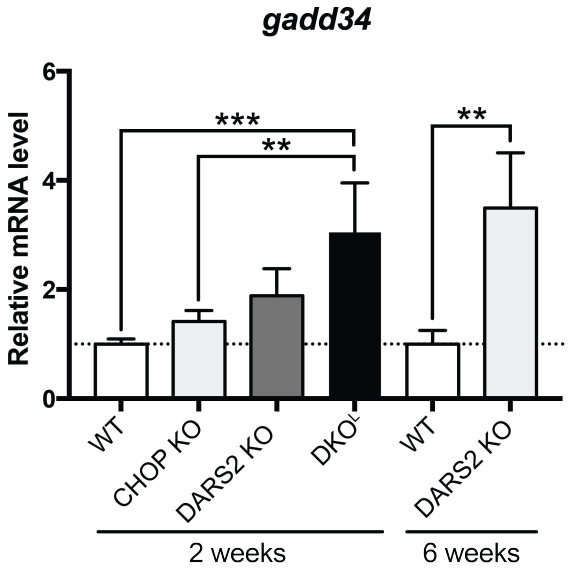

Figure 3.19: CHOP deficiency in DARS2 KO mice does not affect the GADD34-mediated negative feedback loop of the ISR.

(E) Assessment of relative *gadd34* mRNA levels in 2 and 6 week old animals by qPCR. Bars represent mean ± SD, samples were normalised to WT mice of the respective age (2 weeks (p17±2): one-way ANOVA; 6 weeks: two-tailed t-test; *p<0.05, **p<0.01, ***p<0.001).

3.1.3.8 Assessment of further potentially relevant, stress-related pathways

3.1.3.8.1 Alterations of downstream effectors of AMPK/ Akt/ mTOR signalling indicate metabolic adaptations to the modified energy status of DKO^{L} hearts

Metabolic pathways are characterised by a high degree of interdependence. As a metabolic organelle, mitochondria contribute to a variety of different pathways such as amino acid metabolism (Owen et al., 2002) or β-oxidation of fatty acids (Drysdale and Lardy, 1953). Therefore, impairing mitochondrial processes, in particular, is equivalent to interference with metabolism, in general. Moreover, it is a well-known phenomenon that, upon the development of cardiomyopathy, the heart is undergoing a switch of substrate preference. Fuel utilisation shifts from the predominant use of fatty acids, processed by fatty acid oxidation, to glucose, the fuel of choice of the foetal heart mainly relying on glycolysis (Lehman and Kelly, 2002). Three kinases deeply involved in regulation of metabolism are (i) AMPK (5'-AMP-activated protein kinase), the 'master regulator of metabolism', (ii) AKT (RAC-alpha serine/threonine-protein kinase), with major importance for the regulation of glucose metabolism, and (iii) mTOR (mammalian target of rapamycin, serine/threonine-protein kinase), triggering anabolism (mTORC1) or promoting cell survival and proliferation (mTORC2) (Saxton and Sabatini, 2017; Whiteman et al., 2002; Yuan et al., 2013).

In order to evaluate possible altered activities, the phosphorylation status of AMPK at Thr172, AKT at Ser473 and mTOR at Ser2448 were analysed (Figure 3.20). Interestingly, none of the kinases exhibited a significantly changed phosphorylation status, except for p-AKT in CHOP KO animals (Figure 3.20A, B). Despite unaltered AMPK or AKT activity, glucose metabolism was demonstrably modified, as shown by increased protein levels of the primary mediator of insulin-stimulated glucose uptake in the heart: GLUT4 (Figure 3.20A, B). GLUT1 functionally complements GLUT4, the primary glucose transporter in the adult heart. The activity of the former one is mainly determined at the transcriptional level (Shao and Tian, 2015). Therefore, GLUT1-encoding *slc2a1* transcript levels in the RNAseq data set were compared: As for GLUT4 on the protein level, *slc2a1* transcript levels were significantly augmented (FC 5.15; $p<10^{-4}$) in DKO^{L} mice, whereas the transcript levels in the other genotypes remained unchanged.

Concerning the recently introduced model of the integrated mitochondrial stress response (ISRmt) proposing mTORC1 complex-dependent ATF4 induction in a mouse model of mitochondrial myopathy (Nikkanen et al., 2016), the phosphorylated and total

protein levels of 4EBP1, a phosphorylation target of mTORC1, were assessed. DARS2 KO and DKO^{L} mice showed increased total 4EBP1 protein levels complemented by increased p-4EBP1 levels in DKO^{L} animals (Figure 3.20C, D). Furthermore, bioinformatic analyses, performed by our collaborators (Prof. Dr. Ivan Topisirovic, Prof. Dr. Ola Larsson and Christian Oertlin) using anota2seq (Oertlin et al., 2019), provided no evidence for considerably altered 4EBP1 activity. Therefore, increased mTORC1 activity in DKO^{L} samples is unlikely. However, these analyses suggested an ATF4-like regulation on the proteomic as well as on the transcriptomic level (data not shown).

Generally, the presented data demonstrate a shift towards enhanced glucose metabolism in DKO^{L} mice, indicating a switch to foetal-like cardiac metabolism, although they fail to provide robust evidence for increased activity of the mTORC1 complex.

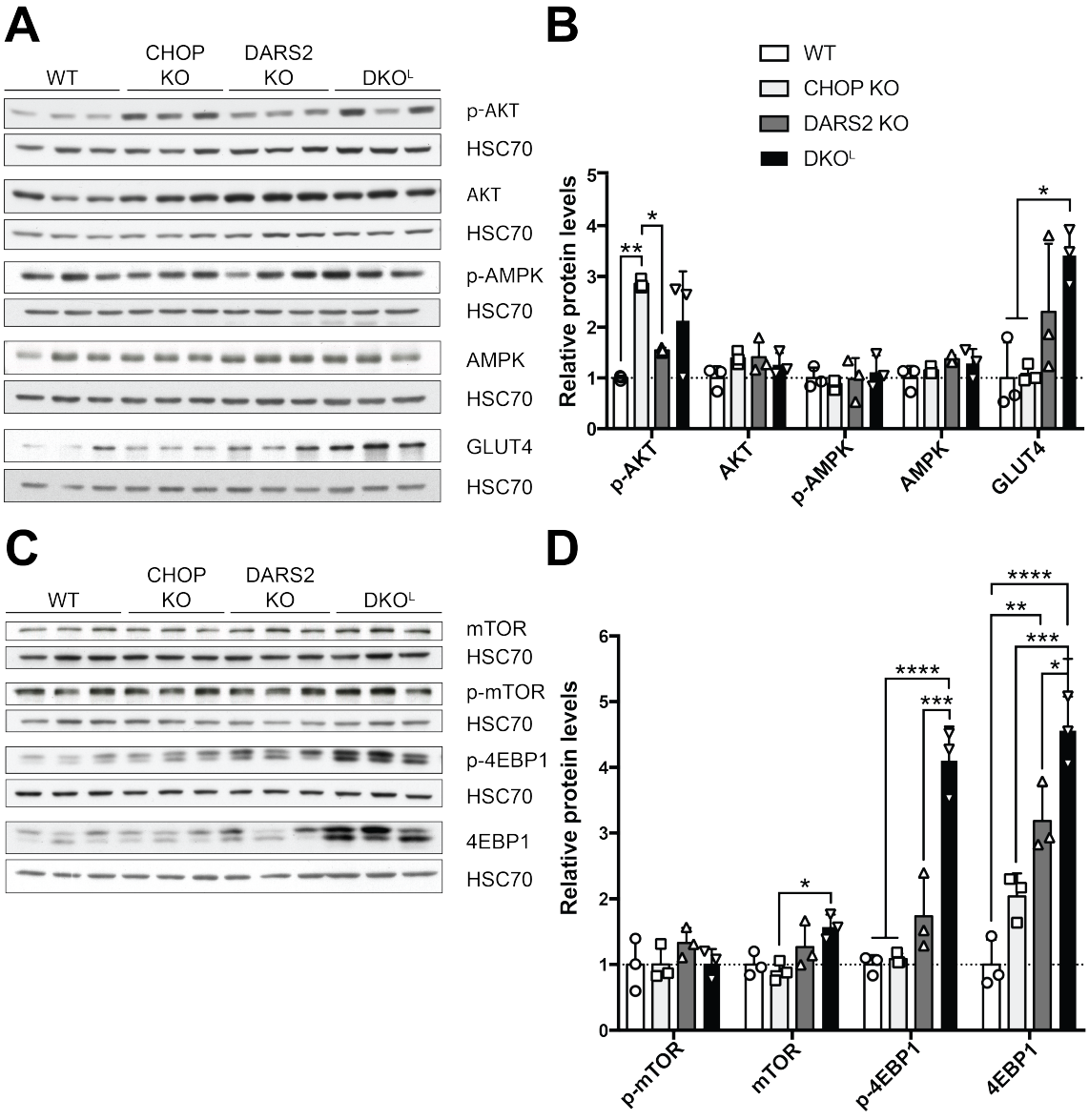

Figure 3.20: GLUT4, 4EBP1 and p-4EBP1 protein levels are increased in DKO^{L} mice.

(A) Western blot analysis and (B) relative protein levels of pSer473 AKT, AKT, pThr172 AMPK, AMPK and GLUT4. (C) Western blot analysis and (D) relative protein levels of mTOR, pSer2448 mTOR, 4EBP1 and pThr37/46 4EBP1. HSC70 serves as loading control. Experiments were performed on cardiac lysates of mice at p17 (±2). Bars represent mean ± SD (One-way ANOVA; *p<0.05, **p<0.01, ***p<0.001, ****p<0.0001).

3.1.3.8.2 Increased p62 levels in DKO^{L} suggest possible changes in autophagy

Previous work of the lab on the DARS2 KO mouse model suggested reduced autophagy as one of the induced stress responses (Dogan et al., 2014). For this reason, the LC3B-I to LC3B-II conversion as well as p62 levels were analysed (Figure 3.21). In contrast to the six week old DARS2 KO mice (Dogan et al., 2014), LC3-I to LC3-II conversion at p17 (±2) was affected neither in DARS2 KO nor in DKO^{L} mice. p62 protein levels, however, showed significant increases in DKO^{L} samples (Figure 3.21), revealing a possible alteration of autophagy (Mizushima et al., 2010).

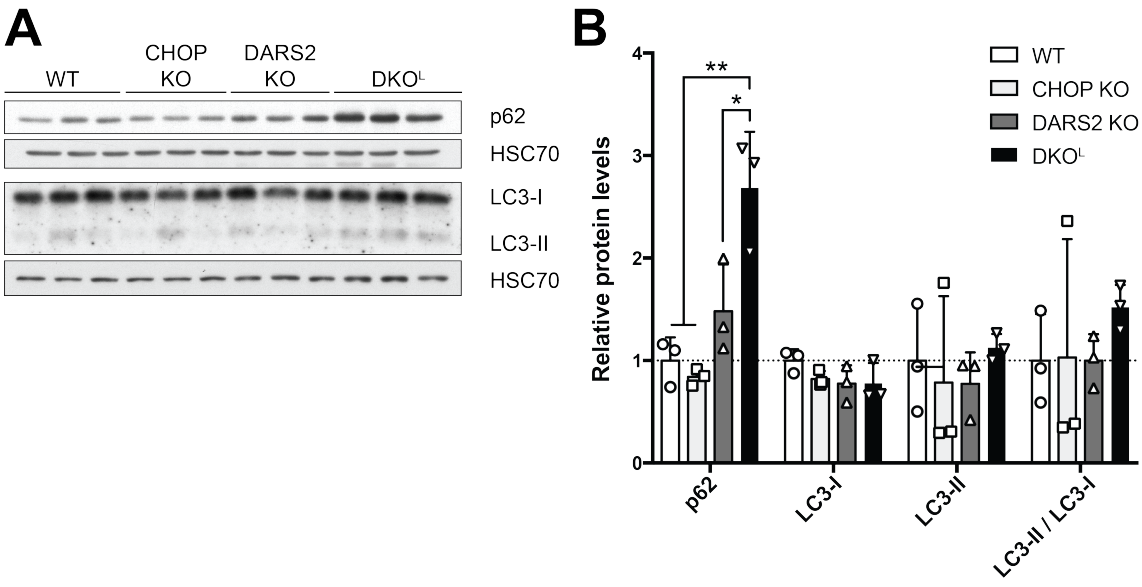

Figure 3.21: DKO^{L} mice exhibit increased p62 protein levels.

(A) Western blot analysis and (B) relative protein levels of p62, LC3-I and LC3-II. HSC70 serves as loading control. Experiments were performed on cardiac lysates of mice at p17 (±2). Bars represent mean ± SD (One-way ANOVA; *p<0.05, **p<0.01).

3.1.3.8.3 Apoptosis is not increased in DKO^{L} mice

The pro-apoptotic role of CHOP during stress conditions such as microbial infection or ER-stress represents one of the best-studied functions of the transcription factor. CHOP-dependent induction of apoptosis can occur via mitochondria-dependent, death receptor or other pathways (Hu et al., 2019). Furthermore, cardiomyocyte apoptosis represents a common feature of dilated cardiomyopathy pathology (Harvey and Leinwand, 2011). Cleaved caspase-3 protein levels were analysed in order to evaluate the potential relevance of apoptosis in DKO^{L} animals. However, cleaved caspase-3 was neither detected in DKO^{L} mice nor in the respective controls (data not shown). As the primary executioner caspase of the apoptotic pathway, cleaved caspase-3 induces PARP (protein poly-ADP-ribosyltransferase) cleavage, one of the hallmarks of apoptosis (Slee et al., 2001). To further confirm the negative cleaved caspase-3 signal, PARP cleavage was assessed. Again, no changes in DKO^{L} samples in comparison to the respective controls were detected (Figure 3.22). One of the protein families that is transcriptionally regulated by CHOP is the BCL-2 family, comprising several pro- and anti-apoptotic proteins. The anti-apoptotic protein BCL-2, for instance, is negatively regulated by CHOP (Rodriguez et al., 2011). In DKO^{L} mice BCL-2 protein levels were significantly increased (Figure 3.22). Taken together, the results provide no evidence for induction of apoptosis in any of the analysed samples, however they confirmed the proposed repressive effect of CHOP on *Bcl-2*, as BCL-2 protein levels were increased in DKO^{L} mice.

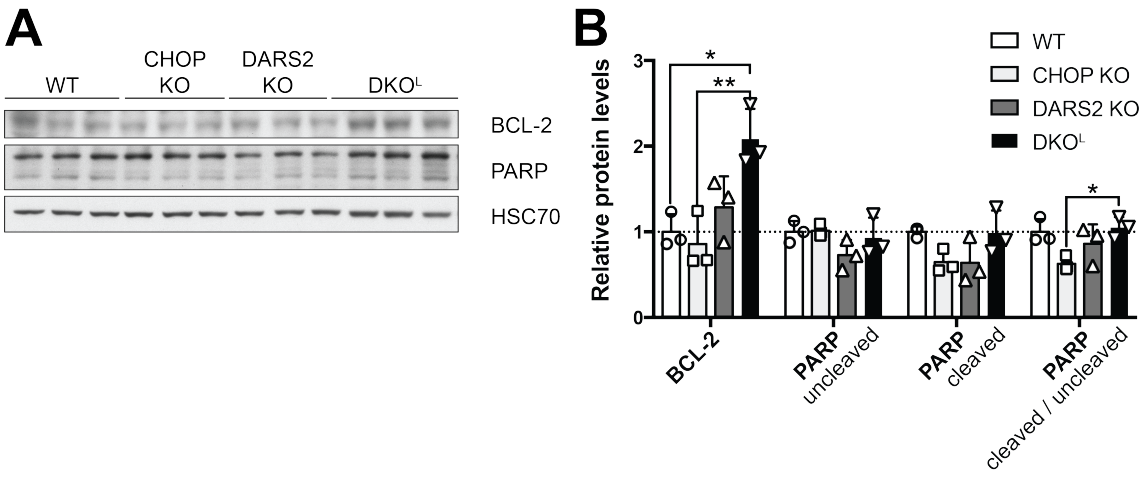

Figure 3.22: Neither DARS2 KO nor DKO^{L} mice display signs of altered apoptotic cell death. (A) Western blot analysis and (B) relative protein levels of BCL-2 and PARP. (C) HSC70 serves as loading control. Experiments were performed on cardiac lysates of mice at p17 (±2). Bars represent mean ± SD (One-way ANOVA; *p<0.05, **p<0.01).

3.1.3.8.4 DKO^{L} mice exhibit elevated ER stress-marker levels

CHOP is known as one of the TFs activated downstream of the UPR^{ER}. Furthermore, increasing attention is attributed to mito-ER communication. For this reason, protein levels of the luminal ER chaperone BiP (binding-immunoglobulin protein) and one of the sensors of the UPR^{ER}, IRE1a (inositol-requiring protein 1), were assessed (Chakrabarti et al., 2011; Lopez-Crisosto et al., 2017). At p6, no changes were detected (data not shown). At p17 (±2), DKO^{L} mice presented significantly increased BiP levels (Figure 3.23). DARS2 KO, as well as selected DKO^{L} mice, exhibited increased IRE1a levels (Figure 3.23). Furthermore, the RNAseq data revealed transcriptional activation of *Atf6* – one of the main TFs mediating the UPR^{ER} – in DKO^{L} mice (DARS2 KO vs. WT: FC 1.33, $p<10^{-4}$; DKO^{L} vs. WT: FC 2.09, $p<10^{-4}$). Collectively, those data indicate that the ER reacts in response to the perturbation of mitochondrial proteostasis induced by deletion of *Dars2* and increases its luminal protein folding capacity by augmenting BiP levels of DKO^{L} animals.

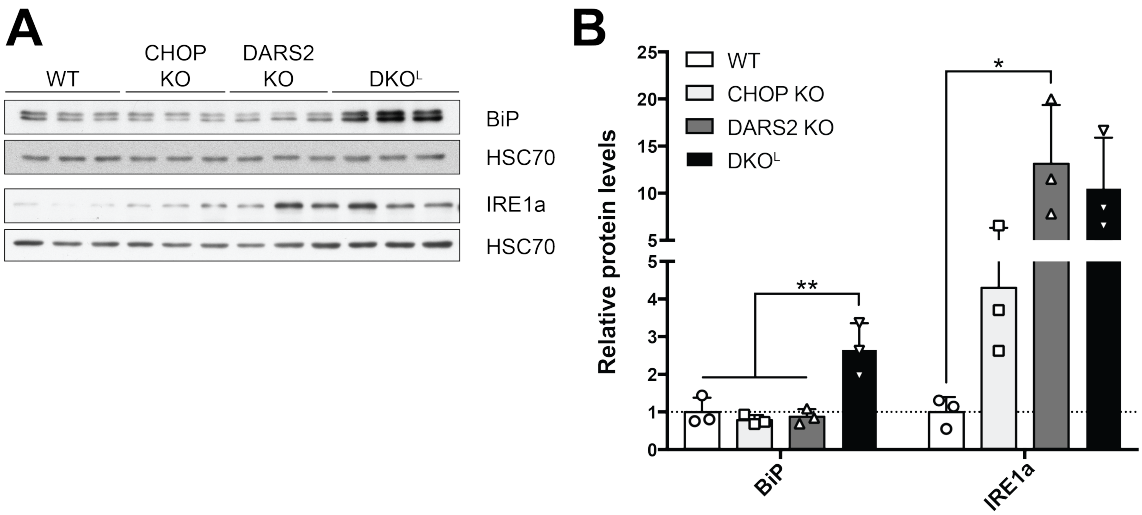

Figure 3.23: DKO^{L} mice increase protein folding capacity of the ER lumen by augmented BiP protein levels.

(A) Western blot analysis and (B) relative protein levels of BiP and IRE1a. (C) HSC70 serves as loading control. Experiments were performed on cardiac lysates of mice at p17 (±2). Bars represent mean ± SD (One-way ANOVA; *p<0.05, **p<0.01).

3.1.4 C/EBPβ is the only identified transcription factor interacting with CHOP in DARS2 KO animals

Since CHOP in DARS2 KO mice affects the activation of the ISR, but not the regulation of *Gadd34* (3.1.3.1-3.1.3.7), alternative explanations for the detrimental consequences of CHOP-deficiency in DKO mice had to be identified. As a bZIP TF, dimerisation of CHOP is a prerequisite in order to bind DNA. Moreover, the DNA binding domain of CHOP is non-functional due to the substitution of several conserved aliphatic and basic residues of the C/EBP family of TFs. Thus CHOP requires a hetero-dimerisation partner that confers DNA binding (Ron and Habener, 1992). CHOP interacting proteins in the DARS2 KO vs. WT background were identified by co-immunoprecipitation and subsequent mass spectrometry (Table 3.3). Among the list of identified proteins, CHOP was expectably the most enriched one. The remaining group of six proteins contained only one more TF: C/EBPβ (Table 3.3).

Table 3.3: Significantly enriched proteins (p<0.05, FC>2) isolated by CHOP co-immunoprecipitation and identified by subsequent mass spectrometry.

Protein names	Gene names	p-value	FC
CCAAT homologous protein	*Chop*	0.0262	4.82
CCAAT/enhancer-binding protein beta	*Cebpb*	0.0064	4.31
DnaJ homolog subfamily C member 11	*Dnajc11*	0.0194	3.25
Lon protease homolog, mitochondrial	*Lonp1*	0.0027	3.43
E3 ubiquitin-protein ligase TRIM21	*Trim21*	0.0069	3.22
Plasminogen activator inhibitor 1 RNA-binding protein	*Serbp1*	0.0218	3.43

3.2 Investigating the mito-specific modulation of the ISR *in vitro*

Previous *in vivo* experiments revealed an accelerated and intensified activation of the ISR in the context of mitochondrial dysfunction induced by deletion of *Dars2* upon CHOP deficiency. In order to shed light on the molecular mechanism behind the observed over-activation of the ISR in general, and ATF4 in particular, additional investigations were performed *in vitro*.

3.2.1 Cellular models of mitochondrial dysfunction and physiological impact of CHOP upon ISR activation

To facilitate mechanistic analyses of the earlier described effects of CHOP deficiency in DKO mice, several *in vitro* models, recapitulating the molecular *in vivo* phenotype as accurately as possible, were established.

Among others, COX10-deficient fibroblasts obtained from the lab of Carlos T. Moraes were utilised. The loss of the assembly factor COX10 impedes complex IV assembly. Interestingly, those fibroblasts are not only complex IV but also complex I-deficient (Diaz et al., 2006). As expected in cells devoid of respiratory complexes I and IV, no respiration-related oxygen consumption by COX10 KO fibroblasts was recorded using Seahorse (data not shown). The ISR activation of COX10 KO fibroblasts, characterised by significant up-regulation of p-eIF2α, ATF4 and ATF4 downstream targets (MTHFD2, ASNS, SHMT2, PYCR1) (Figure 3.24A, B), was comparable to the situation in DARS2 KO and DKO^{L} mice described before (Figure 3.15). Additionally, ISR inhibitor (ISRIB) treatments indisputably confirmed the ISR as the cause of ATF4 up-regulation. ISRIB treatments lead to a rapid decrease of ATF4 protein levels in cells displaying severe mitochondrial dysfunction. 4h treatment duration were sufficient to revert ATF4 levels to the WT situation in COX10 KO fibroblast (data not shown). For visible effects on ATF4 downstream targets longer treatment durations were necessary. After 48h of ISRIB treatment, partial restoration of the WT situation was observed in COX10-deficient cells (Figure 3.24A, B). Several reasons for the discrepancy between the results of ATF4 and ATF4 downstream targets should be considered. First, ATF4 protein levels need to be decreased in order to reduce the transcription of the respective target genes. Second, the already present mRNA moieties of ATF4 targets need to be degraded in order to prevent the synthesis of the respective proteins. Third, ATF4 is known for its extremely

short half-life that is characteristic for stress-responsive proteins (Dey et al., 2010). This short half-life might not apply to its respective downstream targets.

In accordance with the published mechanism of ISR inhibition by ISRIB, based on the alleviation of eIF2B inhibition by phosphorylated eIF2α (Sidrauski et al., 2015), p-eIF2α levels were not affected by the inhibitor (Figure 3.24A).

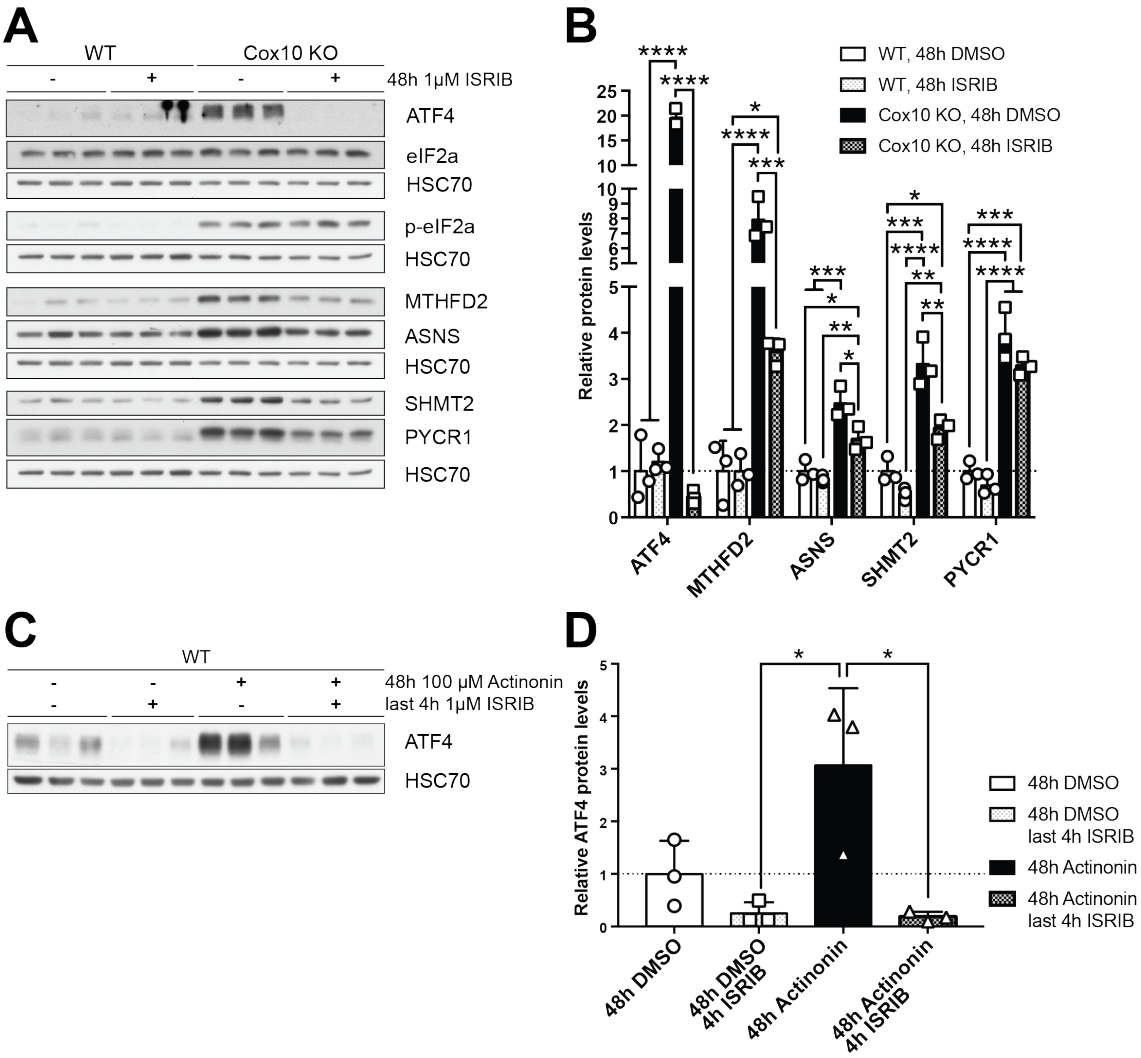

Figure 3.24: Mitochondrial dysfunction-induced ATF4 up-regulation is fully attributable to ISR activation.

(A) Western blot analysis and (B) relative protein levels of ISR markers in immortalised COX10 KO and control fibroblasts. (C) Western blot analysis and (D) relative protein levels of ATF4 in immortalised MEFs treated with DMSO (control, 48h), actinonin (48h) and/or ISRIB (4h). HSC70 serves as loading control. Bars represent mean ± SD (One-way ANOVA; *p<0.05, **p<0.01, ***p<0.001, ****p<0.0001).

A second cell culture model further confirmed ISR-dependent ATF4 up-regulation. 48h of actinonin treatment robustly induced mitochondrial dysfunction in immortalised mouse embryonic fibroblasts (MEFs). Actinonin, a potent peptide deformylase inhibitor,

interferes with mitochondrial translation. Peptide deformylase is required for mitochondrial translation in order to remove the starter methionine's formyl group of the nascent polypeptide chain, when the latter one emerges from the exit tunnel of the mitoribosome (Chen et al., 2000). Additionally, actinonin was shown to deplete mitochondrial ribosomes, rRNAs and mRNAs as well as to block cell proliferation (Richter et al., 2013). As observed before in COX10-deficient cells, 4h of ISRIB treatment prevented up-regulation of ATF4 induced by 48h actinonin treatment in MEFs (Figure 3.24C, D).

In order to evaluate how well the selected *in vitro* treatment recapitulates the effects of CHOP-deficiency observed during mitochondrial dysfunction *in vivo*, CHOP KO MEFs were subjected to 48h of actinonin treatment (Figure 3.25A, B). In line with previous results (3.1.3.2, 3.1.3.3), ATF4 mRNA activation upon mitochondrial dysfunction – detected at the transcript level here – occured prematurely in CHOP-deficient cells (Figure 3.25A). Calling back to mind the chronology of the ISR, were preferential translation of *atf4* mRNA precedes induction of ATF4 targets such as *mthfd2* and *atf4*, it is not surprising to observe a simultaneous increase of those transcripts.

Juxtaposition of actinonin-treated WT and CHOP KO MEFs facilitated the evaluation of physiologic effect of CHOP deficiency during mitochondrial dysfunction *in vitro* (Figure 3.25B). The comparison of the linearised growth curves during the exponential growth phase of both cell lines revealed a much stronger negative effect on CHOP-deficient MEFs. As opposed to CHOP KO MEFs, growth rates of untreated and actinonin-treated WT MEFs did not differ significantly from each other.

Most interestingly, ISRIB treatments partially rescued the negative effect induced by mitochondrial dysfunction in CHOP KO MEFs ($p=0.056$). In contrast to CHOP KO MEFs, a mild (though not significant) negative effect of ISRIB on the growth rates of actinonin-treated WT MEFs was observed (Figure 3.25B).

Taken together, the discussed *in vitro* studies showed, that mitochondrial dysfunction activates ATF4 up-regulation solely via the ISR. Furthermore, the premature activation of the stress response upon CHOP deficiency and the resulting negative effect on the physiological level observed in the DKO^{L} mice were recapitulated in actinonin-treated CHOP KO MEFs.

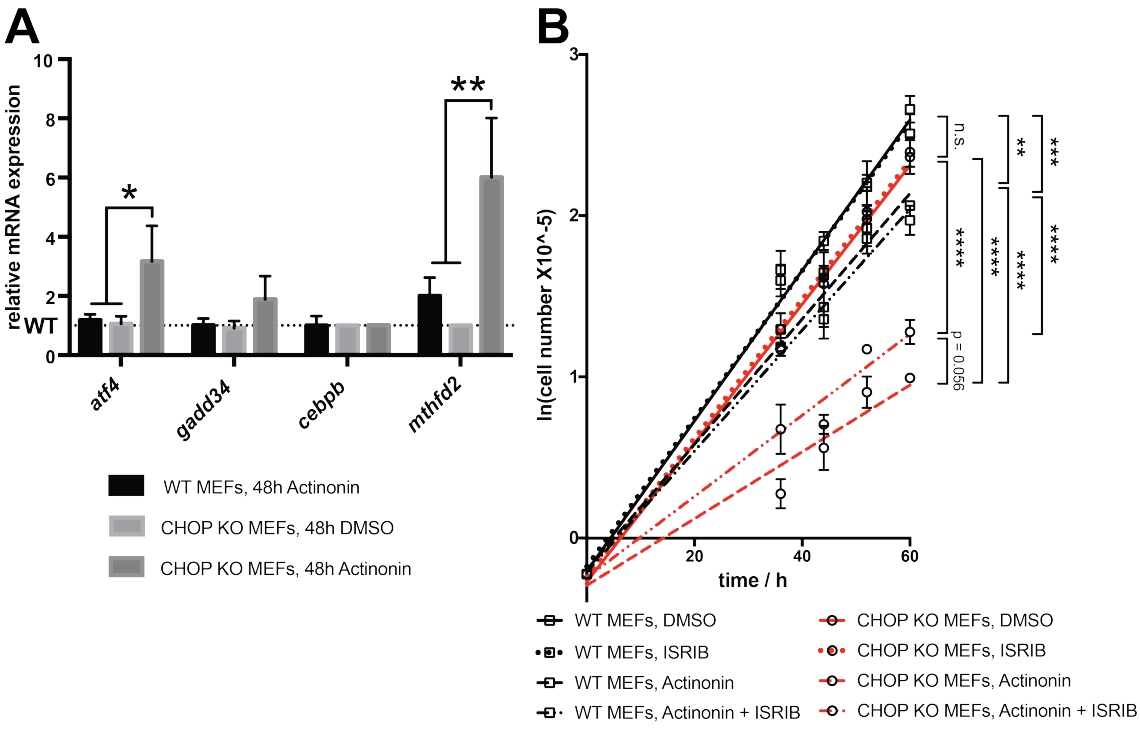

Figure 3.25: Inhibition of the ISR induced by mitochondrial dysfunction is beneficial under conditions of CHOP deficiency.

(A) Relative mRNA levels of ISR markers and *cebpb* in actinonin-treated (48h) CHOP KO MEFs and respective controls determined by qPCR. Samples were normalised to DMSO-treated WT MEFs. (B) Linearised growth curves of respective exponential growth phases of WT and CHOP KO MEFs under the specified conditions. Treatment durations correspond to respective growth times. Curves were determined using linear regression. Based on the calculated slopes for each condition Prism 7 software determined the probability of each possible pair of slopes being equal (n=3). Bars represent mean ± SD (*p<0.05, **p<0.01, ***p<0.001, ****p<0.0001).

3.2.2 CHOP deficiency modulates the protein levels of C/EBPβ isoforms

As the transcriptomic analyses did not provide evidence for a CHOP-regulated sub-set of transcripts but rather indicated a general repressive effect on ISR target gene activation, possible interaction partners of CHOP had been determined. Strikingly, the only identified interacting TF in DARS2 KO hearts was C/EBPβ, which was the second most-enriched protein after CHOP in the co-immunoprecipitation assay (3.1.4). Since further analyses on tissue samples were not possible due to antibody issues, subsequent experiments were performed *in vitro*.

The protein levels of the three C/EBPβ isoforms LAP* (liver activating protein*), LAP (liver activating protein) and LIP (liver inhibiting protein) were assessed in both cell

culture models introduced beforehand (Figure 3.26). Previous studies had shown, that the proportion of the short isoform LIP to the two longer isoforms LAP* and LAP modulates the cellular response to ER stress (Li et al., 2008). Similarly, the protein levels of the C/EBPβ isoforms explicitly responded to the increased mitochondrial stress level in COX10 KO fibroblasts. LAP* and LAP levels increased approximately two to three-fold. LIP levels, however, increased up to eight-fold (Figure 3.26A, B). Additional experiments with other cellular models confirmed the general trends of the results as mentioned before. As one example of several, the response of actinonin-treated WT MEFs is shown below (Figure 3.26C, D). Most notably, LIP levels failed to increase in the CHOP-deficient background. Moreover, LAP* and LAP protein levels tend to be reduced in those cells, independent of the treatment.

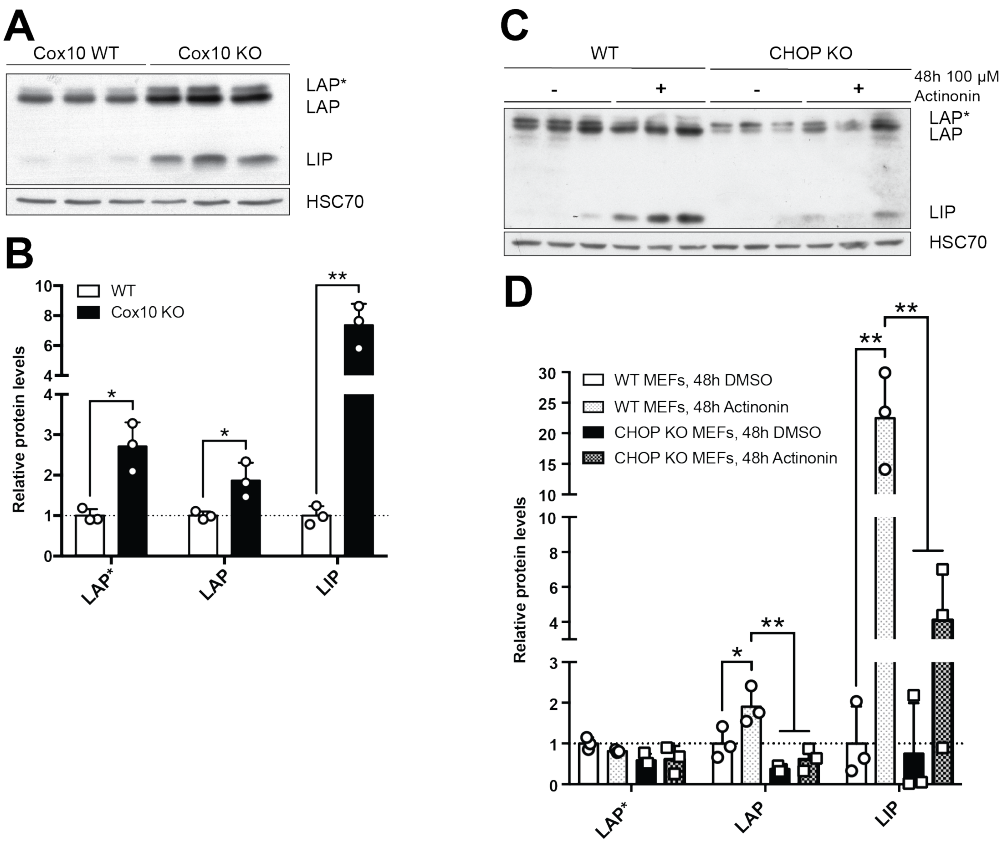

Figure 3.26: CHOP-deficient cells exhibit an altered response to mitochondrial dysfunction on the level of the C/EBPβ isoforms.

Western blot analysis of the three CEBPβ isoforms LAP*, LAP and LIP in COX10 KO fibroblasts (A) and actinonin-treated (48h) CHOP KO MEFs (C) along with the respective controls. HSC70 serves as loading control. (B, D) Quantification of Western blot analysis in (A) and (C). Bars represent mean ± SD (One-way ANOVA; *p<0.05, **p<0.01).

Interestingly, a particular relationship, termed as a *molecular symbiosis*, between the TFs CHOP and LIP had been previously described in the context of ER stress. According

to the proposed model, CHOP – preferentially interacting with the C/EBPβ isoform LIP – requires LIP to enter the nucleus. In contrast to CHOP, LIP has not only a functional nuclear localisation sequence (NLS) but also a nuclear export signal (NES), which results in re-export of the TF and subsequent proteasomal degradation in the absence of CHOP. Therefore, upon induction of ER stress, increasing CHOP protein levels entail LIP accumulation too, as CHOP facilitates its nuclear retention (Chiribau et al., 2010).

Taken together, it appeared that C/EBPβ levels alter upon mitochondrial dysfunction. Among all three isoforms, LIP exhibits the sharpest increase, which is impaired by loss of *Chop.*

3.2.3 LIP and LAP act as functional antagonists for transcriptional regulation of *Atf4*

The third alternative start codon of the C/EBPβ mRNA initiating translation of LIP is located after the sequence sections encoding the transactivation domains (TADs). Therefore, the short C/EBPβ isoform LIP harbours no TADs. This structural feature represents the main difference between LIP and the two longer isoforms LAP* and LAP. Contrary to LAP* or LAP, LIP primarily acts as a repressor and negatively impacts on *Atf4* expression in the context of UV irradiation (Descombes and Schibler, 1991; Dey et al., 2012). In order to test whether the functional antagonism of LAP*/LAP and LIP also applies to the context of the ISR activation induced by mitochondrial dysfunction, several experiments in C/EBPβ KO MEFs complemented with either LAP or LIP were performed (Figure 3.27). C/EBPβ KO MEFs, as well as LIP and LAP-encoding plasmids, were kindly provided by Maria Hatzoglou (Chiribau et al., 2010). Since LAP* and LAP are functionally not different from each other, additional experiments comprising LAP* over-expression were not performed.

Complementation of C/EBPβ KO MEFs with LAP or LIP was achieved by transfection. The hygromycin resistance-conferring plasmids, encoding the respective protein isoforms under control of the endogenous promoter, facilitated the subsequent hygromycin-based selection of stably transfected cells. As already suspected, the functional antagonism of LAP and LIP regarding the regulation of *Atf4* expression in the context of mitochondrial dysfunction was confirmed. The increase of ATF4 protein levels in LAP expressing C/EBPβ KO MEFs was significantly higher than in C/EBPβ KO MEFs (Figure 3.27A, B). Furthermore, despite only feeble LIP expression in stably transfected C/EBPβ KO MEFs, presence of LIP tended to attenuate the increase of ATF4

protein levels in actinonin-treated cells (Figure 3.27C, D). However, the significance level was not reached under those conditions.

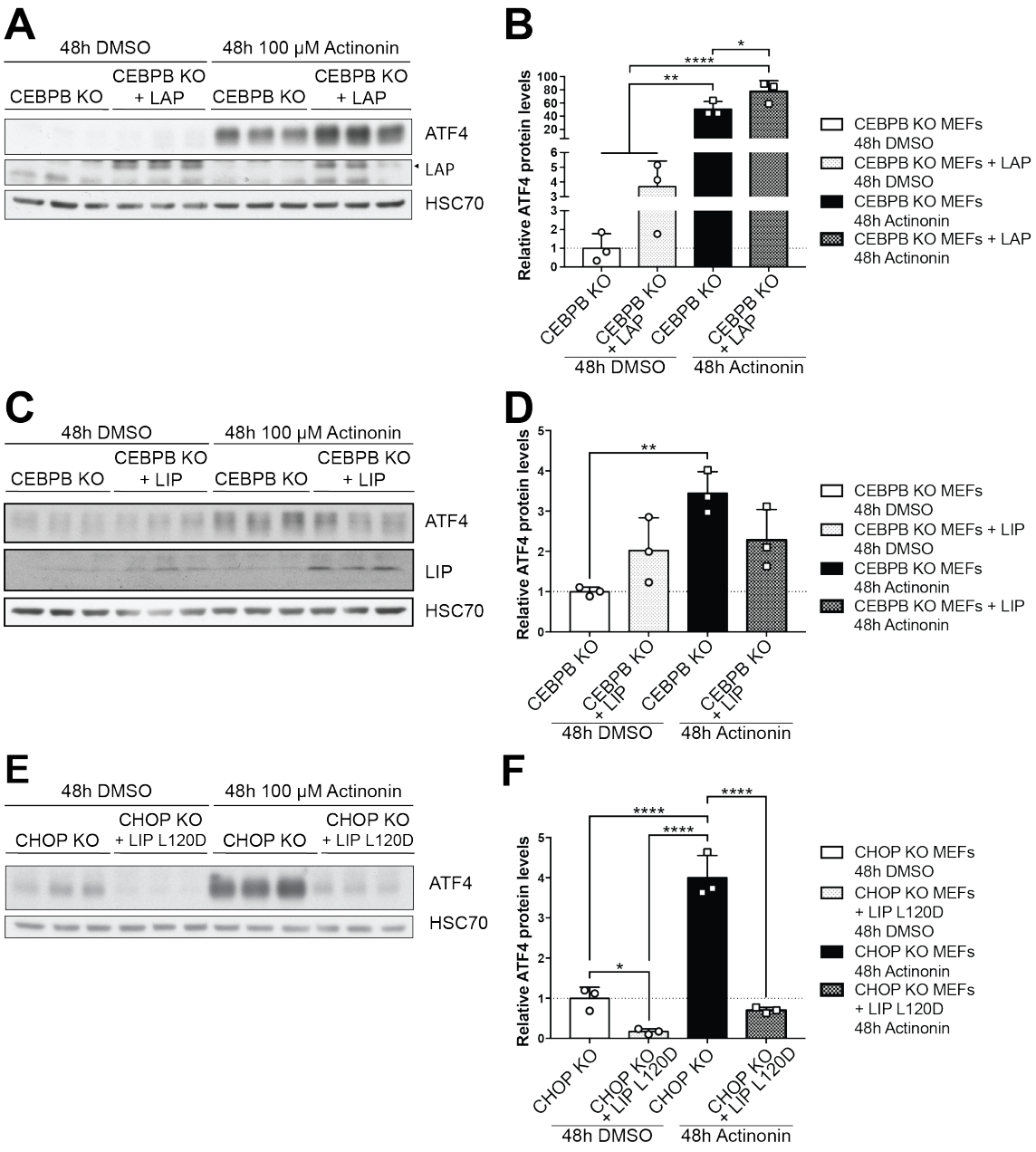

Figure 3.27: Nuclear retention of LIP represses ATF4 activation.

(A) Western blot analysis and (B) relative protein levels of ATF4 and LAP in actinonin-treated (48h) C/EBPβ KO MEFs with or without stable over-expression of LAP along with the respective controls. (C) Western blot analysis and (D) relative protein levels of ATF4 and LIP in actinonin-treated (48h) C/EBPβ KO MEFs with or without stable over-expression of LIP along with the respective controls. (E) Western blot analysis and (F) relative protein levels of ATF4 in actinonin-treated (48h) CEBPβ KO MEFs with or without stable over-expression of the LIP L120D point mutant along with the respective controls. Bars represent mean ± SD (One-way ANOVA; *p<0.05, **p<0.01, ***p<0.001, ****p<0.0001).

The molecular symbiosis between CHOP and LIP, as well as the results of LAP and LIP over-expression in actinonin-treated C/EBPβ KO MEFs (Figure 3.26A-D), imply insufficient nuclear retention of LIP as possible cause of excessive ATF4 up-regulation in the context of mitochondrial dysfunction upon CHOP deficiency. In order to test this hypothesis, the leucine amino acid residue located at position 120 in LIP, in the heart of the protein's NES (Williams et al., 1997), was mutated to aspartate to disrupt the NES. Strikingly, stable over-expression of LIP L120D in CHOP KO MEFs abolished increase of ATF4 protein levels by actinonin treatment (Figure 3.27E, F).

Collectively the data suggest a major, CHOP-dependent role for LIP in regulation of *Atf4* expression during mitochondrial dysfunction.

4 Discussion

The knowledge of the close relation between mitochondrial with cellular, organ- or even organism-related homeostasis vigorously increased during the past decades. Numerous studies addressing mitochondrial function and dys-function but also the underlying mechanisms of primarily non-mitochondrial diseases and the ageing process contributed to the remarkable gain of knowledge. The central role of mitochondria in for instance (i) steering fuel utilisation for energy production, (ii) synthesis of nucleotides, amino acids, lipids and iron-sulphur clusters, but also (iii) cell-fate determining pathways like apoptosis emphasises the importance of mitochondria as metabolic and signalling hubs (Friedman and Nunnari, 2014; Galluzzi et al., 2018; Nunnari and Suomalainen, 2012; Schaefer et al., 2004; Wallace, 2005). As such, retrograde communication with the nucleus, facilitating concerted action in response to alterations ranging from the intra-organellar to the intra-organismal level, is of high importance. Understanding the underlying signalling pathways of those complex regulatory networks, e.g. induced by loss of mitochondrial homeostasis, can provide precious entry points for therapeutical approaches.

The present study focused on one specific case of mito-nuclear communication: the induction of the stress-responsive TF CHOP upon mitochondrial dysfunction. CHOP was firstly described in the context of mitochondrial stress responses as a crucial component of the UPR^{mt} ensuring the induction of mitochondrial chaperones and proteases in answer to disrupted proteostasis of the organelle (Aldridge et al., 2007; Martinus et al., 1996; Zhao et al., 2002). Our studies revealed CHOP to be one of the first stress-related TFs up-regulated in the heart in response to mitochondrial dysfunction induced by heart

and skeletal muscle-specific deletion of *Dars2*, thereby suggesting a potential role in the early phase of the anterograde response (Dogan et al., 2014).

For this study, a newly-generated double knock-out mouse model deficient for DARS2 (heart and skeletal-muscle specific) and CHOP (whole-body) as well as several cell culture models were combined for reasons of mutual complementation in order to reach the previously defined objectives.

4.1 DARS2 KO mice as an appropriate tool to investigate general stress responses induced by mitochondrial dysfunction

Previous studies in the lab clearly defined the main characteristics of the cardiac phenotype in DARS2 KO animals: progressive development of OXPHOS deficiency and dilated cardiomyopathy resulting in a significantly reduced life expectancy of the mice to approximately seven weeks of age (Dogan et al., 2014). This pathology is prevalent for cardiac phenotypes of mitochondrial mutants and not a DARS2-specific phenomenon, as also mutations targeting other mitochondrial processes than translation show similar phenotypes. An excellent overview was given by Kühl and co-workers in a comparative study of five heart and skeletal muscle-specific mouse models targeting the mitochondrial replication (*Twinkle* KO), mtDNA maintenance (*Tfam* KO), mtDNA transcription (*Polrmt* KO), RNA stability/processing (*Lrpprc* KO) and the translation process (*Mterf4* KO), respectively. The disruption of the before-mentioned processes central for mtDNA expression always resulted in OXPHOS deficiency, cardiomyopathy and early death at six to 21 weeks of age (Kuhl et al., 2017).

On the molecular level, much attention was given to the remodelling of the serine biosynthetic and the 1-C pathway in response to mitochondrial dysfunction during the last years. The tight relationship between the function of the respiratory chain and serine synthesis as well as 1-C metabolism was investigated in a cell culture model with inducible expression of a dominant-negative mutant version of POLG. It was shown, that the increase of serine synthesis is impaired from the mitochondrial generation of formate through the 1-C cycle and that those metabolic alterations were mediated by the TF ATF4 (Bao et al., 2016). Similar rewiring of metabolism was reported for the 'Deletor' mouse, a model of slowly progressing mitochondrial myopathy. The accumulation of multiple mtDNA deletions in those animals lead to up-regulation of serine synthesis and impairment of folate-dependent biosynthetic pathways in the skeletal muscle (Nikkanen

et al., 2016). Also, the present study demonstrated markedly increased serine synthesis and remodelling of the 1-C cycle in hearts of DARS2 KO and DKO mice as well as in distinct cell culture models, underscoring the initiation of a response attributable to mitochondrial dysfunction in general, and not to DARS2 deficiency in particular.

Further evidence supporting the notion of a general relevance of the observations made in DARS2 KO mice for mitochondrial stress responses are provided by the direct comparison of DARS2 KO and DKO mice. DKO^{L} and DARS2 KO animals showed comparable OXPHOS assembly defects around p17. However, OXPHOS assembly defects at that age coincided with severe inhibition of mitochondrial translation and a respiratory defect only in DKO^{L} and not in DARS2 KO mice. Hence, deletion of *Dars2* alone is not resulting in severe inhibition of mitochondrial translation at p17. The assembly defects accompanied by only mild translation defects in DARS2 KO mice rather suggest on-going protein synthesis enabled by misincorporation of amino acids substituting aspartate residues in newly synthesised proteins. The deletion of *Chop* in the DARS2 KO background revealed the existence of secondary responses modifying the mitochondrial translation process, in addition to the primary defect triggered by deletion of *Dars2.* Thus it appears essential for future projects to understand the mechanism delaying or alternatively causing accelerated loss of mitochondrial translation in DARS2 KO and DKO mice, respectively. Possible entry points to investigate causes of translational inhibition beyond DARS2 deficiency are (i) mitochondrial f-Met levels, that are potentially affected by the re-routing of the 1-C cycle, (ii) investigation of the driving forces leading to the structural defects observed on TEM pictures, and (iii) monitoring of mitochondrial protein import and its possible inhibition by accumulation of misfolded proteins in the mitochondrial matrix.

4.2 CHOP deficiency results in severe deregulation of the ISR characterised by ATF4 over-activation

CHOP is well-known for its apoptosis-related role within the ISR pathway that was extensively studied in the context of the UPR^{ER}, where the PERK-dependent branch of the stress response activates the ISR (Ron, 2002). Nevertheless, initiation of the ISR can occur in response to various types of stresses and by several cellular compartments (Pakos-Zebrucka et al., 2016). Even though the upstream signalling events are still a matter of debate, mitochondrial dysfunction as a trigger of the ISR is commonly accepted in the field. For example, ISR activation was evidenced in mice with neuron-specific

deletion of the mitochondrial fission protein DRP1. Interestingly, augmented ATF4 levels and increased p-eIF2α/eIF2α ratio used as a read-out for an activated ISR were also accompanied by increased *chop* mRNA levels (Restelli et al., 2018). Furthermore, the direct dependence of CHOP expression from the eIF2α/ATF4 axis in the context of mitochondrial dysfunction was shown in cell culture models with impaired mtDNA expression caused by mtDNA depletion or translational inhibition (Michel et al., 2015).

Strikingly, transcriptomic and proteomic analyses provided strong evidence for CHOP as a regulator of the ISR. Deletion of *Chop* in the DARS2-deficient background resulted in a reinforced transcriptional signature of ATF4. Furthermore, transcriptional induction of ATF4 targets conveyed into similar changes in the proteomic data set. On the protein level, accentuated ISR in DKO^{L} compared to DARS2 KO mice became apparent by a significantly increased proportion of phosphorylated eIF2α - representing the central hub of the ISR - and augmented ATF4 protein levels - the central TF of the ISR (Pakos-Zebrucka et al., 2016). In summary, DKO mice exhibited a premature and strong activation of the ISR. The presented *in vivo* results provide solid evidence for a significant role of ATF4 in the response to mitochondrial stress and thereby further confirm published results acquired in several *in vitro* cell culture models of pharmacologically induced mitochondrial dysfunction (Quirós et al., 2017).

4.3 First *in vivo* evidence for a translational switch from acute to chronic ISR

Beside ATF4 activation, eIF2α phosphorylation also results in global inhibition of CAP-dependent protein synthesis. In the field of mitochondrial dysfunction, inhibition of protein synthesis by the ISR is often assumed upon detection of ISR, but commonly not further explored. For the present project, inhibition of CAP-dependent protein synthesis was confirmed in DKO^{E} mice at p13. This raised the question how the animals are able to survive for approximately four more days. Unexpectedly, protein synthesis of DKO^{L} mice is not only partially, but fully restored around p17. Those surprising results are consistent with recent data published in a cell culture model of ER stress, revealing a translation initiation reprogramming during chronic ISR activation. According to the proposed model, two translational switches are induced subsequently: First, during the acute phase of the ISR, only stress-responsive mRNAs are translated. Second, upon persisting chronic ISR activation, global translation is re-initiated in an eIF4F-independent but eIF3-dependent manner, resulting in parallel execution of stress-specific and global translation. The

second translational switch appeared to have beneficial effects within the studied *in vitro* model, preventing initiation of cell death (Guan et al., 2017). The present study in DKO mice provided first-time *in vivo* evidence for the switch from acute to chronic ISR along with the alterations on the level of cytoplasmic protein synthesis. Furthermore, the presented results demonstrate, that the model of the chronic ISR also applies to the context of mitochondrial dysfunction and is not limited to ER stress.

Nevertheless, the execution of two translational programmes results in a significantly increased energy demand, protein synthesis being considered as one of the most energy consuming processes in the cell (Lane and Martin, 2010). With regard to the strong respiratory defect of the animal model used for the present study, initiation of chronic ISR most probably represents a further challenge to the animals' energy resources. In addition, sudden re-initiation of global protein synthesis equates to increased ER stress due to a rapidly increasing amounts of proteins entering the ER for further processing. This configuration provides a potential explanation for the increase of ER stress markers observed during the terminal stage of DKO^{L} mice.

4.4 Putative signals upstream of eIF2α phosphorylation

The study design of this project was mainly oriented towards downstream aspects of eIF2α phosphorylation. However, the upstream signalling events initiating the signalling pathway in the context of mitochondrial dysfunction remain an issue of great interest. eIF2α is known to be phosphorylated by four different kinases, that become activated by distinct types of stress: PKR, PERK, HRI and GCN2. The particular major activating stressors are dsRNA, ER stress, heme deficiency and amino acid deprivation (Donnelly et al., 2013). Except PERK, all kinases were previously proposed as potential inducers of the ISR in response to mitochondrial stress (Michel et al., 2015; Rath et al., 2012; Restelli et al., 2018; Taniuchi et al., 2016). Unfortunately, the wide range of models (from cell culture to mice), tissues (from intestinal epithelial cells to neurons) and methods used to investigate mitochondrial dysfunction in the mentioned publications (e.g. ΔOTC expression, DRP1 deletion, FCCP treatment) complicate the evaluation of these results.

A recent publication examining endogenous intracellular dsRNAs interacting with PKR revealed dsRNAs of mitochondrial origin as the most strongly represented group. In addition, partial rescue of stress-induced eIF2α phosphorylation could be achieved by knock-down of *polrmt* (Kim et al., 2018). Considering the increase of selected mitochondrial transcripts, the gradual decline of the mitochondrial membrane potential

as well as the observed structural defects of mitochondria in DARS2 KO and DKO mice, a possible role for PKR should be assessed in future analyses.

Increased BiP levels as a marker for ER stress were detected in both, DARS2 KO (data not shown) and DKO^{L} mice during the respective terminal stages of the animals. Therefore, the involvement of PERK in sustaining ISR activation during the chronic phase of the ISR should be considered.

Re-evaluation of the proteomics data provided indications for iron deficiency and enhancement of heme biosynthesis in DKO^{L} mice. First, iron storage protein Ferritin H (FTH1) levels are significantly decreased in DKO^{L} animals. Ferritin H is mainly regulated post-transcriptionally. *Fth1* transcripts are actively recruited from monosomes to polysomes in the presence of iron (Rogers and Munro, 1987; Zähringer et al., 1976). Hence, decreased Ferritin H protein levels are most likely a result of decreased iron levels. Second, Ferrochelatase is significantly increased in DARS2 KO and DKO^{L} mice. Ferrochelatase catalyses the last step of heme synthesis, incorporating a ferrous atom in protoporphyrinogen IX (Pelley, 2012). Those modifications point towards altered iron metabolism and are raising the possibility of ISR activation via the eIF2α kinase HRI.

GCN2 is sensing amino acid deprivation through accumulation of uncharged tRNAs using a histidyl tRNA synthetase-domain (Vazquez de Aldana et al., 1994; Wek et al., 1995). In this regard, the significantly decreased histidine levels in early-state DARS2 KO mice around p17 suggest GCN2 activation as a potential cause of early eIF2α phosphorylation. However, histidine levels of early-stage DKO^{E} mice are not available, and no difference was detected in late-stage DKO^{L} animals. Apart from decreased amino acid levels, increased tRNA levels could also result in GCN2 activation. Notably, increased ATF4 protein levels in the context of cancer were shown to be caused by the MYC-dependent increase of cytoplasmic tRNA levels leading to GCN2 activation (Tameire et al., 2019). Moreover, potential relevance of the TF MYC for mitochondrial stress responses was described for several mouse models of severe mitochondrial dysfunction (Kuhl et al., 2017). Interestingly, ATF4 and MYC share a considerable amount of transcriptional targets and were shown to co-occupy promoter regions of genes with functions in amino acid transport (Tameire et al., 2019). MYC promotes cell growth and proliferation by providing building blocks through increased anabolism and promotion of protein synthesis (Stine et al., 2015). Considering those findings, the transcriptional activation of *Myc* in DARS2 KO and DKO mice represents an important indication with a significance extending beyond the possible induction of GCN2 activation. Hence, not only amino acid and cytoplasmic tRNA levels should be subject of further investigations to clarify a possible role of GCN2, but also the general role of MYC in the context of mitochondrial dysfunction needs to be analysed more precisely.

In conclusion, several models for eIF2α phosphorylation in DARS2 KO and DKO mice are conceivable, including the cooperation of two or more kinases. Assessment of the phosphorylation status of all four eIF2α kinases along with further analyses suggested above are required, in order to drive forward the understanding of the exact mechanisms upstream of eIF2α phosphorylation.

4.5 CHOP is not required for *in vivo* activation of UPR^{mt} markers

Albeit the prominent ISR signature in DARS2 KO and DKO mice, the UPR^{mt}, as the first CHOP-associated mito-specific stress response, had also to be taken into consideration.

Inaugural *in vitro* studies demonstrated CHOP-dependent induction of a nuclear gene expression programme supposed to promote mitochondrial proteostasis by increased expression of mitochondrial chaperones and proteases (Zhao et al., 2002). Whereas partially only validated by reporter assays, proteins such as HSP60, HSP10 or YME1L1 were subsequently employed as *bona fide* UPR^{mt} markers (Aldridge et al., 2007; Zhao et al., 2002). Subsequent *in vitro* studies extended the list of mammalian UPR^{mt} markers with e.g. mtHSP70 and LONP1 (Fiorese et al., 2016). It should be noted that those results were obtained solely by analyses performed on the transcript level. The mentioned study did not comment on CHOP, but proposed the TF ATF5 as mediator of the mammalian UPR ^{mt}, in analogy to ATFS-1 known from the *C.elegans*-specific pathway. However, these results not necessarily contradict the inaugural work based on CHOP, as CHOP is a known transcriptional regulator of ATF5 (Teske et al., 2013).

With regard to the present study performed on DARS2 KO and DKO mice, CHOP does not seem to be essential for the transcriptional activation of UPR^{mt}-associated genes. Transcriptional activation of mitochondrial chaperones and proteases related to the signalling pathway was not blocked in DKO^{L} mice. On the contrary, UPR^{mt} associated transcripts showed a significant increase in comparison to DARS2 KOs. However, the biological significance of this transcriptional activation, accepted as a gold standard for detection of UPR^{mt} activation according to a recent review (Münch, 2018), remains disputable. In the present case, those transcriptional changes did not implicate elevated protein levels of the respective mitochondrial chaperones and proteases in DKO^{L} mice. Considering the late-onset increase of respective UPR^{mt} markers in DARS2 KO mice on the protein level (detectable only at six weeks of age) and in accordance with the observations made in the Deletor mouse introduced earlier (Forsstrom et al., 2019), the

data suggest a subordinate role for the UPR^{mt} in the mentioned *in vivo* models. The biologically relevant induction of mitochondrial chaperones and proteases on the protein level arises late in the chronology of pathological changes. This leads to the question, to what extent mitochondrial homeostasis can be improved at this advanced stage of mitochondrial dysfunction. Moreover, the concept of the UPR^{mt} would benefit from further consolidation in general, as the widely used UPR^{mt} markers certainly require a more profound validation.

4.6 Mitochondrial deficiency induced by loss of *Dars2* entails considerable changes in cardiac metabolism that occur prematurely upon CHOP deficiency

4.6.1 General pathological changes associated with mitochondrial dysfunction in the myocardium

According to the resting metabolic rates determined for major organs in humans, both heart and kidney display the highest resting energy expenditure (Elia, 1992; Wang et al., 2010). Interference with cardiac mitochondrial energy production frequently results in activation of adaptive but also maladaptive alterations of the organ's energy metabolism. Development of cardiomyopathy, for instance, is commonly observed under the described conditions (Kelly and Strauss, 1994). Hence, cardiomyopathy developed by DARS2 KO and DKO^{L} mice was not surprising. However, it is interesting to note that DKO mice exhibited premature development of cardiac pathologies in comparison to DARS2 KO mice. Considering the coinciding onset of cardiomyopathy with the transition from the acute to the chronic stage of the ISR, a possible involvement of the ISR in the disease progression needs to be taken into account.

From a metabolic point of view, DKO mice display the classical switch from energy production mainly based on fatty acid oxidation to a foetal-like metabolic profile relying primarily on glucose utilisation. Significantly increased *nppa* and *nppb* levels detected in DKO^{L} mice provide further evidence for the re-expression of the foetal gene program (Ellen Kreipke et al., 2016; Lehman and Kelly, 2002; Ritterhoff and Tian, 2017). Also, a

trend towards reduced ATP levels in DKO^{L} mice was detected. According to the “energy starvation” hypothesis of heart failure, suboptimal ATP supply predisposes for the contractile dysfunction observed during heart failure (Katz, 1998). In the heart, CK (creatine kinase) represents a spatial and temporal ATP buffer, generating high cytosolic ATP concentrations at the site of consumption out of phospho-creatine and ADP. It has been shown previously, that ATP flux through CK in hearts of patients with mild-to-moderate chronic heart failure is reduced already before a significant reduction of ATP levels is detectable. Furthermore, evidence for a deficit in energy supply of failing human hearts was provided (Weiss et al., 2005). Hence, the detection of a trend towards diminished ATP concentration in the hearts of DKO^{L} mice might suggest a progressed state of heart failure.

Besides contractile dysfunction as discussed above, also ventricular arrhythmias are tightly associated with heart failure (Packer, 1985). Strikingly, single cardiomyocytes with severe mitochondrial dysfunction are sufficient to promote cardiac arrhythmia. Using the K320E-$Twinkle^{Myo}$ mouse exhibiting accelerated accumulation of mtDNA deletions it was shown, that already 0.6% of COX-negative cardiomyocytes result in spontaneous ventricular premature contractions and atrioventricular blocks (Baris et al., 2015). Considering the severe impairment of ETC function in both, DARS2 KO and DKO mice, the occurrence of cardiac arrhythmias in those animals further contributing to the pathology seem likely.

Furthermore, alarming citrate levels were detected in hearts of DKO^{L} mice. As compared to WT samples, a 5.6-fold increase of the metabolite had been determined. It was previously shown in patient cells harbouring mtDNA mutations, that upon severe OXPHOS impairment glutamine metabolism is altered and feeds the reductive TCA cycle, resulting in increased citrate synthesis (Chen et al., 2018). Increased intracellular citrate levels can engender intracellular acidosis, leading to hypocalcemia caused by reduced availability of Ca^{2+}. Importantly, cardiac contraction is induced by Ca^{2+}-release from the sarcoplasmic reticulum. Ca^{2+}-release occurs in close proximity to mitochondria. As a result of increased Ca^{2+} uptake by mitochondria during this phase, the TCA cycle and the ETC are transiently activated, inducing increased ATP production. Therefore, reduced Ca^{2+} availability caused by citrate-driven metabolic acidosis contributes to reduced contractility of the heart. The excitation of muscle fibres is damped, and ATP production-coupling in mitochondria with the muscle contraction provided by Ca^{2+} is impaired (Orchard and Kentish, 1990; Poole-Wilson, 1982; Porter et al., 2011). Therefore, increased citrate levels negatively impact on cardiac physiology of DKO^{L} mice via impairment of the excitation-contraction-metabolism coupling. Furthermore, additional effects of elevated citrate levels on regulation of metabolic enzymes or

chromatin dynamics by acetylation have to be taken into consideration (Wellen et al., 2009; Zhao et al., 2010).

4.6.2 ATF4-specific metabolic alterations induced by the activation of the ISR

Induction of anabolic programmes by ATF4 activation becomes evident on closer inspection of transcriptional ATF4 targets. In DKO mice, re-inforced increases of amino acid transporters (e.g. SLC38A2, SLC7A5), amino acid metabolic enzymes (e.g. ASNS, PHGDH) and tRNA synthetases (e.g. GARS, NARS) determined in DARS2 KO mice were ascertained on the mRNA and protein level. Mass spectrometric analyses of amino acid levels in cardiac samples further confirmed the observed trend, as 15 out of 19 recorded amino acids showed significant increases in DKO^{L} mice. However, this overall increase is most probably not entirely attributable to ATF4-related changes, as also branched-chain amino acids (BCAAs: Ile, Leu and Val) were affected and BCAA catabolism is known to be impaired during cardiac dysfunction and hypertrophy (Ritterhoff and Tian, 2017). The metabolic rewiring caused by the transition of acute to chronic ISR in general, and activation of ATF4 in particular, results in the induction of anabolic pathways and thus a significantly increased energy demand in hearts of DKO^{L} mice.

As a regulator of growth and metabolism, mTORC1 is controlled by an extensive variety of signals such as cellular energy levels (via AMPK) or nutrients (especially amino acids) (Goberdhan et al., 2016). Therefore, generally increased amino acid levels in DKO^{L} mice provide a possible explanation for the minor signs of mTORC1 activation detected in the animals. Nevertheless, the data indicate that mTORC1 activation plays a subordinate role in our model of mitochondrial dysfunction and rather represents a consequence than the cause of ATF4 activation.

This conclusion is of particular interest, as an inverse relationship between mTORC1 and ATF4 was shown in the Deletor mouse. Strikingly, treatment of Deletor mice with rapamycin, an inhibitor of mTORC1, resulted in decreased *atf4* mRNA levels and were accompanied by arrested disease progression (Khan et al., 2017). Control of ATF4 by mTORC1 was shown to occur on the post-transcriptional level by regulation of mRNA stability and translation (Park et al., 2017). As a whole, the described findings summarise the mutual interference between ISR and mTORC1 via amino acid and *atf4* transcript levels (Papadopoli et al., 2019). Moreover, these insights highlight the necessity to

understand the upstream events of ISR in DARS2 KO and DKO mice as well as mTORC1 activation in Deletor mice, respectively.

Intriguingly, bringing the most recent publication of the Deletor mouse model into accordance with the findings mentioned above is challenging. First, *atf4* transcript levels in Deletor mice are unchanged up to the age of 22 months (Forsstrom et al., 2019), contrary to the previous paper reporting significant changes on the mRNA as well as on the protein level (Khan et al., 2017). Instead, a significant contribution of ATF3 and ATF5 to the progression of the integrated mitochondrial stress response (ISR^{mt}) proposed by the Suomalainen laboratory earlier, was suggested (Forsstrom et al., 2019; Suomalainen and Battersby, 2017). Second, mTORC1, previously classified upstream of ATF4 and FGF21 activation (Khan et al., 2017), is not considered as the regulator of the ISR^{mt} anymore. Conversely, an FGF21-dependent regulation of the ISR^{mt} was proposed (Forsstrom et al., 2019). Interestingly, actinonin-treated murine myoblasts displayed an ATF4-dependent, but ATF3 and ATF5-independent ISR^{mt}. The post-mitotic nature of the analysed skeletal muscle samples issued from Deletor mice versus the proliferative nature of the myoblast cell line was proposed as a possible explanation for the described differences between the two model systems (Forsstrom et al., 2019). Due to insights gained from analyses performed on DKO mice, this explanation might be questioned. Analyses of DKO mice were also performed on a post-mitotic tissue, the murine heart. Possible alternative explanations might include the severity of the disease, tissue-specific effects or the age and therefore the developmental state at which the disease peaks.

4.7 The interplay between LIP and CHOP is essential for adjusted transcriptional regulation of *Atf4* during severe mitochondrial dysfunction

Net transcription of a specific gene represents the result of complex signal integration taking place at several regulatory levels, including the activity of activating or repressing TFs on the promoter level. Therefore, increased *Atf4* transcription upon loss of *Chop* might result from augmented activation, decreased repression or a combinatory effect of both.

Interestingly, C/EBPβ was identified as CHOP interactor in DARS2 KO hearts. Like CHOP, C/EBPβ is a pleiotropic TF contributing among other things to regulation of hematopoiesis as well as homeostasis of several tissues such as bone, skin or fat (Begay

et al., 2018). C/EBPβ is primarily regulated on the translational level. One of its peculiarities is the sequence of three consecutive in-frame start codons on the protein-coding mRNA, giving rise to the three C/EBPβ protein isoforms LAP* (liver activating protein*, 38 kDa, full lengh), LAP (liver activating protein, 35 kDa) and LIP (liver inhibitory protein, 20 kDa, devoid of the TADs present in LAP* and LAP) (Descombes and Schibler, 1991). Both longer isoforms and LIP are characterised by an antagonistic relationship, as the names already indicate. In many cases target genes (e.g. *Mafb*, coding for a TF involved in osteoclastogenesis) are positively regulated by LAP*/LAP, whereas LIP binding represses the respective locus. As the DBD is identical in all three isoforms, the regulation occurs via the modulation of the LAP*/LAP vs. LIP ratio (Smink et al., 2009; Tsukada et al., 2011).

Based on *in vitro* analyses assessing (i) the response of all three C/EBPβ isoforms LAP*, LAP and LIP to mitochondrial dysfunction, and (ii) the impact of individual isoforms on *Atf4* expression the following mechanism underlying ISR over-activation in DKO mice is proposed:

Loss of CHOP impairs the increase of the C/EBPβ isoform LIP, normally occurring upon mitochondrial dysfunction. CHOP was previously shown to prevent the re-export of LIP from the nucleus in the context of ER stress, thereby preventing cytoplasmic degradation of LIP (Chiribau et al., 2010).

Additionally, nuclear retention of LIP via mutation of the NES (LIP L120D) abolished the increase of ATF4 protein levels upon actinonin treatment in CHOP-deficient MEFs. Those results are in line with an earlier report studying the causes of variable ATF4 expression in response to eIF2α phosphorylation upon distinct stress conditions such as ER stress or UV irradiation. It was shown, that UV irradiation LIP-dependently represses *Atf4* transcription. Furthermore, evidence for beneficial effects of eIF2α phosphorylation as well as enhanced cell survival due to repression of *Atf4* during UV irradiation were provided (Dey et al., 2012).

Taken together, CHOP-mediated nuclear retention of LIP upon mitochondrial dysfunction represents a novel regulating screw in the context of the mito-specific modulation of the ISR, contributing to the adjustment of *Atf4* expression executed by the repressive impact of LIP on the *Atf4* promoter (Figure 4.1).

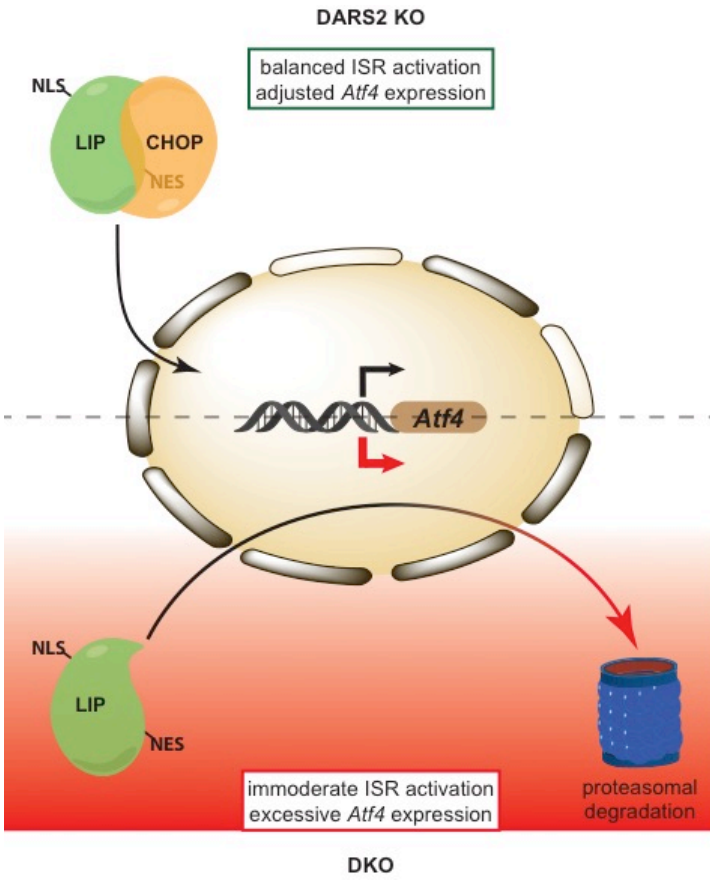

Figure 4.1: Model of CHOP-mediated nuclear retention of LIP, exerting repressive effects on the *Atf4* promoter.

Increased CHOP protein levels triggered by mitochondrial dysfunction-related ISR activation facilitate nuclear retention of LIP. The latter TF negatively affects *Atf4* transcription. In the absence of CHOP, LIP re-export and subsequent proteasomal degradation abrogate the repressive effect of LIP on the *Atf4* promoter, resulting in increased *Atf4* expression.

However, further investigations are necessary to provide deeper mechanistic details on the LIP-mediated repression of *Atf4.* Owing to the characteristics of the C/EBP family of TFs (Tsukada et al., 2011), pre-formed LIP-containing dimers binding to the *Atf4* promoter as well as the replacement of a single subunit within a promoter-bound dimer by LIP need to be considered. Also, LIP-containing dimers might be of homo- or hetero-dimeric nature. On the one hand, transcriptional inhibition could be achieved by binding of TF dimers fully devoid of TADs (e.g. LIP homodimers or LIP-CHOP heterodimers, respectively). However, experiments in CHOP KO MEFs revealed, that CHOP is dispensable for repression of *Atf4* transcription. On the other hand, mechanisms including the replacement of the activating C/EBPβ isoforms LAP* or LAP by LIP in *Atf4* promoter-binding dimers should be taken into consideration, too. The presence of LIP in the respective dimers would thereby revert the LAP*/LAP-mediated positive effect on transcription. The determination of the dimer composition upon mitochondrial

dysfunction during future investigations will certainly advance the understanding of underlying mechanistic details. Moreover, direct comparison of LIP dimer composition during mitochondrial dysfunction and UV irradiation could provide further insights into stress-specific fine-tuning of the ISR in response to different types of stress.

4.8 Summary

In consideration of beforehand discussed accumulated pathological developments caused by mitochondrial dysfunction and resulting metabolic alterations in DKO mice, heart failure appears as the most plausible cause of death. Significant changes contributing to pathology are summarised below (Figure 4.2).

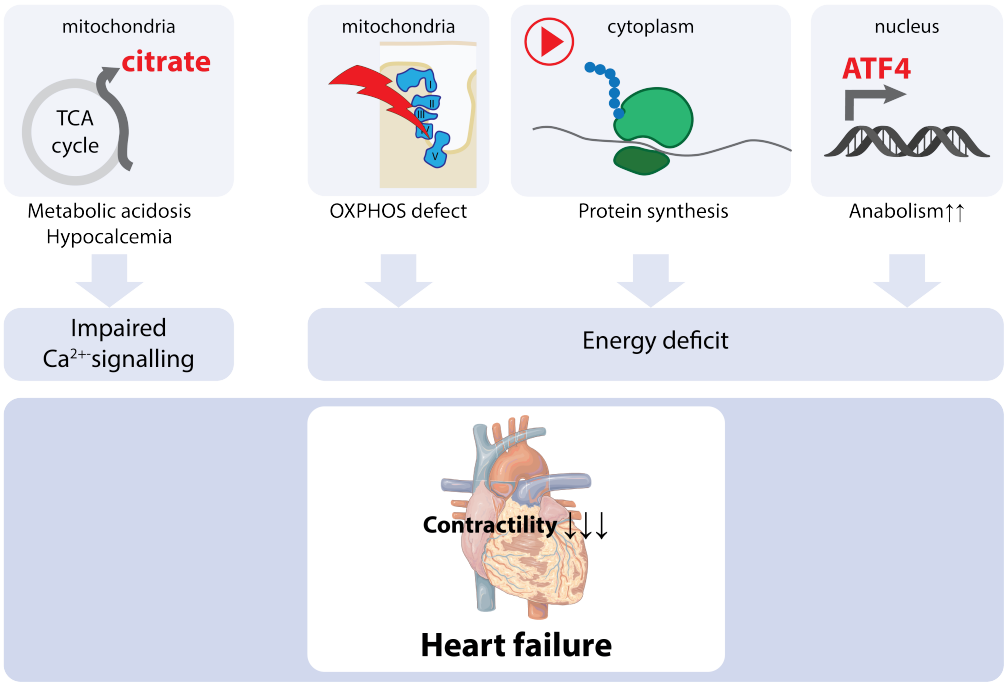

Figure 4.2: Events contributing DKO mice pathology.

Referring to the earlier defined research aims for this study investigating the role of CHOP in the context of mitochondrial dysfunction, following insights were gained:

First, deletion of *Chop* has detrimental effects in conditions of severe mitochondrial dysfunction as shown by animal (DARS2/CHOP DKO mice) or cell culture-based experiments (actinonin-treated CHOP KO MEFs), resulting in significantly shortened life expectancy or reduced growth rates, respectively.

Second, under the given circumstances CHOP modulates the progression of the ISR, a stress pathway induced in many models of mitochondrial dysfunction (Arnould et al., 2015; Dogan et al., 2014; Forsstrom et al., 2019; Kuhl et al., 2017; Quirós et al., 2017).

Third, CHOP negatively regulates transcriptional activation of *Atf4* via the nuclear retention of the inhibitory C/EBPβ isoform LIP, thereby adding a supplementary regulatory layer to the ISR.

This study provided evidence for the deleterious consequences of ISR deregulation resulting in ATF4 over-activation. The discussed findings give rise to further questions concerning (i) the benefit of the ISR, (ii) specific conditions impairing a beneficial equilibrium between activation and inhibition of the stress response and (iii) about ATF4 as a potential therapeutic target for pathological developments triggered by inappropriate ISR activation. Obviously, the respective answers strongly depend on the specific situation, determined for instance by the nature and severity of the ISR initiating stress or the affected tissue. Therefore, the coordinated efforts of many researchers are required in the future in order to recognise the greater picture.

References

Agaronyan, K., Morozov, Y.I., Anikin, M., and Temiakov, D. (2015). Mitochondrial biology. Replication-transcription switch in human mitochondria. Science *347*, 548-551.

Akram, M. (2014). Citric acid cycle and role of its intermediates in metabolism. Cell Biochem Biophys *68*, 475-478.

Al-Attar, S., and de Vries, S. (2013). Energy transduction by respiratory metallo-enzymes: From molecular mechanism to cell physiology. Coordination Chemistry Reviews *257*, 64-80.

Aldridge, J.E., Horibe T Fau - Hoogenraad, N.J., and Hoogenraad, N.J. (2007). Discovery of genes activated by the mitochondrial unfolded protein response (mtUPR) and cognate promoter elements.

Ameri, K., and Harris, A.L. (2008). Activating transcription factor 4. The International Journal of Biochemistry & Cell Biology *40*, 14-21.

Amunts, A., Brown, A., Toots, J., Scheres, S.H.W., and Ramakrishnan, V. (2015). Ribosome. The structure of the human mitochondrial ribosome. Science *348*, 95-98.

Anderson, S., Bankier, A.T., Barrell, B.G., de Bruijn, M.H.L., Coulson, A.R., Drouin, J., Eperon, I.C., Nierlich, D.P., Roe, B.A., Sanger, F., et al. (1981). Sequence and organization of the human mitochondrial genome. Nature *290*, 457-465.

Andrews, R.M., Kubacka, I., Chinnery, P.F., Lightowlers, R.N., Turnbull, D.M., and Howell, N. (1999). Reanalysis and revision of the Cambridge reference sequence for human mitochondrial DNA. Nat Genet *23*, 147.

Arnold, I., Pfeiffer, K., Neupert, W., Stuart, R.A., and Schagger, H. (1998). Yeast mitochondrial F1F0-ATP synthase exists as a dimer: identification of three dimer-specific subunits. EMBO J *17*, 7170-7178.

Arnould, T., Michel, S., and Renard, P. (2015). Mitochondria Retrograde Signaling and the UPR(mt): Where Are We in Mammals? International Journal of Molecular Sciences *16*, 18224-18251.

Baker, B.M., Nargund, A.M., Sun, T., and Haynes, C.M. (2012). Protective Coupling of Mitochondrial Function and Protein Synthesis via the eIF2α Kinase GCN-2. PLOS Genetics *8*, e1002760.

Balachandran, S., Roberts, P.C., Brown, L.E., Truong, H., Pattnaik, A.K., Archer, D.R., and Barber, G.N. (2000). Essential role for the dsRNA-dependent protein kinase PKR in innate immunity to viral infection. Immunity *13*, 129-141.

Bao, X.R., Ong, S.-E., Goldberger, O., Peng, J., Sharma, R., Thompson, D.A., Vafai, S.B., Cox, A.G., Marutani, E., Ichinose, F., et al. (2016). Mitochondrial dysfunction remodels one-carbon metabolism in human cells. eLife *5*, e10575.

Baradaran, R., Berrisford, J.M., Minhas, G.S., and Sazanov, L.A. (2013). Crystal structure of the entire respiratory complex I. Nature *494*, 443-448.

Baris, O.R., Ederer, S., Neuhaus, J.F., von Kleist-Retzow, J.C., Wunderlich, C.M., Pal, M., Wunderlich, F.T., Peeva, V., Zsurka, G., Kunz, W.S., et al. (2015). Mosaic Deficiency in Mitochondrial Oxidative Metabolism Promotes Cardiac Arrhythmia during Aging. Cell Metab *21*, 667-677.

Begay, V., Baumeier, C., Zimmermann, K., Heuser, A., and Leutz, A. (2018). The C/EBPbeta LIP isoform rescues loss of C/EBPbeta function in the mouse. Sci Rep *8*, 8417.

Bertolotti, A., Zhang, Y., Hendershot, L.M., Harding, H.P., and Ron, D. (2000). Dynamic interaction of BiP and ER stress transducers in the unfolded-protein response. Nat Cell Biol *2*, 326-332.

Bogenhagen, D.F. (2012). Mitochondrial DNA nucleoid structure. Biochim Biophys Acta *1819*, 914-920.

Bohovych, I., and Khalimonchuk, O. (2016). Sending Out an SOS: Mitochondria as a Signaling Hub. Frontiers in Cell and Developmental Biology *4*, 109.

Bolster, D.R., Crozier, S.J., Kimball, S.R., and Jefferson, L.S. (2002). AMP-activated Protein Kinase Suppresses Protein Synthesis in Rat Skeletal Muscle through Down-regulated Mammalian Target of Rapamycin (mTOR) Signaling. Journal of Biological Chemistry *277*, 23977-23980.

Butow, R.A., and Avadhani, N.G. (2004). Mitochondrial Signaling: The Retrograde Response. Molecular Cell *14*, 1-15.

Cai, Y.C., Bullard, J.M., Thompson, N.L., and Spremulli, L.L. (2000). Interaction of mitochondrial elongation factor Tu with aminoacyl-tRNA and elongation factor Ts. J Biol Chem *275*, 20308-20314.

Cao, Z., Umek, R.M., and McKnight, S.L. (1991). Regulated expression of three C/EBP isoforms during adipose conversion of 3T3-L1 cells. Genes Dev *5*, 1538-1552.

Carrara, M., Prischi, F., Nowak, P.R., Kopp, M.C., and Ali, M.M. (2015). Noncanonical binding of BiP ATPase domain to Ire1 and Perk is dissociated by unfolded protein CH1 to initiate ER stress signaling. Elife *4*.

Chakrabarti, A., Chen, A.W., and Varner, J.D. (2011). A review of the mammalian unfolded protein response. Biotechnology and Bioengineering *108*, 2777-2793.

Chandel, Navdeep S. (2015). Evolution of Mitochondria as Signaling Organelles. Cell Metabolism *22*, 204-206.

Chefalo, P.J., Oh, J., Rafie-Kolpin, M., Kan, B., and Chen, J.J. (1998). Heme-regulated eIF-2alpha kinase purifies as a hemoprotein. Eur J Biochem *258*, 820-830.

Chen, D.Z., Patel, D.V., Hackbarth, C.J., Wang, W., Dreyer, G., Young, D.C., Margolis, P.S., Wu, C., Ni, Z.-J., Trias, J., et al. (2000). Actinonin, a Naturally Occurring Antibacterial Agent, Is a Potent Deformylase Inhibitor. Biochemistry *39*, 1256-1262.

Chen, H., Pan, Y.X., Dudenhausen, E.E., and Kilberg, M.S. (2004). Amino acid deprivation induces the transcription rate of the human asparagine synthetase gene through a timed program of expression and promoter binding of nutrient-responsive basic region/leucine zipper transcription factors as well as localized histone acetylation. J Biol Chem *279*, 50829-50839.

Chen, Q., Kirk, K., Shurubor, Y.I., Zhao, D., Arreguin, A.J., Shahi, I., Valsecchi, F., Primiano, G., Calder, E.L., Carelli, V., et al. (2018). Rewiring of Glutamine Metabolism Is a Bioenergetic Adaptation of Human Cells with Mitochondrial DNA Mutations. Cell Metab *27*, 1007-1025 e1005.

Chinnery, P.F. (1993). Mitochondrial Disorders Overview. In GeneReviews((R)). M.P. Adam, H.H. Ardinger, R.A. Pagon, S.E. Wallace, L.J.H. Bean, K. Stephens, and A. Amemiya, eds. (Seattle (WA)).

Chiribau, C.-B., Gaccioli, F., Huang, C.C., Yuan, C.L., and Hatzoglou, M. (2010). Molecular Symbiosis of CHOP and C/EBPβ Isoform LIP Contributes to Endoplasmic Reticulum Stress-Induced Apoptosis. Molecular and Cellular Biology *30*, 3722.

Chrzanowska-Lightowlers, Z.M.A., Pajak, A., and Lightowlers, R.N. (2011). Termination of Protein Synthesis in Mammalian Mitochondria. Journal of Biological Chemistry *286*, 34479-34485.

Connor, J.H., Weiser, D.C., Li, S., Hallenbeck, J.M., and Shenolikar, S. (2001). Growth arrest and DNA damage-inducible protein GADD34 assembles a novel signaling complex containing protein phosphatase 1 and inhibitor 1. Mol Cell Biol *21*, 6841-6850.

Craven, L., Alston, C.L., Taylor, R.W., and Turnbull, D.M. (2017). Recent Advances in Mitochondrial Disease. Annu Rev Genomics Hum Genet *18*, 257-275.

Davies, K.M., Anselmi, C., Wittig, I., Faraldo-Gomez, J.D., and Kuhlbrandt, W. (2012). Structure of the yeast F1Fo-ATP synthase dimer and its role in shaping the mitochondrial cristae. Proc Natl Acad Sci U S A *109*, 13602-13607.

Deng, J., Harding, H.P., Raught, B., Gingras, A.C., Berlanga, J.J., Scheuner, D., Kaufman, R.J., Ron, D., and Sonenberg, N. (2002). Activation of GCN2 in UV-irradiated cells inhibits translation. Curr Biol *12*, 1279-1286.

Descombes, P., and Schibler, U. (1991). A liver-enriched transcriptional activator protein, LAP, and a transcriptional inhibitory protein, LIP, are translated from the sam mRNA. Cell *67*, 569-579.

Dey, S., Baird, T.D., Zhou, D., Palam, L.R., Spandau, D.F., and Wek, R.C. (2010). Both Transcriptional Regulation and Translational Control of ATF4 Are Central to the Integrated Stress Response. Journal of Biological Chemistry *285*, 33165-33174.

Dey, S., Savant, S., Teske, B.F., Hatzoglou, M., Calkhoven, C.F., and Wek, R.C. (2012). Transcriptional Repression of ATF4 Gene by CCAAT/Enhancer-binding Protein β (C/EBPβ) Differentially Regulates Integrated Stress Response. Journal of Biological Chemistry *287*, 21936-21949.

Diaz, F., Fukui, H., Garcia, S., and Moraes, C.T. (2006). Cytochrome c Oxidase Is Required for the Assembly/Stability of Respiratory Complex I in Mouse Fibroblasts. Molecular and Cellular Biology *26*, 4872.

Dogan, Sukru A., Pujol, C., Maiti, P., Kukat, A., Wang, S., Hermans, S., Senft, K., Wibom, R., Rugarli, Elena I., and Trifunovic, A. (2014). Tissue-Specific Loss of DARS2 Activates Stress Responses Independently of Respiratory Chain Deficiency in the Heart. Cell Metabolism *19*, 458-469.

Donnelly, N., Gorman, A.M., Gupta, S., and Samali, A. (2013). The eIF2alpha kinases: their structures and functions. Cell Mol Life Sci *70*, 3493-3511.

Drysdale, G.R., and Lardy, H.A. (1953). Fatty acid oxidation by a soluble enzyme system from mitochondria. J Biol Chem *202*, 119-136.

Durieux, J., Wolff, S., and Dillin, A. (2011). The Cell-Non-Autonomous Nature of Electron Transport Chain-Mediated Longevity. Cell *144*, 79-91.

Elia, M. (1992). Organ and tissue contribution to metabolic rate. In Energy metabolism: tissue determinants and cellular corollaries. T.H. Kinney JM, ed. (New York: Raven Press), pp. 61–80.

Ellen Kreipke, R., Wang, Y., Miklas, J.W., Mathieu, J., and Ruohola-Baker, H. (2016). Metabolic remodeling in early development and cardiomyocyte maturation. Semin Cell Dev Biol *52*, 84-92.

Ernster, L., and Schatz, G. (1981). Mitochondria: a historical review. J Cell Biol *91*, 227s-255s.

Falkenberg, M. (2018). Mitochondrial DNA replication in mammalian cells: overview of the pathway. Essays Biochem *62*, 287-296.

Falkenberg, M., Larsson, N.G., and Gustafsson, C.M. (2007). DNA replication and transcription in mammalian mitochondria. Annu Rev Biochem *76*, 679-699.

Fawcett, T.W., Martindale, J.L., Guyton, K.Z., Hai, T., and Holbrook, N.J. (1999). Complexes containing activating transcription factor (ATF)/cAMP-responsive-element-binding protein (CREB) interact with the CCAAT/enhancer-binding protein (C/EBP)-ATF composite site to regulate Gadd153 expression during the stress response. Biochem J *339 (Pt 1)*, 135-141.

Fiorese, Christopher J., Schulz, Anna M., Lin, Y.-F., Rosin, N., Pellegrino, Mark W., and Haynes, Cole M. (2016). The Transcription Factor ATF5 Mediates a Mammalian Mitochondrial UPR. Current Biology *26*, 2037-2043.

Fontanesi, F., Soto, I.C., Horn, D., and Barrientos, A. (2006). Assembly of mitochondrial cytochrome c-oxidase, a complicated and highly regulated cellular process. Am J Physiol Cell Physiol *291*, C1129-1147.

Forsstrom, S., Jackson, C.B., Carroll, C.J., Kuronen, M., Pirinen, E., Pradhan, S., Marmyleva, A., Auranen, M., Kleine, I.M., Khan, N.A., et al. (2019). Fibroblast Growth Factor 21 Drives Dynamics of Local and Systemic Stress Responses in Mitochondrial Myopathy with mtDNA Deletions. Cell Metab.

Fribley, A.M., Miller, J.R., Brownell, A.L., Garshott, D.M., Zeng, Q., Reist, T.E., Narula, N., Cai, P., Xi, Y., Callaghan, M.U., et al. (2015). Celastrol induces unfolded protein response-dependent cell death in head and neck cancer. Exp Cell Res *330*, 412-422.

Friedman, J.R., and Nunnari, J. (2014). Mitochondrial form and function. Nature *505*, 335.

Galluzzi, L., Yamazaki, T., and Kroemer, G. (2018). Linking cellular stress responses to systemic homeostasis. Nat Rev Mol Cell Biol *19*, 731-745.

Gardner, B.M., and Walter, P. (2011). Unfolded proteins are Ire1-activating ligands that directly induce the unfolded protein response. Science *333*, 1891-1894.

Gaur, R., Grasso, D., Datta, P.P., Krishna, P.D., Das, G., Spencer, A., Agrawal, R.K., Spremulli, L., and Varshney, U. (2008). A single mammalian mitochondrial translation initiation factor functionally replaces two bacterial factors. Mol Cell *29*, 180-190.

Ghezzi, D., and Zeviani, M. (2012). Assembly factors of human mitochondrial respiratory chain complexes: physiology and pathophysiology. Adv Exp Med Biol *748*, 65-106.

Giannattasio, S., Liu, Z., Thornton, J., and Butow, R.A. (2005). Retrograde Response to Mitochondrial Dysfunction Is Separable from TOR1/2 Regulation of Retrograde Gene Expression. Journal of Biological Chemistry *280*, 42528-42535.

Gilkerson, R.W., Selker, J.M., and Capaldi, R.A. (2003). The cristal membrane of mitochondria is the principal site of oxidative phosphorylation. FEBS Lett *546*, 355-358.

Glover, J.N., and Harrison, S.C. (1995). Crystal structure of the heterodimeric bZIP transcription factor c-Fos-c-Jun bound to DNA. Nature *373*, 257-261.

Goberdhan, D.C., Wilson, C., and Harris, A.L. (2016). Amino Acid Sensing by mTORC1: Intracellular Transporters Mark the Spot. Cell Metab *23*, 580-589.

Goodman, C.A., and Hornberger, T.A. (2013). Measuring protein synthesis with SUnSET: a valid alternative to traditional techniques? Exercise and sport sciences reviews *41*, 107-115.

Gorman, G.S., Chinnery, P.F., DiMauro, S., Hirano, M., Koga, Y., McFarland, R., Suomalainen, A., Thorburn, D.R., Zeviani, M., and Turnbull, D.M. (2016). Mitochondrial diseases. Nature Reviews Disease Primers *2*, 16080.

Guan, B.-J., van Hoef, V., Jobava, R., Elroy-Stein, O., Valasek, L.S., Cargnello, M., Gao, X.-H., Krokowski, D., Merrick, W.C., Kimball, S.R., et al. (2017). A Unique ISR Program Determines Cellular Responses to Chronic Stress. Molecular Cell *68*, 885-900.e886.

Guan, B.J., Krokowski, D., Majumder, M., Schmotzer, C.L., Kimball, S.R., Merrick, W.C., Koromilas, A.E., and Hatzoglou, M. (2014). Translational control during endoplasmic reticulum stress beyond phosphorylation of the translation initiation factor eIF2alpha. J Biol Chem *289*, 12593-12611.

Han, A.P., Yu, C., Lu, L., Fujiwara, Y., Browne, C., Chin, G., Fleming, M., Leboulch, P., Orkin, S.H., and Chen, J.J. (2001). Heme-regulated eIF2alpha kinase (HRI) is required for translational regulation and survival of erythroid precursors in iron deficiency. EMBO J *20*, 6909-6918.

Haque, M.E., and Spremulli, L.L. (2008). Roles of the N- and C-terminal domains of mammalian mitochondrial initiation factor 3 in protein biosynthesis. J Mol Biol *384*, 929-940.

Harbauer, Angelika B., Zahedi, René P., Sickmann, A., Pfanner, N., and Meisinger, C. (2014). The Protein Import Machinery of Mitochondria—A Regulatory Hub in Metabolism, Stress, and Disease. Cell Metabolism *19*, 357-372.

Harding, H.P., Novoa, I., Zhang, Y., Zeng, H., Wek, R., Schapira, M., and Ron, D. (2000). Regulated Translation Initiation Controls Stress-Induced Gene Expression in Mammalian Cells. Molecular Cell *6*, 1099-1108.

Harding, H.P., Zhang, Y., and Ron, D. (1999). Protein translation and folding are coupled by an endoplasmic-reticulum-resident kinase. Nature *397*, 271-274.

Harding, H.P., Zhang, Y., Zeng, H., Novoa, I., Lu, P.D., Calfon, M., Sadri, N., Yun, C., Popko, B., Paules, R., et al. (2003). An Integrated Stress Response Regulates Amino Acid Metabolism and Resistance to Oxidative Stress. Molecular Cell *11*, 619-633.

Harvey, P.A., and Leinwand, L.A. (2011). Cellular mechanisms of cardiomyopathy. The Journal of Cell Biology *194*, 355.

Hattori, T., Ohoka, N., Hayashi, H., and Onozaki, K. (2003). C/EBP homologous protein (CHOP) up-regulates IL-6 transcription by trapping negative regulating NF-IL6 isoform. FEBS Letters *541*, 33-39.

Haynes, C.M., Petrova, K., Benedetti, C., Yang, Y., and Ron, D. (2007). ClpP Mediates Activation of a Mitochondrial Unfolded Protein Response in C. elegans. Developmental Cell *13*, 467-480.

Haynes, C.M., Yang, Y., Blais, S.P., Neubert, T.A., and Ron, D. (2010). The Matrix Peptide Exporter HAF-1 Signals a Mitochondrial UPR by Activating the Transcription Factor ZC376.7 in C. elegans. Molecular Cell *37*, 529-540.

He, K., Zheng, X., Li, M., Zhang, L., and Yu, J. (2016a). mTOR inhibitors induce apoptosis in colon cancer cells via CHOP-dependent DR5 induction on 4E-BP1 dephosphorylation. Oncogene *35*, 148-157.

He, Y., Hara, H., and Núñez, G. (2016b). Mechanism and Regulation of NLRP3 Inflammasome Activation. Trends in Biochemical Sciences *41*, 1012-1021.

Horibe, T., and Hoogenraad, N.J. (2007). The Chop Gene Contains an Element for the Positive Regulation of the Mitochondrial Unfolded Protein Response. PLOS ONE *2*, e835.

Hu, H., Tian, M., Ding, C., and Yu, S. (2019). The C/EBP Homologous Protein (CHOP) Transcription Factor Functions in Endoplasmic Reticulum Stress-Induced Apoptosis and Microbial Infection. Frontiers in Immunology *9*, 3083.

Hutchin, T., Haworth, I., Higashi, K., Fischel-Ghodsian, N., Stoneking, M., Saha, N., Arnos, C., and Cortopassi, G. (1993). A molecular basis for human hypersensitivity to aminoglycoside antibiotics. Nucleic Acids Res *21*, 4174-4179.

Ill-Raga, G., Tajes, M., Busquets-Garcia, A., Ramos-Fernandez, E., Vargas, L.M., Bosch-Morato, M., Guivernau, B., Valls-Comamala, V., Eraso-Pichot, A., Guix, F.X., et al. (2015). Physiological Control of Nitric Oxide in Neuronal BACE1 Translation by Heme-Regulated eIF2alpha Kinase HRI Induces Synaptogenesis. Antioxid Redox Signal *22*, 1295-1307.

Ishikawa, F., Akimoto, T., Yamamoto, H., Araki, Y., Yoshie, T., Mori, K., Hayashi, H., Nose, K., and Shibanuma, M. (2009). Gene Expression Profiling Identifies a Role for CHOP During Inhibition of the Mitochondrial Respiratory Chain. The Journal of Biochemistry *146*, 123-132.

Iurlaro, R., and Muñoz-Pinedo, C. (2016). Cell death induced by endoplasmic reticulum stress. The FEBS Journal *283*, 2640-2652.

Jackson, R.J., Hellen, C.U., and Pestova, T.V. (2010). The mechanism of eukaryotic translation initiation and principles of its regulation. Nat Rev Mol Cell Biol *11*, 113-127.

Jacobs, H.T., and Holt, I.J. (1998). The Mitochondrial Genetic System. In Mitochondrial DNA Mutations in Aging, Disease and Cancer. K.K. Singh, ed. (Berlin, Heidelberg: Springer Berlin Heidelberg), pp. 43-83.

Jäger, S., Handschin, C., St.-Pierre, J., and Spiegelman, B.M. (2007). AMP-activated protein kinase (AMPK) action in skeletal muscle via direct phosphorylation of PGC-1α. Proceedings of the National Academy of Sciences *104*, 12017.

Janky, R.s., Verfaillie, A., Imrichová, H., Van de Sande, B., Standaert, L., Christiaens, V., Hulselmans, G., Herten, K., Naval Sanchez, M., Potier, D., et al. (2014). iRegulon: From a Gene List to a Gene Regulatory Network Using Large Motif and Track Collections. PLOS Computational Biology *10*, e1003731.

Jhas, B. (2012). Chronic Mitochondrial Translation Inhibition Alters Metabolic Phenotype and Stemness Properties of a Leukemic Cell Line. In Institute of Medical Sciences (Toronto: University of Toronto), p. 110.

John, P., and Whatley, F.R. (1975). Paracoccus denitrificans and the evolutionary origin of the mitochondrion. Nature *254*, 495-498.

Jonckheere, A.I., Smeitink, J.A., and Rodenburg, R.J. (2012). Mitochondrial ATP synthase: architecture, function and pathology. J Inherit Metab Dis *35*, 211-225.

Jousse, C., Oyadomari, S., Novoa, I., Lu, P., Zhang, Y., Harding, H.P., and Ron, D. (2003). Inhibition of a constitutive translation initiation factor 2alpha phosphatase, CReP, promotes survival of stressed cells. J Cell Biol *163*, 767-775.

Jovaisaite, V., and Auwerx, J. (2015). The mitochondrial unfolded protein response—synchronizing genomes. Current Opinion in Cell Biology *33*, 74-81.

Katz, A.M. (1998). Is the failing heart energy depleted? Cardiol Clin *16*, 633-644, viii.

Kelly, D.P., and Strauss, A.W. (1994). Inherited cardiomyopathies. N Engl J Med *330*, 913-919.

Khan, N.A., Nikkanen, J., Yatsuga, S., Jackson, C., Wang, L., Pradhan, S., Kivelä, R., Pessia, A., Velagapudi, V., and Suomalainen, A. (2017). mTORC1 Regulates Mitochondrial Integrated Stress Response and Mitochondrial Myopathy Progression. Cell Metabolism *26*, 419-428.e415.

Kilberg, M.S., Balasubramanian, M., Fu, L., and Shan, J. (2012). The Transcription Factor Network Associated With the Amino Acid Response in Mammalian Cells. Advances in Nutrition *3*, 295-306.

Kilberg, M.S., Shan, J., and Su, N. (2009). ATF4-dependent transcription mediates signaling of amino acid limitation. Trends in Endocrinology & Metabolism *20*, 436-443.

Kim, Y., Park, J., Kim, S., Kim, M., Kang, M.G., Kwak, C., Kang, M., Kim, B., Rhee, H.W., and Kim, V.N. (2018). PKR Senses Nuclear and Mitochondrial Signals by Interacting with Endogenous Double-Stranded RNAs. Mol Cell *71*, 1051-1063 e1056.

Korennykh, A., and Walter, P. (2012). Structural basis of the unfolded protein response. Annu Rev Cell Dev Biol *28*, 251-277.

Korhonen, J.A., Pham, X.H., Pellegrini, M., and Falkenberg, M. (2004). Reconstitution of a minimal mtDNA replisome in vitro. EMBO J *23*, 2423-2429.

Krishnamoorthy, T., Pavitt, G.D., Zhang, F., Dever, T.E., and Hinnebusch, A.G. (2001). Tight Binding of the Phosphorylated α Subunit of Initiation Factor 2 (eIF2α) to the Regulatory Subunits of Guanine Nucleotide Exchange Factor eIF2B Is Required for Inhibition of Translation Initiation. Molecular and Cellular Biology *21*, 5018.

Krug, A.K., Gutbier, S., Zhao, L., Pöltl, D., Kullmann, C., Ivanova, V., Förster, S., Jagtap, S., Meiser, J., Leparc, G., et al. (2014). Transcriptional and metabolic adaptation of human neurons to the mitochondrial toxicant MPP+. Cell Death & Disease *5*, e1222-e1222.

Kuhl, I.A.-O., Miranda, M.A.-O.X., Atanassov, I.A.-O., Kuznetsova, I., Hinze, Y., Mourier, A., Filipovska, A.A.-O., and Larsson, N.A.-O.X. (2017). Transcriptomic and proteomic

landscape of mitochondrial dysfunction reveals secondary coenzyme Q deficiency in mammals. LID - 10.7554/eLife.30952 [doi] LID - e30952 [pii].

Kuhlbrandt, W. (2015). Structure and function of mitochondrial membrane protein complexes. BMC Biol *13*, 89.

Kukat, C., Wurm, C.A., Spahr, H., Falkenberg, M., Larsson, N.G., and Jakobs, S. (2011). Super-resolution microscopy reveals that mammalian mitochondrial nucleoids have a uniform size and frequently contain a single copy of mtDNA. Proc Natl Acad Sci U S A *108*, 13534-13539.

Kurland, C.G., and Andersson, S.G.E. (2000). Origin and Evolution of the Mitochondrial Proteome. Microbiology and Molecular Biology Reviews *64*, 786.

Landschulz, W.H., Johnson, P.F., and McKnight, S.L. (1989). The DNA binding domain of the rat liver nuclear protein C/EBP is bipartite. Science *243*, 1681-1688.

Lane, N., and Martin, W. (2010). The energetics of genome complexity. Nature *467*, 929.

Lapuente-Brun, E., Moreno-Loshuertos, R., Acin-Perez, R., Latorre-Pellicer, A., Colas, C., Balsa, E., Perales-Clemente, E., Quiros, P.M., Calvo, E., Rodriguez-Hernandez, M.A., et al. (2013). Supercomplex assembly determines electron flux in the mitochondrial electron transport chain. Science *340*, 1567-1570.

Larsson, N.-G. (2010). Somatic Mitochondrial DNA Mutations in Mammalian Aging. Annual Review of Biochemistry *79*, 683-706.

Lehman, J.J., and Kelly, D.P. (2002). Transcriptional Activation Of Energy Metabolic Switches In The Developing And Hypertrophied Heart. Clinical and Experimental Pharmacology and Physiology *29*, 339-345.

Lemaire, P.A., Anderson, E., Lary, J., and Cole, J.L. (2008). Mechanism of PKR Activation by dsRNA. J Mol Biol *381*, 351-360.

Lemieux, H., Semsroth, S., Antretter, H., Höfer, D., and Gnaiger, E. (2011). Mitochondrial respiratory control and early defects of oxidative phosphorylation in the failing human heart. The International Journal of Biochemistry & Cell Biology *43*, 1729-1738.

Lewis, S.C., Uchiyama, L.F., and Nunnari, J. (2016). ER-mitochondria contacts couple mtDNA synthesis with mitochondrial division in human cells. Science *353*, aaf5549.

Li, Y., Bevilacqua, E., Chiribau, C.-B., Majumder, M., Wang, C., Croniger, C.M., Snider, M.D., Johnson, P.F., and Hatzoglou, M. (2008). Differential Control of the CCAAT/Enhancer-binding Protein β (C/EBPβ) Products Liver-enriched Transcriptional Activating Protein (LAP) and Liver-enriched Transcriptional Inhibitory Protein (LIP) and

the Regulation of Gene Expression during the Response to Endoplasmic Reticulum Stress. Journal of Biological Chemistry *283*, 22443-22456.

Liao, X., and Butow, R.A. (1993). RTG1 and RTG2: Two yeast genes required for a novel path of communication from mitochondria to the nucleus. Cell *72*, 61-71.

Lin, Y.-F., and Haynes, C.M. (2016). Metabolism and the UPR^{mt}. Molecular Cell *61*, 677-682.

Lin, Y.-F., Schulz, A.M., Pellegrino, M.W., Lu, Y., Shaham, S., and Haynes, C.M. (2016). Maintenance and propagation of a deleterious mitochondrial genome by the mitochondrial unfolded protein response. Nature *533*, 416.

Lodish, U.H., Lodish, H., Berk, A., Kaiser, C.A., Kaiser, C., Kaiser, U.C.A., Krieger, M., Scott, M.P., Bretscher, A., and Ploegh, H. (2008). Molecular Cell Biology. (W. H. Freeman).

Lomakin, I.B., and Steitz, T.A. (2013). The initiation of mammalian protein synthesis and mRNA scanning mechanism. Nature *500*, 307-311.

Lopez, M.F., Kristal, B.S., Chernokalskaya, E., Lazarev, A., Shestopalov, A.I., Bogdanova, A., and Robinson, M. (2000). High-throughput profiling of the mitochondrial proteome using affinity fractionation and automation. Electrophoresis *21*, 3427-3440.

Lopez-Crisosto, C., Pennanen, C., Vasquez-Trincado, C., Morales, P.E., Bravo-Sagua, R., Quest, A.F.G., Chiong, M., and Lavandero, S. (2017). Sarcoplasmic reticulum–mitochondria communication in cardiovascular pathophysiology. Nature Reviews Cardiology *14*, 342.

Lu, M., Lawrence, D.A., Marsters, S., Acosta-Alvear, D., Kimmig, P., Mendez, A.S., Paton, A.W., Paton, J.C., Walter, P., and Ashkenazi, A. (2014). Opposing unfolded-protein-response signals converge on death receptor 5 to control apoptosis. Science *345*, 98.

Lyons, G.E., Muhlebach, S., Moser, A., Masood, R., Paterson, B.M., Buckingham, M.E., and Perriard, J.C. (1991). Developmental regulation of creatine kinase gene expression by myogenic factors in embryonic mouse and chick skeletal muscle. Development *113*, 1017.

Mai, N., Chrzanowska-Lightowlers, Z.M., and Lightowlers, R.N. (2017). The process of mammalian mitochondrial protein synthesis. Cell Tissue Res *367*, 5-20.

Marciniak, S.J., Yun, C.Y., Oyadomari, S., Novoa, I., Zhang, Y., Jungreis, R., Nagata, K., Harding, H.P., and Ron, D. (2004). CHOP induces death by promoting protein

synthesis and oxidation in the stressed endoplasmic reticulum. Genes & development *18*, 3066-3077.

Margulis, L. (1970). Origin of Eukaryotic Cells: Evidence and Research Implications for a Theory of the Origin and Evolution of Microbial, Plant, and Animal Cells on the Precambrian Earth. (Yale University Press).

Martinus, R.D., Garth, G.P., Webster, T.L., Cartwright, P., Naylor, D.J., Høj, P.B., and Hoogenraad, N.J. (1996). Selective Induction of Mitochondrial Chaperones in Response to Loss of the Mitochondrial Genome. European Journal of Biochemistry *240*, 98-103.

McCullough, K.D., Martindale, J.L., Klotz, L.-O., Aw, T.-Y., and Holbrook, N.J. (2001). Gadd153 Sensitizes Cells to Endoplasmic Reticulum Stress by Down-Regulating Bcl2 and Perturbing the Cellular Redox State. Molecular and Cellular Biology *21*, 1249.

McEwen, E., Kedersha, N., Song, B., Scheuner, D., Gilks, N., Han, A., Chen, J.J., Anderson, P., and Kaufman, R.J. (2005). Heme-regulated inhibitor kinase-mediated phosphorylation of eukaryotic translation initiation factor 2 inhibits translation, induces stress granule formation, and mediates survival upon arsenite exposure. J Biol Chem *280*, 16925-16933.

Michel, S., Canonne, M., Arnould, T., and Renard, P. (2015). Inhibition of mitochondrial genome expression triggers the activation of CHOP-10 by a cell signaling dependent on the integrated stress response but not the mitochondrial unfolded protein response. Mitochondrion *21*, 58-68.

Mikelsaar, R. (1983). Human mitochondrial genome and the evolution of methionine transfer ribonucleic acids. Journal of Theoretical Biology *105*, 221-232.

Miller, M., Shuman, J.D., Sebastian, T., Dauter, Z., and Johnson, P.F. (2003). Structural basis for DNA recognition by the basic region leucine zipper transcription factor CCAAT/enhancer-binding protein alpha. J Biol Chem *278*, 15178-15184.

Minczuk, M., He, J., Duch, A.M., Ettema, T.J., Chlebowski, A., Dzionek, K., Nijtmans, L.G., Huynen, M.A., and Holt, I.J. (2011). TEFM (c17orf42) is necessary for transcription of human mtDNA. Nucleic Acids Res *39*, 4284-4299.

Miralles Fuste, J., Shi, Y., Wanrooij, S., Zhu, X., Jemt, E., Persson, O., Sabouri, N., Gustafsson, C.M., and Falkenberg, M. (2014). In vivo occupancy of mitochondrial single-stranded DNA binding protein supports the strand displacement mode of DNA replication. PLoS Genet *10*, e1004832.

Mitchell, P. (1976). Possible molecular mechanisms of the protonmotive function of cytochrome systems. J Theor Biol *62*, 327-367.

Mizushima, N., Yoshimori, T., and Levine, B. (2010). Methods in Mammalian Autophagy Research. Cell *140*, 313-326.

Mootha, V.K., Arai, A.E., and Balaban, R.S. (1997). Maximum oxidative phosphorylation capacity of the mammalian heart. American Journal of Physiology-Heart and Circulatory Physiology *272*, H769-H775.

Morozov, Y.I., Agaronyan, K., Cheung, A.C.M., Anikin, M., Cramer, P., and Temiakov, D. (2014). A novel intermediate in transcription initiation by human mitochondrial RNA polymerase. Nucleic Acids Res *42*, 3884-3893.

Münch, C. (2018). The different axes of the mammalian mitochondrial unfolded protein response. BMC Biology *16*, 81.

Nargund, A.M., Pellegrino, M.W., Fiorese, C.J., Baker, B.M., and Haynes, C.M. (2012). Mitochondrial Import Efficiency of ATFS-1 Regulates Mitochondrial UPR Activation. Science *337*, 587.

Nikkanen, J., Forsström, S., Euro, L., Paetau, I., Kohnz, Rebecca A., Wang, L., Chilov, D., Viinamäki, J., Roivainen, A., Marjamäki, P., et al. (2016). Mitochondrial DNA Replication Defects Disturb Cellular dNTP Pools and Remodel One-Carbon Metabolism. Cell Metabolism *23*, 635-648.

Novoa, I., Zeng, H., Harding, H.P., and Ron, D. (2001). Feedback inhibition of the unfolded protein response by GADD34-mediated dephosphorylation of eIF2alpha. J Cell Biol *153*, 1011-1022.

Novoa, I., Zhang, Y., Zeng, H., Jungreis, R., Harding, H.P., and Ron, D. (2003). Stress-induced gene expression requires programmed recovery from translational repression. The EMBO Journal *22*, 1180-1187.

Nunnari, J., and Suomalainen, A. (2012). Mitochondria: In Sickness and in Health. Cell *148*, 1145-1159.

Oertlin, C., Lorent, J., Murie, C., Furic, L., Topisirovic, I., and Larsson, O. (2019). Generally applicable transcriptome-wide analysis of translation using anota2seq.

Oka, T., Hikoso, S., Yamaguchi, O., Taneike, M., Takeda, T., Tamai, T., Oyabu, J., Murakawa, T., Nakayama, H., Nishida, K., et al. (2012). Mitochondrial DNA that escapes from autophagy causes inflammation and heart failure. Nature *485*, 251-255.

Orchard, C.H., and Kentish, J.C. (1990). Effects of changes of pH on the contractile function of cardiac muscle. American Journal of Physiology-Cell Physiology *258*, C967-C981.

Owen, O.E., Kalhan, S.C., and Hanson, R.W. (2002). The Key Role of Anaplerosis and Cataplerosis for Citric Acid Cycle Function. Journal of Biological Chemistry *277*, 30409-30412.

Oyadomari, S., and Mori, M. (2004). Roles of CHOP/GADD153 in endoplasmic reticulum stress. Cell Death Differ *11*, 381-389.

Packer, M. (1985). Sudden unexpected death in patients with congestive heart failure: a second frontier. Circulation *72*, 681-685.

Pain, V.M. (1996). Initiation of protein synthesis in eukaryotic cells. Eur J Biochem *236*, 747-771.

Pakos-Zebrucka, K., Koryga, I., Mnich, K., Ljujic, M., Samali, A., and Gorman, A.M. (2016). The integrated stress response. EMBO Reports *17*, 1374-1395.

Papa, L., and Germain, D. (2014). SirT3 regulates the mitochondrial unfolded protein response. Mol Cell Biol *34*, 699-710.

Papa, S., Martino, P.L., Capitanio, G., Gaballo, A., De Rasmo, D., Signorile, A., and Petruzzella, V. (2012). The oxidative phosphorylation system in mammalian mitochondria. Adv Exp Med Biol *942*, 3-37.

Papadopoli, D., Boulay, K., Kazak, L., Pollak, M., Mallette, F., Topisirovic, I., and Hulea, L. (2019). mTOR as a central regulator of lifespan and aging. F1000Res *8*.

Parikh, V.S., Conrad-Webb, H., Docherty, R., and Butow, R.A. (1989). Interaction between the yeast mitochondrial and nuclear genomes influences the abundance of novel transcripts derived from the spacer region of the nuclear ribosomal DNA repeat. Molecular and Cellular Biology *9*, 1897.

Parikh, V.S., Morgan, M.M., Scott, R., Clements, L.S., and Butow, R.A. (1987). The mitochondrial genotype can influence nuclear gene expression in yeast. Science *235*, 576.

Park, Y., Reyna-Neyra, A., Philippe, L., and Thoreen, C.C. (2017). mTORC1 Balances Cellular Amino Acid Supply with Demand for Protein Synthesis through Post-transcriptional Control of ATF4. Cell Reports *19*, 1083-1090.

Pelley, J.W. (2012). 12 - Amino Acid and Heme Metabolism. In Elsevier's Integrated Review Biochemistry (Second Edition). J.W. Pelley, ed. (Philadelphia: W.B. Saunders), pp. 99-107.

Poole-Wilson, P.A. (1982). Acidosis and Contractility of Heart Muscle. Ciba Foundation Symposium 87 - Metabolic Acidosis, 58-76.

Porter, G.A., Jr., Hom, J., Hoffman, D., Quintanilla, R., de Mesy Bentley, K., and Sheu, S.S. (2011). Bioenergetics, mitochondria, and cardiac myocyte differentiation. Prog Pediatr Cardiol *31*, 75-81.

Posse, V., and Gustafsson, C.M. (2017). Human Mitochondrial Transcription Factor B2 Is Required for Promoter Melting during Initiation of Transcription. J Biol Chem *292*, 2637-2645.

Quiros, P.M., Goyal, A., Jha, P., and Auwerx, J. (2017). Analysis of mtDNA/nDNA Ratio in Mice. Curr Protoc Mouse Biol *7*, 47-54.

Quirós, P.M., Prado, M.A., Zamboni, N., D'Amico, D., Williams, R.W., Finley, D., Gygi, S.P., and Auwerx, J. (2017). Multi-omics analysis identifies ATF4 as a key regulator of the mitochondrial stress response in mammals. The Journal of Cell Biology *216*, 2027-2045.

Rafie-Kolpin, M., Chefalo, P.J., Hussain, Z., Hahn, J., Uma, S., Matts, R.L., and Chen, J.J. (2000). Two heme-binding domains of heme-regulated eukaryotic initiation factor-2alpha kinase. N terminus and kinase insertion. J Biol Chem *275*, 5171-5178.

Rainbolt, T.K., Atanassova, N., Genereux, Joseph C., and Wiseman, R.L. (2013). Stress-Regulated Translational Attenuation Adapts Mitochondrial Protein Import through Tim17A Degradation. Cell Metabolism *18*, 908-919.

Rampelt, H., Zerbes, R.M., van der Laan, M., and Pfanner, N. (2017). Role of the mitochondrial contact site and cristae organizing system in membrane architecture and dynamics. Biochim Biophys Acta Mol Cell Res *1864*, 737-746.

Rath, E., Berger, E., Messlik, A., Nunes, T., Liu, B., Kim, S.C., Hoogenraad, N., Sans, M., Sartor, R.B., and Haller, D. (2012). Induction of dsRNA-activated protein kinase links mitochondrial unfolded protein response to the pathogenesis of intestinal inflammation. Gut *61*, 1269.

Restelli, L.M., Oettinghaus, B., Halliday, M., Agca, C., Licci, M., Sironi, L., Savoia, C., Hench, J., Tolnay, M., Neutzner, A., et al. (2018). Neuronal Mitochondrial Dysfunction Activates the Integrated Stress Response to Induce Fibroblast Growth Factor 21. Cell Rep *24*, 1407-1414.

Richter, U., Lahtinen, T., Marttinen, P., Myöhänen, M., Greco, D., Cannino, G., Jacobs, Howard T., Lietzén, N., Nyman, Tuula A., and Battersby, Brendan J. (2013). A Mitochondrial Ribosomal and RNA Decay Pathway Blocks Cell Proliferation. Current Biology *23*, 535-541.

Ritterhoff, J., and Tian, R. (2017). Metabolism in cardiomyopathy: every substrate matters. Cardiovasc Res *113*, 411-421.

Robberson, D.L., Kasamatsu, H., and Vinograd, J. (1972). Replication of mitochondrial DNA. Circular replicative intermediates in mouse L cells. Proc Natl Acad Sci U S A *69*, 737-741.

Rodriguez, D., Rojas-Rivera, D., and Hetz, C. (2011). Integrating stress signals at the endoplasmic reticulum: The BCL-2 protein family rheostat. Biochimica et Biophysica Acta (BBA) - Molecular Cell Research *1813*, 564-574.

Rogers, J., and Munro, H. (1987). Translation of ferritin light and heavy subunit mRNAs is regulated by intracellular chelatable iron levels in rat hepatoma cells. Proceedings of the National Academy of Sciences *84*, 2277.

Ron, D. (2002). Translational control in the endoplasmic reticulum stress response. The Journal of Clinical Investigation *110*, 1383-1388.

Ron, D., and Habener, J.F. (1992). CHOP, a novel developmentally regulated nuclear protein that dimerizes with transcription factors C/EBP and LAP and functions as a dominant-negative inhibitor of gene transcription.

Rorbach, J., Richter, R., Wessels, H.J., Wydro, M., Pekalski, M., Farhoud, M., Kuhl, I., Gaisne, M., Bonnefoy, N., Smeitink, J.A., et al. (2008). The human mitochondrial ribosome recycling factor is essential for cell viability. Nucleic Acids Res *36*, 5787-5799.

Rosilio, C., Nebout, M., Imbert, V., Griessinger, E., Neffati, Z., Benadiba, J., Hagenbeek, T., Spits, H., Reverso, J., Ambrosetti, D., et al. (2015). L-type amino-acid transporter 1 (LAT1): a therapeutic target supporting growth and survival of T-cell lymphoblastic lymphoma/T-cell acute lymphoblastic leukemia. Leukemia *29*, 1253-1266.

Rossignol, R., Faustin, B., Rocher, C., Malgat, M., Mazat, J.P., and Letellier, T. (2003). Mitochondrial threshold effects. Biochem J *370*, 751-762.

Rutkowski, D.T., Arnold, S.M., Miller, C.N., Wu, J., Li, J., Gunnison, K.M., Mori, K., Sadighi Akha, A.A., Raden, D., and Kaufman, R.J. (2006). Adaptation to ER stress is mediated by differential stabilities of pro-survival and pro-apoptotic mRNAs and proteins. PLoS Biol *4*, e374.

Rutter, J., Winge, D.R., and Schiffman, J.D. (2010). Succinate dehydrogenase - Assembly, regulation and role in human disease. Mitochondrion *10*, 393-401.

Saunders, L.R., and Barber, G.N. (2003). The dsRNA binding protein family: critical roles, diverse cellular functions. FASEB J *17*, 961-983.

Saxton, R.A., and Sabatini, D.M. (2017). mTOR Signaling in Growth, Metabolism, and Disease. Cell *169*, 361-371.

Schaefer, A.M., Taylor, R.W., Turnbull, D.M., and Chinnery, P.F. (2004). The epidemiology of mitochondrial disorders--past, present and future. Biochim Biophys Acta *1659*, 115-120.

Schagger, H., and Pfeiffer, K. (2000). Supercomplexes in the respiratory chains of yeast and mammalian mitochondria. EMBO J *19*, 1777-1783.

Scheuner, D., Patel, R., Wang, F., Lee, K., Kumar, K., Wu, J., Nilsson, A., Karin, M., and Kaufman, R.J. (2006). Double-stranded RNA-dependent protein kinase phosphorylation of the alpha-subunit of eukaryotic translation initiation factor 2 mediates apoptosis. J Biol Chem *281*, 21458-21468.

Schmidt, E.K., Clavarino, G., Ceppi, M., and Pierre, P. (2009). SUnSET, a nonradioactive method to monitor protein synthesis. Nature Methods *6*, 275-277.

Schon, E.A., DiMauro, S., and Hirano, M. (2012). Human mitochondrial DNA: roles of inherited and somatic mutations. Nat Rev Genet *13*, 878-890.

Seiferling, D., Szczepanowska, K., Becker, C., Senft, K., Hermans, S., Maiti, P., König, T., Kukat, A., and Trifunovic, A. (2016). Loss of CLPP alleviates mitochondrial cardiomyopathy without affecting the mammalian UPR<sup>mt</sup&gt. EMBO reports *17*, 953.

Shao, D., and Tian, R. (2015). Glucose Transporters in Cardiac Metabolism and Hypertrophy. Comprehensive Physiology, 331-351.

Shenoy, A.R., Wellington, D.A., Kumar, P., Kassa, H., Booth, C.J., Cresswell, P., and MacMicking, J.D. (2012). GBP5 Promotes NLRP3 Inflammasome Assembly and Immunity in Mammals. Science *336*, 481.

Shi, Y., Dierckx, A., Wanrooij, P.H., Wanrooij, S., Larsson, N.-G., Wilhelmsson, L.M., Falkenberg, M., and Gustafsson, C.M. (2012). Mammalian transcription factor A is a core component of the mitochondrial transcription machinery. Proceedings of the National Academy of Sciences *109*, 16510.

Shpilka, T., and Haynes, C.M. (2017). The mitochondrial UPR: mechanisms, physiological functions and implications in ageing. Nature Reviews Molecular Cell Biology *19*, 109.

Sidrauski, C., McGeachy, A.M., Ingolia, N.T., and Walter, P. (2015). The small molecule ISRIB reverses the effects of eIF2alpha phosphorylation on translation and stress granule assembly. Elife *4*.

Sissler, M., González-Serrano, L.E., and Westhof, E. (2017). Recent Advances in Mitochondrial Aminoacyl-tRNA Synthetases and Disease. Trends in Molecular Medicine *23*, 693-708.

Slee, E.A., Adrain, C., and Martin, S.J. (2001). Executioner Caspase-3, -6, and -7 Perform Distinct, Non-redundant Roles during the Demolition Phase of Apoptosis. Journal of Biological Chemistry *276*, 7320-7326.

Smink, J.J., Begay, V., Schoenmaker, T., Sterneck, E., de Vries, T.J., and Leutz, A. (2009). Transcription factor C/EBPbeta isoform ratio regulates osteoclastogenesis through MafB. EMBO J *28*, 1769-1781.

Soleimanpour-Lichaei, H.R., Kuhl, I., Gaisne, M., Passos, J.F., Wydro, M., Rorbach, J., Temperley, R., Bonnefoy, N., Tate, W., Lightowlers, R., et al. (2007). mtRF1a is a human mitochondrial translation release factor decoding the major termination codons UAA and UAG. Mol Cell *27*, 745-757.

Song, B., Scheuner, D., Ron, D., Pennathur, S., and Kaufman, R.J. (2008). Chop deletion reduces oxidative stress, improves beta cell function, and promotes cell survival in multiple mouse models of diabetes. J Clin Invest *118*, 3378-3389.

Spinelli, J.B., and Haigis, M.C. (2018). The multifaceted contributions of mitochondria to cellular metabolism. Nature Cell Biology *20*, 745-754.

Stefano, G.B., Bjenning, C., Wang, F., Wang, N., and Kream, R.M. (2017). Mitochondrial Heteroplasmy. Adv Exp Med Biol *982*, 577-594.

Stewart, J.B., and Larsson, N.-G. (2014). Keeping mtDNA in Shape between Generations. PLOS Genetics *10*, e1004670.

Stine, Z.E., Walton, Z.E., Altman, B.J., Hsieh, A.L., and Dang, C.V. (2015). MYC, Metabolism, and Cancer. Cancer Discovery *5*, 1024.

Suomalainen, A., and Battersby, B.J. (2017). Mitochondrial diseases: the contribution of organelle stress responses to pathology. Nature Reviews Molecular Cell Biology *19*, 77.

Tameire, F., Verginadis, II, Leli, N.M., Polte, C., Conn, C.S., Ojha, R., Salas Salinas, C., Chinga, F., Monroy, A.M., Fu, W., et al. (2019). ATF4 couples MYC-dependent translational activity to bioenergetic demands during tumour progression. Nat Cell Biol *21*, 889-899.

Taniuchi, S., Miyake, M., Tsugawa, K., Oyadomari, M., and Oyadomari, S. (2016). Integrated stress response of vertebrates is regulated by four eIF2α kinases. Scientific Reports *6*, 32886.

Teske, B.F., Fusakio, M.E., Zhou, D., Shan, J., McClintick, J.N., Kilberg, M.S., and Wek, R.C. (2013). CHOP induces activating transcription factor 5 (ATF5) to trigger apoptosis in response to perturbations in protein homeostasis. Mol Biol Cell *24*, 2477-2490.

Timmis, J.N., Ayliffe, M.A., Huang, C.Y., and Martin, W. (2004). Endosymbiotic gene transfer: organelle genomes forge eukaryotic chromosomes. Nature Reviews Genetics *5*, 123-135.

Topf, U., Uszczynska-Ratajczak, B., and Chacinska, A. (2019). Mitochondrial stress-dependent regulation of cellular protein synthesis. Journal of Cell Science *132*, jcs226258.

Trifunovic, A., Wredenberg, A., Falkenberg, M., Spelbrink, J.N., Rovio, A.T., Bruder, C.E., Bohlooly, Y.M., Gidlof, S., Oldfors, A., Wibom, R., et al. (2004). Premature ageing in mice expressing defective mitochondrial DNA polymerase. Nature *429*, 417-423.

Tsuboi, M., Morita, H., Nozaki, Y., Akama, K., Ueda, T., Ito, K., Nierhaus, K.H., and Takeuchi, N. (2009). EF-G2mt is an exclusive recycling factor in mammalian mitochondrial protein synthesis. Mol Cell *35*, 502-510.

Tsukada, J., Yoshida, Y., Kominato, Y., and Auron, P.E. (2011). The CCAAT/enhancer (C/EBP) family of basic-leucine zipper (bZIP) transcription factors is a multifaceted highly-regulated system for gene regulation. Cytokine *54*, 6-19.

Tucker, E.J., Hershman, S.G., Kohrer, C., Belcher-Timme, C.A., Patel, J., Goldberger, O.A., Christodoulou, J., Silberstein, J.M., McKenzie, M., Ryan, M.T., et al. (2011). Mutations in MTFMT underlie a human disorder of formylation causing impaired mitochondrial translation. Cell Metab *14*, 428-434.

Vafai, S.B., and Mootha, V.K. (2012). Mitochondrial disorders as windows into an ancient organelle. Nature *491*, 374.

van den Bogert, C., and Kroon, A.M. (1981). Tissue distribution and effects on mitochondrial protein synthesis of tetracyclines after prolonged continuous intravenous administration to rats. Biochem Pharmacol *30*, 1706-1709.

Vazquez de Aldana, C.R., Wek, R.C., Segundo, P.S., Truesdell, A.G., and Hinnebusch, A.G. (1994). Multicopy tRNA genes functionally suppress mutations in yeast eIF-2 alpha kinase GCN2: evidence for separate pathways coupling GCN4 expression to unchanged tRNA. Molecular and Cellular Biology *14*, 7920.

Wagle, P., Nikolic, M., and Frommolt, P. (2015). QuickNGS elevates Next-Generation Sequencing data analysis to a new level of automation. BMC Genomics *16*, 487.

Wallace, D.C. (2005). A mitochondrial paradigm of metabolic and degenerative diseases, aging, and cancer: a dawn for evolutionary medicine. Annu Rev Genet *39*, 359-407.

Wang, C., and Youle, R.J. (2009). The role of mitochondria in apoptosis*. Annual review of genetics *43*, 95-118.

Wang, J., Wilhelmsson, H., Graff, C., Li, H., Oldfors, A., Rustin, P., Bruning, J.C., Kahn, C.R., Clayton, D.A., Barsh, G.S., et al. (1999). Dilated cardiomyopathy and atrioventricular conduction blocks induced by heart-specific inactivation of mitochondrial DNA gene expression. Nat Genet *21*, 133-137.

Wang, M., and Kaufman, R.J. (2016). Protein misfolding in the endoplasmic reticulum as a conduit to human disease. Nature *529*, 326-335.

Wang, Z., Ying, Z., Bosy-Westphal, A., Zhang, J., Schautz, B., Later, W., Heymsfield, S.B., and Muller, M.J. (2010). Specific metabolic rates of major organs and tissues across adulthood: evaluation by mechanistic model of resting energy expenditure. Am J Clin Nutr *92*, 1369-1377.

Wanrooij, S., Fuste, J.M., Farge, G., Shi, Y., Gustafsson, C.M., and Falkenberg, M. (2008). Human mitochondrial RNA polymerase primes lagging-strand DNA synthesis in vitro. Proc Natl Acad Sci U S A *105*, 11122-11127.

Weiss, R.G., Gerstenblith, G., and Bottomley, P.A. (2005). ATP flux through creatine kinase in the normal, stressed, and failing human heart. Proc Natl Acad Sci U S A *102*, 808-813.

Wek, S.A., Zhu, S., and Wek, R.C. (1995). The histidyl-tRNA synthetase-related sequence in the eIF-2 alpha protein kinase GCN2 interacts with tRNA and is required for activation in response to starvation for different amino acids. Mol Cell Biol *15*, 4497-4506.

Wellen, K.E., Hatzivassiliou, G., Sachdeva, U.M., Bui, T.V., Cross, J.R., and Thompson, C.B. (2009). ATP-citrate lyase links cellular metabolism to histone acetylation. Science *324*, 1076-1080.

West, A.P., Khoury-Hanold, W., Staron, M., Tal, M.C., Pineda, C.M., Lang, S.M., Bestwick, M., Duguay, B.A., Raimundo, N., MacDuff, D.A., et al. (2015). Mitochondrial DNA stress primes the antiviral innate immune response. Nature *520*, 553.

Westermann, B. (2010). Mitochondrial fusion and fission in cell life and death. Nature Reviews Molecular Cell Biology *11*, 872-884.

Whiteman, E.L., Cho, H., and Birnbaum, M.J. (2002). Role of Akt/protein kinase B in metabolism. Trends in Endocrinology & Metabolism *13*, 444-451.

Williams, S.C., Angerer, N.D., and Johnson, P.F. (1997). C/EBP proteins contain nuclear localization signals imbedded in their basic regions. Gene Expr *6*, 371-385.

Yang, Y., Liu, L., Naik, I., Braunstein, Z., Zhong, J., and Ren, B. (2017). Transcription Factor C/EBP Homologous Protein in Health and Diseases. Front Immunol *8*, 1612.

Ye, J., Kumanova, M., Hart, L.S., Sloane, K., Zhang, H., De Panis, D.N., Bobrovnikova-Marjon, E., Diehl, J.A., Ron, D., and Koumenis, C. (2010). The GCN2-ATF4 pathway is critical for tumour cell survival and proliferation in response to nutrient deprivation. EMBO J *29*, 2082-2096.

Yoneda, T., Benedetti, C., Urano, F., Clark, S.G., Harding, H.P., and Ron, D. (2004). Compartment-specific perturbation of protein handling activates genes encoding mitochondrial chaperones. Journal of Cell Science *117*, 4055.

Yuan, H.-X., Xiong, Y., and Guan, K.-L. (2013). Nutrient Sensing, Metabolism, and Cell Growth Control. Molecular Cell *49*, 379-387.

Zähringer, J., Baliga, B.S., and Munro, H.N. (1976). Novel mechanism for translational control in regulation of ferritin synthesis by iron. Proceedings of the National Academy of Sciences *73*, 857.

Zhao, Q., Wang, J., Levichkin, I.V., Stasinopoulos, S., Ryan, M.T., and Hoogenraad, N.J. (2002). A mitochondrial specific stress response in mammalian cells. The EMBO Journal *21*, 4411-4419.

Zhao, S., Xu, W., Jiang, W., Yu, W., Lin, Y., Zhang, T., Yao, J., Zhou, L., Zeng, Y., Li, H., et al. (2010). Regulation of cellular metabolism by protein lysine acetylation. Science *327*, 1000-1004.

Zinszner, H., Kuroda, M., Wang, X., Batchvarova, N., Lightfoot, R.T., Remotti, H., Stevens, J.L., and Ron, D. (1998). CHOP is implicated in programmed cell death in response to impaired function of the endoplasmic reticulum. Genes & development *12*, 982-995.

Erklärung

Ich versichere, dass ich die von mir vorgelegte Dissertation selbstständig angefertigt, die benutzten Quellen und Hilfsmittel vollständig angegeben und die Stellen der Arbeit − einschließlich Tabellen, Karten und Abbildungen −, die anderen Werken im Wortlaut oder dem Sinn nach entnommen sind, in jedem Einzelfall als Entlehnung kenntlich gemacht habe; dass diese Dissertation noch keiner anderen Fakultät oder Universität zur Prüfung vorgelegen hat; dass sie − abgesehen von unten angegebenen Teilpublikationen − noch nicht veröffentlicht worden ist, sowie, dass ich eine solche Veröffentlichung vor Abschluss des Promotionsverfahrens nicht vornehmen werde.

Die Bestimmungen der Promotionsordnung sind mir bekannt. Die von mir vorgelegte Dissertation ist von Prof. Dr. Aleksandra Trifunovic betreut worden.

Köln, den 4. Dezember 2019